

1 **A Bivalent Molecular Glue Linking Lysine Acetyltransferases to Oncogene-
2 induced Cell Death**

3 **AUTHORS:**

4 Meredith N. Nix^{1,2*}, Sai Gourisankar^{1*}, Roman C. Sarott^{1†}, Brendan G. Dwyer^{1†}, Sabin.
5 A. Nettles^{3†}, Michael M. Martinez¹, Hind Abuzaid³, Haopeng Yang⁵, Yanlan Wang³, Juste
6 M. Simanauskaite³, Bryan A. Romero¹, Hannah M. Jones¹, Andrey Krokhitin³, Tara N.
7 Lowensohn², Lei Chen⁶, Cara Low¹, Mark M. Davis⁶, Daniel Fernandez⁷, Tinghu Zhang¹,
8 Michael R. Green^{5#}, Stephen M. Hinshaw^{1#}, Nathanael S. Gray^{1#}, Gerald R. Crabtree^{3,4#}

9
10 **AFFILIATIONS:**

11 ¹Department of Chemical and Systems Biology, Stanford University, Stanford, CA, USA

12 ²Department of Chemistry, Stanford University, Stanford, CA, USA

13 ³Department of Pathology, Stanford University, Stanford, CA, USA

14 ⁴Department of Developmental Biology, Stanford University, Stanford, CA, USA

15 ⁵Department of Lymphoma- & Myeloma, University of Texas MD Anderson Cancer
16 Center, Houston, TX, USA

17 ⁶Department of Microbiology and Immunology, Stanford University, Stanford, CA, USA

18 ⁷Macromolecular Structure, Nucleus at Sarafan ChEM-H, Stanford University, Stanford,
19 CA, USA

20 *these authors contributed equally to this work

21 †these authors contributed equally to this work

22 #Correspondence should be addressed to Michael R. Green:
23 MGreen5@mdanderson.org, Stephen M. Hinshaw: hinshaw@stanford.edu, Nathanael S.
24 Gray: nsgray01@stanford.edu, and Gerald R. Crabtree: crabtree@stanford.edu (lead
25 contact)

26 **SUMMARY:**

27 Developing cancer therapies that induce robust death of the malignant cell is critical to
28 prevent relapse. Highly effective strategies, such as immunotherapy, exemplify this
29 observation. Here we provide the structural and molecular underpinnings for an approach
30 that leverages chemical induced proximity to produce specific cell killing of diffuse large
31 B cell lymphoma, the most common non-Hodgkin's lymphoma. We develop KAT-TCIPs
32 (lysine acetyltransferase transcriptional/epigenetic chemical inducers of proximity) that
33 redirect p300 and CBP to activate programmed cell death genes normally repressed by
34 the oncogenic driver, BCL6. Acute treatment rapidly reprograms the epigenome to initiate
35 apoptosis and repress c-MYC. The crystal structure of the chemically induced p300-BCL6
36 complex reveals how chance interactions between the two proteins can be systematically
37 exploited to produce the exquisite potency and selectivity of KAT-TCIPs. Thus, the
38 malignant function of an oncogenic driver can be co-opted to activate robust cell death,
39 with implications for precision epigenetic therapies.

40 **KEYWORDS:** lysine acetyltransferases, induced proximity, lymphoma, transcription

47 **INTRODUCTION**

48

49 The paralogous lysine acetyltransferases (KATs) p300 (E1A-associated protein p300,
50 encoded by *EP300*) and CBP (CREB-binding protein, encoded by *CREBBP*), are
51 essential regulators of gene expression in healthy and malignant cells¹. p300 and CBP
52 (hereafter: p300/CBP) bind and catalyze histone acetylation, interact with transcription
53 factors (TFs), and activate transcription at promoters and enhancers^{2,3}. A catalytic KAT
54 domain (86% identity between p300/CBP)⁴⁻⁶, an acetyl-lysine-binding bromodomain (97%
55 identity), and several other conserved protein-interaction domains facilitate these
56 functions^{7,8}. In diverse cancers, p300/CBP support the expression of oncogenic networks
57 by activating clusters of gene-regulatory regions called super-enhancers⁸⁻¹³. No
58 p300/CBP inhibitor has received regulatory approval for oncology¹⁴⁻¹⁸. Given the
59 physiological role of p300/CBP in activating transcription, we sought to develop small
60 molecules that redirect them to induce the expression of proapoptotic pathways in cancer.

61

62 We pursued this objective by developing chemical inducers of proximity (CIPs). CIPs are
63 small molecules that rewire protein-protein interactions. The realization that induced
64 proximity governs diverse cellular processes such as signal transduction, post-
65 translational-modification, and epigenetic regulation¹⁹ has led to the development of CIPs
66 for therapeutic purposes. Proteolysis-targeting chimeras (PROTACs), which rely on
67 inducing the proximity of a ubiquitin ligase to degrade a target protein, exemplify this
68 concept²⁰. Cyclosporin A²¹, FK506²² (tacrolimus) and rapamycin²³ (sirolimus) belong to a
69 related class of clinical proximity-inducing small molecules. Structural studies by
70 Schreiber and Clardy showed that these compounds facilitate the formation of protein
71 complexes by creating a composite binding surface containing the small molecule and
72 the two binding proteins²⁴. A high degree of cooperative binding enables the potency and
73 selectivity of the CIP²⁵. Small molecules that facilitate the cooperative assembly of
74 complexes between unrelated proteins have come to be known as molecular glues²⁶.

75

76 While CIPs are emerging as preclinical tools to degrade p300/CBP in hematological
77 malignancies and solid cancers²⁷⁻³⁰, the development of p300/CBP-redirecting CIPs
78 remains limited. Thus far, efforts have largely relied on transgene overexpression³¹,
79 protein tags³²⁻³⁴, or large, DNA-binding pyrrole-imidazole polyamide moieties³⁵; these
80 technologies are not easily translatable to the clinic. Two notable recent exceptions are
81 CIPs^{36,37} that harness KAT activity to inactivate a relatively rare³⁸, mutant form of p53 via
82 targeted p53 acetylation in genetically unmodified cells.

83

84 Our laboratories recently introduced a class of CIPs termed transcriptional/epigenetic
85 chemical inducers of proximity (TCIPs) that relocalize transcriptional activators to
86 chromatin bound by DNA sequence-specific TFs^{39,40}. We previously synthesized TCIPs
87 that redirect the RNA Polymerase II elongation-associated factors BRD4 and CDK9 to
88 BCL6, a TF that represses pro-apoptotic and growth arrest genes⁴¹⁻⁴³ and is
89 overexpressed in 40 to 60% of diffuse large B cell lymphomas (DLBCLs)⁴⁴. These
90 molecules rewire BCL6 to activate transcriptionally silent proapoptotic pathways and
91 potently kill cells. They offer an alternative therapeutic strategy to kill DLBCL cells when
92 compared to inhibitors or degraders of BCL6⁴⁵⁻⁴⁹ and have been chemically optimized for

93 *in vivo* administration⁴⁰. The broad applicability of this approach hinges on (i) identifying
94 a diverse set of activators that can be rewired and (ii) developing molecular glues that
95 induce favorable protein-protein interactions. The latter requires structural studies of
96 critical ternary complexes to drive chemical optimization of cooperativity.
97

98 Here, we developed lysine acetyltransferase TCIPs (KAT-TCIPs) that redirect p300/CBP
99 to BCL6. We used a systematic chemical design cascade to discover molecules that are
100 exquisitely selective to both protein partners and potent in DLBCL cells (cell proliferation
101 IC₅₀ ~0.8 nM). KAT-TCIPs redistributed p300/CBP-catalyzed chromatin acetylation and
102 activated BCL6-regulated gene expression. These molecular effects led to potent
103 induction of pro-apoptotic proteins and durable repression of the oncogene c-MYC (IC₅₀
104 ~ 0.8 nM). A co-crystal structure of the KAT-TCIP in complex with p300 and BCL6 and
105 biophysical analyses demonstrated that selectivity and potency arise from the chance
106 formation of complementary protein-protein interactions on the composite drug-protein
107 interface. Thus, CIPs that redirect p300/CBP can be systematically designed to be precise
108 and powerful killers of cancer cells.
109

110 RESULTS

112 Design and activity of KAT-TCIPs

114 To explore the potential of harnessing co-activating lysine acetyltransferase activity for
115 transcriptional activation, we synthesized a library of bivalent compounds designed to
116 recruit p300/CBP to BCL6-bound genes (Fig. 1A). These bivalent compounds link the
117 BCL6 BTB-domain-binding ligand BI-3812⁴⁸ to p300/CBP-specific bromodomain (BD)
118 inhibitors, including GNE-781⁵⁰ and Cmpd33⁵¹, via conjugatable handles identified from
119 X-ray co-crystal structures (Supplemental Fig. 1A, B). A diverse library of alkyl, PEG, and
120 rigid linkers was employed to increase the probability of generating cell-permeable TCIPs
121 that induce productive ternary complexes (Supplemental Fig. 1A, 1B).
122

123 To test the KAT-TCIP library, we used a BCL6-controlled green fluorescent protein (GFP)
124 reporter gene in the DLBCL cell line KARPAS422 (K422)³⁹. One compound, which we
125 named **TCIP3** (Fig. 1B), produced the highest GFP signal, 10-times greater than DMSO
126 treatment (Fig. 1C and Supplemental Fig. 1C). We observed a hook effect in GFP
127 activation, a characteristic of bivalent molecules in which high concentrations of a
128 compound saturate binding to either protein partner and prevent productive ternary
129 complex formation^{52,53}. To distinguish the effects of ternary complex formation from
130 p300/CBP^{BD} or BCL6^{BTB} inhibition while controlling for drug size and cellular permeability,
131 we synthesized negative controls containing the **TCIP3** linker but that lack the ability to
132 bind either BCL6^{BTB} (**NEG1**) or p300/CBP^{BD} (**NEG2**) (Fig. 1B). When compared with
133 **TCIP3**, **NEG1** and **NEG2** remained similarly membrane-permeable and potent binders of
134 either p300/CBP^{BD} or BCL6^{BTB}, respectively, as measured by cellular probe-displacement
135 assays (nanoBRET⁵⁴) (Supplemental Fig. 1D, E). Neither **NEG1** nor **NEG2** activated GFP
136 expression, supporting ternary complex-dependent activity (Fig. 1C).
137

138 Given the ability of p300/CBP KAT-TCIPs to activate the BCL6 reporter gene, we
139 investigated their effects on the viability of DLBCL. In a 72-hour cell viability assay, **TCIP3**
140 inhibited the proliferation of SUDHL5 DLBCL cells with an average IC₅₀ of 0.8 nM (Fig.
141 1D). **TCIP3** was over 1,000 times more cytotoxic than either **NEG1** or **NEG2**, and nearly
142 all GNE-781-based KAT-TCIPs were 10 – 38,000-times more potent than the co-inhibition
143 of p300/CBP and BCL6 (Fig. 1D, Supplemental Fig. 2A). In these cell proliferation/viability
144 assays, **TCIP3** was 238-times more potent than the p300/CBP KAT catalytic-site inhibitor
145 A-485¹⁵ and 12 times more potent than a p300/CBP PROTAC dCBP-1³⁰ (Fig. 1D). Thus,
146 **TCIP3** produces a potent anti-proliferative effect in DLBCL cells.
147

148 **TCIP3** exhibited substantially reduced cytotoxicity in B and T cells isolated from primary
149 tonsillar lymphocytes of two separate donors and in primary human fibroblasts, as
150 compared to its effects on SUDHL5 cells, and was less toxic than GNE-781, dCBP-1, and
151 A-485 (Supplemental Fig. 2B, 2C). Because **TCIP3** exhibited cancer-specific cytotoxicity
152 and was less toxic than p300/CBP-targeting agents in untransformed cells, we assessed
153 the generality of these observations by testing the sensitivity of seven different lymphoma
154 and leukemia lines. These included six lymphoma lines with high, medium, and low levels
155 of BCL6 expression and one leukemia cell line (K562) with negligible BCL6 (Fig. 1E).
156 There was a statistically significant correlation between BCL6 levels and area under the
157 curve (AUC) values upon **TCIP3** treatment (Pearson's *R* = -0.89, *P* = 0.0074). Co-
158 treatment of the same cell lines with GNE-781 and BI-3812 produced no such correlation.
159 Over 7 days of treatment, **TCIP3** inhibited the viability of high-BCL6 lines SUDHL5, K422,
160 DB, and DAUDI at comparable potencies (1.2 nM, 4.0 nM, 9.8 nM, and 6.9 nM,
161 respectively), approximately 200 to 1000 times greater than the co-treatment of the
162 inhibitors GNE-781 and BI-3812 (Fig. 1E, Supplemental Fig. 2D, 2E). In cells with low
163 BCL6 levels, **TCIP3** performed equivalently to the co-treatment of GNE-781 and BI-3812
164 (Fig. 1E, Supplemental Fig. 2D, 2E).
165

166 Each BCL6-high lymphoma cell line we tested originated from a germinal center B cell
167 (GCB)-derived lymphoma in which dysregulation of BCL6 drives cancer progression by
168 repressing pro-apoptotic and growth arrest genes⁴¹. p300/CBP are constitutively
169 expressed at similar levels and are essential genes in most cells⁵⁵. If **TCIP3** suppresses
170 malignant cell growth by using high BCL6 expression to sequester p300/CBP from its
171 acetyltransferase and transcriptional substrates, increasing BCL6 levels would increase
172 cellular sensitivity. To directly test this model, we overexpressed the BTB domain of BCL6
173 in BCL6-low K562 cells. This construct codes for the BTB domain, which binds **TCIP3**,
174 but not the DNA-binding zinc finger domains of BCL6 that might localize to death genes
175 on chromatin. This line is otherwise sensitive to p300/CBP acetyltransferase inhibition⁵⁵.
176 Overexpressing BCL6^{BTB} did not increase sensitivity to **TCIP3** (Supplemental Fig. 2F).
177 Thus, **TCIP3** activity requires not only high levels of BCL6, but also BCL6 that is actively
178 repressing antiproliferative and cell death gene expression. Together, our data indicate
179 that chemically induced recruitment of p300/CBP to BCL6 by **TCIP3** produces a potent,
180 gain-of-function effect distinct from the effects caused by protein inhibition, sequestration,
181 or degradation.
182
183

184 **Selective ternary complex formation in cells is required for activity**

185
186 We investigated the relationship between p300/CBP-BCL6 ternary complex formation
187 and the activity of KAT-TCIPs. First, to characterize the ternary complex biochemically,
188 we assessed the KAT-TCIP library using TR-FRET with labeled recombinant p300^{BD},
189 CBP^{BD}, and BCL6^{BTB} domains (Supplemental Fig. 3A). Almost all compounds in our KAT-
190 TCIP library induced p300/CBP-BCL6 ternary complexes and had antiproliferative activity
191 (Supplemental Fig. 3B). **TCIP3** showed one of the highest increases in p300^{BD}-BCL6^{BTB}
192 TR-FRET signal with an AUC 23-times higher than **NEG1** (16-times higher in CBP^{BD}-
193 BCL6^{BTB} TR-FRET) and 18-times higher than **NEG2** (25-times higher in CBP^{BD}-BCL6^{BTB}
194 TR-FRET) (Supplemental Fig. 3C, D).

195
196 To probe how the formation of the ternary complex affects cellular viability, we treated
197 SUDHL5 cells with 1 nM of **TCIP3** and co-treated these cells with one of three different
198 BCL6^{BTB} inhibitors: BI-3812⁴⁸, GSK137⁴⁹, and an analog of CCT373566 (CCT373566a,
199 Supplemental File 1) with a matched exit vector to BI-3812⁴⁶. We carried out a similar
200 **TCIP3** co-treatment experiment with the p300/CBP^{BD} inhibitor, GNE-781⁵⁰. Co-treatment
201 with each of these inhibitors buffered the effects of **TCIP3** on cell viability (Fig. 2A, B).
202 These results establish that the activity of **TCIP3** depends on its dual engagement with
203 p300/CBP and BCL6.

204
205 The human genome encodes 62 structurally homologous bromodomains⁵⁶ and 183
206 proteins with BTB domains⁵⁷. To assess the selectivity of **TCIP3**, we conducted mass
207 spectrometry of proteins immunoprecipitated (IP) with either p300 or BCL6 after 2 hours
208 of 1 nM **TCIP3** addition to SUDHL5 cells (IP-MS) (Supplemental Table 1).
209 Immunoprecipitation using an anti-p300 antibody produced exclusive enrichment of BCL6
210 ($P = 1.8 \times 10^{-9}$, $\log_2(\text{fold change}) = 4.0$) (Fig. 2C, Supplemental Fig. 3E, Supplemental
211 Table 1). The sole proteins that showed statistically significant co-enrichment after
212 immunoprecipitation with an anti-FLAG antibody from cells with FLAG inserted C-
213 terminally to the *BCL6* gene (Methods) were CBP ($P < 0.0001$, $\log_2(\text{fold change}) = 3.7$)
214 and p300 (no peptides detected in DMSO, imputed adj $P < 0.05$, $\log_2(\text{fold change}) = 3.7$)
215 (Fig. 2D, Supplemental Fig. 3F, Supplemental Table 1). Despite BROMOscan data
216 suggesting **TCIP3** may also engage BRPF1 at high compound concentrations (10 μ M,
217 Supplemental Fig. 3G), no other bromodomain-containing proteins were enriched (adj. P
218 < 0.05 , $|\log_2(\text{fold change})| > 2$). To validate these results in a genetically unmodified cell,
219 we immunoprecipitated BCL6 using an antibody raised against its native sequence and
220 observed enrichment of both p300 and CBP (Supplemental Fig. 3H). Our proteomic data
221 indicate that **TCIP3** is selective for both p300/CBP and BCL6 inside living cells.

222
223 **Rapid acetylation of BCL6 and BCL6-proximal chromatin**

224
225 Biochemical specificity of **TCIP3** in forming a BCL6-p300/CBP ternary complex and the
226 requirement of the complex for cytotoxicity implicates a proximity-dependent molecular
227 mechanism of cell death. We examined the molecular effects of **TCIP3** in endogenous
228 cells at the chromatin, RNA, and protein levels. We focused on acetylation of protein and

229 chromatin substrates because p300/CBP has been described as acetylating a wide range
230 of target substrates in its proximity⁶.

231
232 First, because p300/CBP-mediated acetylation of BCL6 at lysines 376, 377, and 379 in
233 its unstructured repression domain 2 (RD2) was reported to derepress BCL6-target gene
234 transcription by inhibiting the binding of repressive complexes to BCL6 without altering its
235 DNA-binding capacity^{58,59}, we assessed **TCIP3**-mediated BCL6 acetylation.
236 Immunoprecipitation of all acetylated proteins from nuclear extracts with a pan-acetyl-
237 lysine antibody showed that **TCIP3** induced a dose-dependent increase of acetylated
238 BCL6 after 1 hour of addition beginning at 1 nM and increasing with compound dose,
239 close to the antiproliferative IC₅₀ value of 0.8 nM in these same cells (Fig. 3A).
240

241 Next, we hypothesized that **TCIP3** can induce p300/CBP to acetylate histone tail lysines
242 near chromosomal BCL6 binding sites. Of the potential histone lysines that undergo
243 acetylation, histone H3-K27 and histone H2B-K20 are of particular interest (H3K27ac and
244 H2BK20ac, respectively) since they co-localize with and are generally considered to mark
245 active enhancers and promoters^{60,61}. To examine the effects of **TCIP3** on histone
246 acetylation, we conducted chromatin immunoprecipitation sequencing (ChIP-seq) for
247 H2BK20ac and H3K27ac after addition of 1 nM **TCIP3** to SUDHL5 cells for 15 min, 1 hour,
248 and 2 hours. 69,719 and 66,995 peaks across all timepoints were reconstructed for
249 H2BK20ac and H3K27ac, respectively. Most of the variance between conditions (~90%)
250 was attributable to compound treatment (Supplemental Fig. 4A). Differential peak
251 analysis detected large gains and losses of acetylation: after 1 hour, 936 H2BK20ac
252 peaks were gained and 4,346 were lost, while 533 H3K27ac peaks were gained and 5,216
253 were lost (Fig. 3B).
254

255 Peaks that gained acetylation were enriched in published regions of BCL6 binding in
256 human B-cell and blood cancer cell lines (Fig. 3C and Supplemental Table 2). Enrichment
257 for BCL6-binding sites was more pronounced in regions that gained H2BK20ac than in
258 regions that gained H3K27ac (Fig. 3C), consistent with the recently reported propensity
259 of p300/CBP to catalyze H2BK20ac⁶⁰. Loci that gained acetylation included pro-apoptotic
260 BCL6 targets such as *ARID3B*⁶² (Fig. 3D). We also identified 7,379 BCL6 binding sites in
261 untreated SUDHL5 cells by CUT&RUN⁶³ (Supplemental Fig. 4B). Comparison with this
262 set of BCL6-bound sites showed that 21% (H3K27ac) to 25% (H2BK20ac) of gained
263 acetylation regions overlapped (Supplemental Fig. 4B). The rapidly induced acetylation
264 detected indicates redirection of p300/CBP acetyltransferase activity to BCL6-proximal
265 DNA by **TCIP3**.
266

267 **Redistribution of p300/CBP activity from oncogenic regulatory regions**

268
269 In contrast to gains in histone acetylation, losses occurred at annotated enhancers and
270 super-enhancers in SUDHL5 cells (Fig. 3E and Supplemental Fig. 4C). Losses of
271 H3K27ac and H2BK20ac were modest in magnitude across these regions but statistically
272 significant (adj. $P \leq 0.05$) after 15 min, 1, and 2 hours of **TCIP3** treatment (Supplemental
273 Fig. 4D). The greatest losses in H3K27ac were concentrated in super-enhancers, broad
274 regions of elevated histone acetylation that regulate the expression of cell-identity and

275 proliferation genes^{10,11,64} (Fig. 3F). These losses were observed at several super-
276 enhancers proximal to master regulators of the germinal center B cell and oncogenic
277 drivers (Fig. 3F), including the *BCL6* gene itself, which contains an intronic enhancer as
278 well as a requisite super-enhancer 150 kilobases upstream⁶⁵ (Supplemental Fig. 4E).
279 Total H3K27ac and H2BK20ac levels did not decrease after 1 nM **TCIP3** treatment at
280 these immediate timepoints (Fig. 3G), indicating that **TCIP3** does not reduce global
281 histone acetylation. This dose and timepoint was nevertheless sufficient to decrease c-
282 MYC and increase the *BCL6*-target p27 (Fig. 3G).

283
284 We were intrigued by the fact that most of the regions that lost acetylation due to **TCIP3**
285 (i.e., enhancers and super-enhancers) were already among the highest-acetylated loci
286 on chromatin before treatment (Fig. 3F, H and Supplemental Fig. 4F). We reasoned that
287 since these regions are considered rich in p300/CBP¹¹, **TCIP3** should produce decreases
288 in p300/CBP-target gene expression concurrent with increases in *BCL6*-regulated genes.
289 The redirection of transcriptional activity should also occur on comparable timescales to
290 the dynamic changes in acetylation observed. RNA-sequencing (RNA-seq) after 30 min,
291 1, 2 and 4 hours of 1 nM **TCIP3** addition in SUDHL5 cells revealed large numbers of
292 genes induced (1,510) and decreased (2,126) (adj. $P \leq 0.05$, $|\log_2(\text{fold change})| \geq 0.5$)
293 (Supplemental Fig. 4G). Consistent with our hypothesis, gene set enrichment analysis
294 showed that *BCL6*-bound genes were up, and p300/CBP-regulated genes were down
295 (Fig. 3I). Most but not all genes near enhancers and super-enhancers that lost H3K27ac
296 decreased in expression (Supplemental Fig. 4H). Overall changes in H3K27ac and gene
297 expression showed a weak but statistically significant positive correlation (Supplemental
298 Fig. 4I), indicating a modest direct relationship between histone acetylation and
299 transcription of nearby genes. This is consistent with published data^{60,66}.

300
301 We conclude that increases in *BCL6* target genes result from the combination of the
302 acetylation and inactivation of *BCL6* protein (Fig. 3A) and p300/CBP recruitment to *BCL6*
303 target genes (Fig. 3B). Meanwhile, redirection of p300/CBP produces decreases of gene
304 expression at its normal targets (Fig. 3F). The effective molecular mechanism of **TCIP3**
305 calls to mind the character of Robin Hood: redistributing p300/CBP from “rich” sites to
306 acetylate and activate “poor” genes, directed by *BCL6* (Fig. 3J).

307
308 **Redistribution partly phenocopies proteomic effects of p300/CBP degradation**
309

310 Given that **TCIP3** redistributed p300/CBP activity, we compared its effects on the cell to
311 those produced by p300/CBP degraders. We first assessed changes in protein
312 expression upon a 10 nM **TCIP3** treatment or a 250 nM dCBP-1 treatment at 6 hours
313 (Supplemental Fig. 5A) and 24 hours (Fig. 4A, Supplemental Fig. 5B). **TCIP3** increased
314 the abundance of both p300 and CBP (p300: adj. $P \leq 0.01$, $\log_2(\text{fold change}) = 0.37$; CBP:
315 adj. $P \leq 0.05$, $\log_2(\text{fold change}) = 0.58$) (Fig. 4A). In contrast, and as expected³⁰, 250 nM
316 dCBP-1 treatment induced statistically significant losses in p300/CBP (p300: adj. $P \leq$
317 0.05, $\log_2(\text{fold change}) = -2.7$; CBP: adj. $P \leq 0.01$, $\log_2(\text{fold change}) = -1.8$) (Supplemental
318 Fig. 5A, B). Matched concentrations of **NEG1** and **NEG2** displayed no significant changes
319 relative to DMSO at either timepoint (Supplemental Fig. 5A, B).

321 Global proteomic changes induced by 10 nM **TCIP3** correlated (Pearson's $R = 0.77$, $P <$
322 0.0001) with those observed upon 250 nM dCBP-1 treatment (Fig. 4A). This was striking
323 not only because we treated cells with 25-times less **TCIP3** than dCBP-1, but also
324 because p300/CBP protein levels increased in abundance due to **TCIP3** (Fig. 4A). Both
325 compounds induced significant decreases (adj. $P \leq 0.05$, $\log_2(\text{fold change}) < -2$) of
326 germinal center B-cell-specific TFs including MEF2B, IRF8, SPIB (PU.1-related)^{3,41,67},
327 and modestly of BCL6 itself (Fig. 4A, Supplemental Fig. 5C). This is consistent with the
328 decreases in transcription observed at the genes encoding these TFs and the decreases
329 in acetylation observed at their super-enhancers (Supplemental Fig. 4H and Fig. 3F).
330 Many proteins which decreased upon p300/CBP degradation by dCBP-1 increased in
331 abundance after **TCIP3** treatment. These included key BCL6-regulated and/or p53-target
332 genes that play critical roles in apoptosis such as BBC3, ARID3A, and ARID3B (Fig. 4A
333 and Supplemental Fig. 5A, B). Significantly increased proteins (adj. $P < 0.05$, $\log_2(\text{fold}$
334 change) > 1.0) were enriched with high confidence (adj. $P < 0.05$) for p53-target and
335 apoptosis proteins by 10 nM **TCIP3** but not 250 nM dCBP1 treatment (Fig. 4B and
336 Supplemental Fig. 5D). Proteomic changes induced by **TCIP3** also correlated with
337 transcriptomic effects (Pearson's $R = 0.31$, $P < 0.0001$); two examples of transcripts and
338 proteins that increased are the BCL6-targets ARID3B and p27/CDKN1B (Fig. 4C, Fig.
339 3G, and Supplemental Fig. 5C). Our comparative proteomic analysis suggests that **TCIP3**
340 is not only more potent at decommissioning p300/CBP-regulated signaling but also
341 uniquely capable of activating apoptotic protein signaling.
342

343 Activation of PUMA and induction of apoptosis

344 Global proteomics experiments revealed that PUMA/BBC3 increased after 24 hours of
345 treatment with **TCIP3** but not dCBP-1 ($\log_2(\text{TCIP3} / \text{DMSO fold change}) = 0.72$; adj. $P =$
346 0.0001) (Fig. 4A). PUMA expression continued to increase more than 6-fold after **TCIP3**-
347 treatment for 48 hours (Fig. 4D, E). PUMA is a Bcl-2 homology 3 (BH3)-only containing
348 pro-apoptotic protein sufficient for apoptosis caused by p53 and other stimuli⁶⁸⁻⁷⁰. In
349 lymphocytes, PUMA is a target of p53, BCL6, and the transcription factor forkhead box
350 O3 (FOXO3), the latter itself a BCL6- and p53-target gene⁷¹. p53 and FOXO3 protein
351 levels did not change significantly by 48 hours (Supplemental Fig. 6A). Significant
352 increases in PUMA levels prompted us to quantify the characteristics and kinetics of
353 apoptotic induction by **TCIP3** by analyzing each stage of the apoptotic signaling cascade.
354 Staining with Annexin V for the externalization of phosphatidylserine, one of the first
355 events in a cell undergoing apoptosis, after 24, 48, and 72 hours of 10 nM **TCIP3**
356 treatment showed that significant increases in Annexin V-positive cells began after 48
357 hours of **TCIP3** treatment (Fig. 4F), concurrent with the dramatic increases in PUMA at
358 this timepoint (Fig. 4D, E). 82% of cells stained positive for Annexin V at 72 hours (Fig.
359 4F). This was 2.9 times higher than DMSO, 2.3 times higher than **NEG1**, and 2.5 times
360 higher than **NEG2** treatment (Fig. 4F, Supplemental Fig. 6B), indicating that apoptosis
361 depended on chemically induced proximity. Levels of cleaved caspase-3, the terminal
362 executioner protease in the apoptotic cascade, increased with parallel kinetics to Annexin
363 V (Supplemental Fig. 6C). DNA fragmentation, as measured by terminal deoxynucleotidyl
364 transferase BrdU-dUTP nick end labeling (TUNEL) (Fig. 4G), and loss of membrane
365 integrity, as measured by Trypan blue staining, both began after 48 hours of compound
366

367 treatment (Supplemental Fig. 6D). While dCBP-1 also induced apoptosis after 72 hours
368 of treatment (Fig. 4F), PUMA was not activated (Fig. 4D,E).

369
370 To determine the period of **TCIP3** treatment that is sufficient to trigger apoptosis, we
371 treated cells with 10 nM **TCIP3** for either 24, 48, or 72 hours, washed cells with
372 phosphate-buffered saline, and replaced cells with compound-free media (Supplemental
373 Fig. 6E). Treatment for the first 24 or 48 hours of a 72-hour experiment was sufficient to
374 induce apoptosis at levels comparable to a 72-hour continuous treatment. The kinetics of
375 apoptosis observed suggest that 24 hours of **TCIP3** exposure is sufficient to activate one
376 or more irreversible apoptotic signals, including PUMA, that manifests as apoptosis over
377 the next 24-48 hours.

378
379 **TCIP3 induces G1 arrest**

380
381 In addition to elevated apoptotic proteins, transcriptomic and proteomic profiling
382 suggested that **TCIP3** may induce cell cycle arrest. We observed elevated levels of cell-
383 cycle inhibitors such as *CDKN1B/p27* accompanied by decreased levels of key master
384 germinal center B cell regulators (Fig. 4A), which regulate cell proliferation⁷²⁻⁷⁴.
385 Accordingly, we analyzed cell cycle progression after treating SUDHL5 cells with 10 nM
386 of **TCIP3**, **NEG1**, **NEG2**, or DMSO for 24 hours. For this, we used fluorescent labels to
387 detect total and newly synthesized DNA during a 2-hour pulse of 5-ethynyl-2'-
388 deoxyuridine (EdU). We observed substantial and significant ($P < 0.01$) enrichment in
389 cells arrested in G0/G1 after treatment with 10 nM **TCIP3** relative to DMSO and a
390 corresponding significant ($P < 0.01$) reduction in S phase cells (Fig. 4H, Supplemental
391 Fig. 6F). Cell cycle arrest after 24 hours was dependent on the ternary complex; none of
392 the negative controls significantly changed the ratio of cells found in any of the cell cycle
393 phases. Arrest in G0/G1 is consistent with decreased abundance of G2/M and mitotic
394 spindle proteins detected by proteomics at 24 hours (Supplemental Fig. 5D). The
395 measurements of apoptosis and cell cycle analysis indicate that **TCIP3** induces
396 concurrent arrest of cell cycle progression and commitment to apoptosis in the first 24
397 hours of treatment, although apoptotic death does not occur until an additional 24-48
398 hours.

399
400 **Comparative pharmacology with BCL6-targeting TCIPs**

401
402 The kinetics of apoptosis induction and cell cycle arrest differed strikingly from previous
403 studies on two other BCL6-targeting TCIPs, TCIP1³⁹ and CDK-TCIP1⁴⁰, which recruit
404 elongation factors associated with RNA Polymerase II to BCL6. To assess how the
405 recruitment of chromatin modifiers to BCL6 differentially perturbs anti-proliferative
406 mechanisms, we directly compared the effects of TCIP1 and CDK-TCIP1 with **TCIP3** on
407 cell death and transcriptional reprogramming. **TCIP3** treatment exhibited slower kinetics
408 of apoptosis induction than TCIP1 (Fig. 4F, G), which recruits the bromodomain and
409 extraterminal domain (BET)-containing family member BRD4 to pro-apoptotic BH3-only
410 genes such as *BIM/BCL2L11* and *PMAIP1*³⁹. Concurrent analysis of the cell cycle and
411 apoptotic effects of TCIP1 and **TCIP3** by TUNEL and total DNA content co-staining
412 showed that while the predominant cellular effect after 24 hours of **TCIP3** treatment is to

413 arrest cells in G1, 24 hours of TCIP1 treatment produces DNA fragmentation (Fig. 4G and
414 Supplemental Fig. 7A). Unbiased clustering of transcriptomic changes mediated by
415 **TCIP3**, TCIP1, and CDK-TCIP1, demonstrated that **TCIP3** produces a substantially
416 different gene expression program that clusters independently from TCIP1 and CDK-
417 TCIP1 (Supplemental Fig. 7B). Only some genes, including a set of cell-cycle-mediators,
418 changed similarly for all three classes of TCIPs. These included *c-MYC* and the BCL6-
419 target *CDKN1B* (p27) (Supplemental Fig. 7B). Only **TCIP3** induced dramatic changes in
420 chromatin acetylation of enhancers and super-enhancers (Supplemental Fig. 7C). These
421 epigenomic effects likely account for the similar proteomic changes observed between
422 **TCIP3** and the p300/CBP degrader dCBP-1. Different molecular mechanisms correlated
423 with a slightly different spectrum of cancer cell lines that were sensitive to each TCIP
424 (Supplemental Fig. 7D). Nevertheless, all TCIPs were highly toxic to BCL6-driven
425 lymphomas. Other sensitivities remain to be explored.

426

427 Rapid and potent *c-MYC* repression

428

429 *c-MYC* transcripts were rapidly and significantly depleted upon 10 nM **TCIP3** treatment
430 (mRNA at 2 hours of 1 nM **TCIP3**, adj. $P \leq 10^{-100}$, $\log_2(\text{fold change}) = -2.71$) (Fig. 5A), and
431 global proteomics showed a complete loss of *c-MYC* peptides after 24 hours (Fig. 5B). *c-*
432 *MYC* is a critical oncogenic driver expressed in all germinal center-derived lymphomas
433 that regulates cell proliferation required for formation and maintenance of germinal
434 centers^{75,76,77}, prompting us to examine the contribution of its loss to the antiproliferative
435 mechanism. *c-MYC* mRNA in SUDHL5 cells treated with 1 nM of **TCIP3** decreased with
436 a $t_{1/2}$ of 33 minutes, and repression persisted over 24 hours (Fig. 5C). *c-MYC* protein
437 decreased following the loss of *c-MYC* mRNA ($t_{1/2} = 2.5$ hours, Supplemental Fig. 8A),
438 indicating that **TCIP3** interferes with transcription of the *c-MYC* gene. Protein repression
439 at 4 hours ($IC_{50} \sim 0.8$ nM, Fig. 5D, E) led to significant (adj. $P < 10^{-10}$) loss of *c-MYC*-target
440 gene expression at the same timepoint and dose (Supplemental Fig. 8B). Thus, **TCIP3**
441 represses transcription of the *c-MYC* gene and the entire MYC-coordinated gene
442 expression network in DLBCL cells.

443 To investigate the mechanism of *c-MYC* repression, we examined whether repression of
444 *c-MYC* transcripts depended on induced proximity of p300/CBP and BCL6 by co-treating
445 SUDHL5 cells with 10 nM **TCIP3** and either 500 nM of BI-3812 or GNE-781 to compete
446 for binding with BCL6 or p300/CBP, respectively. Co-treatment with BI-3812 almost
447 completely restored *c-MYC* levels to baseline, and co-treatment with 500 nM of GNE-781
448 restored *c-MYC* levels to those observed with GNE-781 treatment alone (Fig. 5F). *c-MYC*
449 repression induced with 500 nM GNE-781 was still more than two times higher than
450 repression in cells treated with 10 nM **TCIP3**. Neither GNE-781, dCBP-1, **NEG1**, **NEG2**,
451 nor the BCL6^{BTB} inhibitor BI-3812 produced comparable *c-MYC* repression at matched
452 concentrations at the transcript or proteomic level (Fig. 5C, B, Supplemental Fig. 8C). The
453 p300/CBP-TCIP3-BCL6 ternary complex is therefore required for **TCIP3**-induced *c-MYC*
454 repression.

455

456

457 *c-MYC* repression across six lymphoma cell lines correlated with BCL6 levels (Fig. 5G).
458 BCL6-high expressing cells SUDHL5 and K422 displayed more pronounced *c-MYC*

459 repression following a 1 nM **TCIP3** treatment than BCL6-low lymphoma cells OCILY19
460 and TOLEDO, or the leukemia line K562 (Fig. 5G). DB, a germinal center B-type
461 lymphoma line with high *BCL6* levels (269 transcripts/million) and a recently identified c-
462 *MYC* chromosomal rearrangement with the breakpoint at its promoter⁷⁸, exhibited less
463 repression (Fig. 5G). Indeed, repression was muted in BCL6-high Burkitt's lymphoma cell
464 lines (DAUDI and RAJI) with the characteristic chromosomal rearrangement of one or
465 both alleles of the *c-MYC* promoter to the immunoglobulin heavy chain regulatory
466 region^{79,80} (Supplemental Fig. 8D). These results imply that **TCIP3** may indirectly disrupt
467 cis-regulation of *c-MYC* transcription. Consistent with this possibility, modest losses of
468 histone acetylation at the *c-MYC* promoter and its known regulatory enhancers^{78,81} were
469 observed only after *c-MYC* repression, likely as a result of lost transcription
470 (Supplemental Fig. 8E, F). This stands in contrast to p300/CBP bromodomain inhibitors,
471 which repress *c-MYC* transcription by displacing p300/CBP binding and activity from *c-MYC*
472 enhancers and promoters^{30,50}. Therefore, **TCIP3**-mediated repression of *c-MYC* is
473 a mechanistically distinct consequence of chemically induced proximity of p300/CBP and
474 BCL6.

475

476 **Restoration of *c-MYC* reverses cell cycle arrest but not death**

477

478 To evaluate the importance of *c-MYC* repression in driving the cellular response to **TCIP3**,
479 we overexpressed doxycycline(dox)-inducible 3x-FLAG-MYC in SUDHL5 cells (TRE-3x-
480 FLAG-MYC) (Fig. 5H). Analysis of the cell cycle at 24 hours indicated that overexpression
481 of *c-MYC* partially reversed the S-phase block caused by 10 nM **TCIP3** (Fig. 5I and
482 Supplemental Fig. 8G). This correlated with a ~3.8-fold proliferative benefit in cells
483 expressing dox-induced MYC and treated with **TCIP3** ($IC_{50} \sim 7.5$ nM), relative to **TCIP3**-
484 treated cells without dox ($IC_{50} \sim 2.0$ nM, Fig. 5J). These data suggest that *c-MYC*
485 repression contributes to the G1 arrest but cannot reverse the cell killing effects of **TCIP3**,
486 which likely involves direct transcriptional activation of pro-apoptotic factors (Figs. 3-4).

487

488 **TCIP3 is a molecular glue**

489

490 The selectivity of **TCIP3** for its binding partners (Fig. 2C, D) and its use of chemical
491 induced proximity to activate cell death led us to ask what features of the three-component
492 assembly containing BCL6-**TCIP3**-p300 drive extraordinary potency and selectivity. To
493 understand the determinants of specific ternary complex formation, we solved the crystal
494 structure of a BCL6-**MNN-02-155**-p300 ternary complex. This KAT-TCIP features a 4-
495 carbon alkyl linker and induces potent activation of the BCL6-target reporter gene and
496 cell death with an IC_{50} comparable to **TCIP3** (Supplemental Fig. 1A, C). The asymmetric
497 unit, resolved to a minimum Bragg spacing of 2.1 Å (Supplemental Table 3), contained a
498 BCL6^{BTB} homodimer and two copies of a p300^{BD} molecule, each tethered to BCL6 by
499 **MNN-02-155** (Fig. 6A, 6B, Supplemental Fig. 9A, B, C, Supplemental Video 1). **MNN-02-**
500 **155** engages p300 and BCL6 without significant rearrangements of the parental
501 monovalent protein-compound structures: GNE-781-CBP⁵⁰ (RMSD = 0.35 Å,
502 Supplemental Figure 9D) and BI-3802-BCL6⁴⁸ (RMSD = 0.43 Å, Supplemental Figure
503 9E). A hydrogen bond connects the carbonyl of p300^{G1085} and the amide nitrogen in the
504 **MNN-02-155** linker (Fig. 6C). Five residues engaged in fortuitous interactions constitute

505 a p300-BCL6 neo-interface: p300^{L1082} contacts BCL6^{S27}, while p300^{Q1083} contacts
506 BCL6^{R24} and BCL6^{R20}. The interactions are primarily hydrophobic in character (Fig. 6D).
507

508 The identification of chemically induced amino acid contacts between p300 and BCL6
509 suggested cooperativity in ternary complex formation⁸², a hallmark of molecular glues^{23,26}.
510 Cooperativity (α) is defined as the ratio of binary to ternary complex dissociation constants
511 (K_{dS}). We followed a reported procedure⁸³ to measure α for p300, defined as the ratio
512 between the K_d for p300-**MNN-02-155** binding versus the K_d for p300-[BCL6-**MNN-02-**
513 **155**] binding. For p300^{WT}, this value was $\alpha \sim 6.8$ (Fig. 6E), indicating strong ternary
514 complex cooperativity. To understand the importance of the aforementioned contacts for
515 KAT-TCIP binding and cooperativity, we measured α for p300Q^{1083A} or p300Q^{1083R} to
516 reduce residue bulk or to introduce positive charge, respectively. Given the crystal
517 structure, the latter mutation would clash with the interacting BCL6^{R24} amino acid side
518 chain (Fig. 6D). p300^{WT} bound more favorably to **MNN-02-155** in the presence of BCL6
519 relative to p300Q^{1083A} and p300Q^{1083R} (Fig. 6E, Supplemental Fig. 10A). The presence of
520 BCL6 did not affect the affinity of GNE-781 to the various p300 mutants (p300Q^{1083A} $\alpha \sim$
521 0.88; p300Q^{1083R} $\alpha \sim 1.0$; Supplemental Fig. 10B). Thus, fortuitous amino acid side chain
522 contact between p300^{Q1083} and BCL6^{BTB} enhances complex formation, providing a
523 biophysical explanation for potency and specificity.
524

525 We next used the cooperativity assay to profile other active GNE-781-derived KAT-TCIPs.
526 **TCIP3** and **MNN-02-155** produced similar α values ($\alpha = 4.2$ and $\alpha = 6.9$, respectively;
527 Supplemental Fig. 10C). We measured weaker cooperativity for compounds that were
528 less cytotoxic such as **MNN-02-156** and **MNN-02-162** (Supplemental Fig. 10C).
529 Correlation between α and cellular potency prompted us to investigate the average three-
530 dimensional linker lengths of each GNE-781-based KAT-TCIP, as measured from
531 predicted 3D conformations (Supplemental Fig. 10D). The computationally predicted
532 linker length (Methods) of **MNN-02-155** (6.6 Å) deviated by less than 1 Å from the
533 measured distance between p300^{BD} and BCL6^{BTB} in the co-crystal structure (6.1 Å),
534 validating this approach (Supplemental Fig. 10D). Compounds with linker lengths from 4
535 to 12 Å demonstrated antiproliferative activity at $IC_{50s} < 10$ nM, and compounds with
536 rigidified linkers were consistently very potent ($IC_{50} < 1$ nM) (Supplemental Fig. 10D).
537 Rigid linkers decrease rotational degrees of freedom and lower the entropic cost of
538 ternary complex formation. Consequently, it is likely that they produce longer-lasting
539 active ternary complexes inside the cell, assuming that membrane permeability is similar.
540 Given the tolerability for a wide range of linker chemistry and the limited plasticity
541 observed at the protein-protein interface in the co-crystal structure, we conclude that
542 many different orientations of p300/CBP relative to BCL6 can support biological activity.
543

544 Finally, we used isothermal calorimetry (ITC) to quantify the binary and ternary complex
545 binding affinities and thermodynamic parameters of p300^{BD}, BCL6^{BTB}, and **TCIP3**
546 (Supplemental Fig. 10E). Calculations of α in both directions of ternary complex formation
547 demonstrated that **TCIP3** exhibits significantly enhanced affinity for the ternary complex
548 compared to binding with either p300^{BD} or BCL6^{BTB} alone ($\alpha^{p300 \text{ into } BCL6:TCIP3} = 3.5$, $\alpha^{BCL6 \text{ into } p300:TCIP3} = 13$, Fig. 6F). These values are comparable to those obtained with TR-FRET
549 (Fig. 6E). Consistent with the expectation that the ΔG of ternary complex formation
550

551 should be the same regardless of whether binding to p300 or BCL6 occurs first, there was
552 only a 4% deviation in the overall free energy of complex formation between the p300
553 and BCL6 mediated binding mechanisms (Supplemental Figure 10F). Our biophysical
554 and structural data confirms that **TCIP3**, by inducing the formation of a cooperative
555 ternary complex containing new, stabilizing interactions between p300/CBP and BCL6,
556 acts as a molecular glue.

557
558 To investigate how the relative orientation of p300^{BD} to BCL6^{BTB} may relate to biological
559 activity, we superimposed the fragment of p300 seen in the p300-**MNN-02-155**-BCL6^{BTB}
560 structure onto a crystal structure of the p300 catalytic core (PDB: 6GYR) containing the
561 catalytic KAT domain^{84,85}, the p300/CBP auto-inhibitory loop (AIL)⁸⁶, and the really
562 interesting new gene (RING) domain which regulates catalytic KAT activity⁸⁴. **MNN-02-**
563 **155** positions active p300 protomers in an orientation compatible with acetylation of BCL6
564 and proximal chromatin (Supplemental Fig. 10G, teal). Moreover, because BCL6 is an
565 obligate homodimer^{87,88}, 2 molecules of p300 should be recruited to BCL6 binding sites
566 over the genome. Superimposition revealed an opportunity for a second p300 protomer
567 (Supplemental Fig. 10G, gray) to interact with each BCL6-bound p300 molecule.
568 Activation by auto-acetylation occurs in trans across a p300 homodimer assembled on a
569 dimeric binding partner⁸⁵, indicating the potential for higher-ordered oligomers to form on
570 chromatin, facilitating KAT trans-acetylation and reinforcing local chromatin acetylation.
571 We propose a model in which **TCIP3** leverages cooperativity to form a stable and
572 enzymatically active p300-BCL6 complex that goes on to initiate gene modulation on
573 chromatin and cell death.

574
575 **DISCUSSION**

576
577 The introduction of KAT-TCIPs expands the toolbox by which we can precisely reprogram
578 endogenous gene expression networks. KATs are prominent therapeutic targets in
579 lymphoma, but available small molecules inhibit their function globally and have the
580 potential to cause multiple on-target toxicities. We alternatively converted a potent p300
581 inhibitor into a bivalent small molecule that leverages chemical induced proximity (CIP)
582 to redirect p300/CBP acetyltransferase activity, triggering cell death in diffuse large B-cell
583 lymphomas. The resulting KAT-TCIPs are small molecules that activate transcription of
584 genes bound by the master transcriptional repressor BCL6, whose dysregulation drives
585 DLBCL progression. The lead KAT-CIP, which we named **TCIP3**, activated BCL6-target
586 gene expression and inhibited proliferation in DLBCL cells at sub-nanomolar IC₅₀s without
587 exhibiting toxicity in non-transformed tonsillar lymphocytes or fibroblasts.

588
589 **TCIP3** potency was contingent on the formation of a ternary complex between **TCIP3**,
590 p300/CBP, and BCL6, which served as a driver of exquisite selectivity (Figs. 2 and 6).
591 Small-molecule-induced cooperative ternary complexes confer beneficial
592 pharmacological properties such as prolonged target residence time^{23,26}, thereby
593 enhancing the likelihood of sustained and potent therapeutic outcomes. Here, we used
594 structural and biophysical analyses to demonstrate that **TCIP3** is a bivalent molecular
595 glue that shares these advantageous characteristics. The crystal structure of a KAT-TCIP
596 in complex with p300 and BCL6 exhibited potency enhancement by fortuitous amino acid

597 contacts independent of plasticity at the protein-protein interface. This suggests that AI-
598 driven docking strategies leveraging existing structures could accelerate the optimization
599 of CIP-enabling compounds for therapeutic purposes.
600

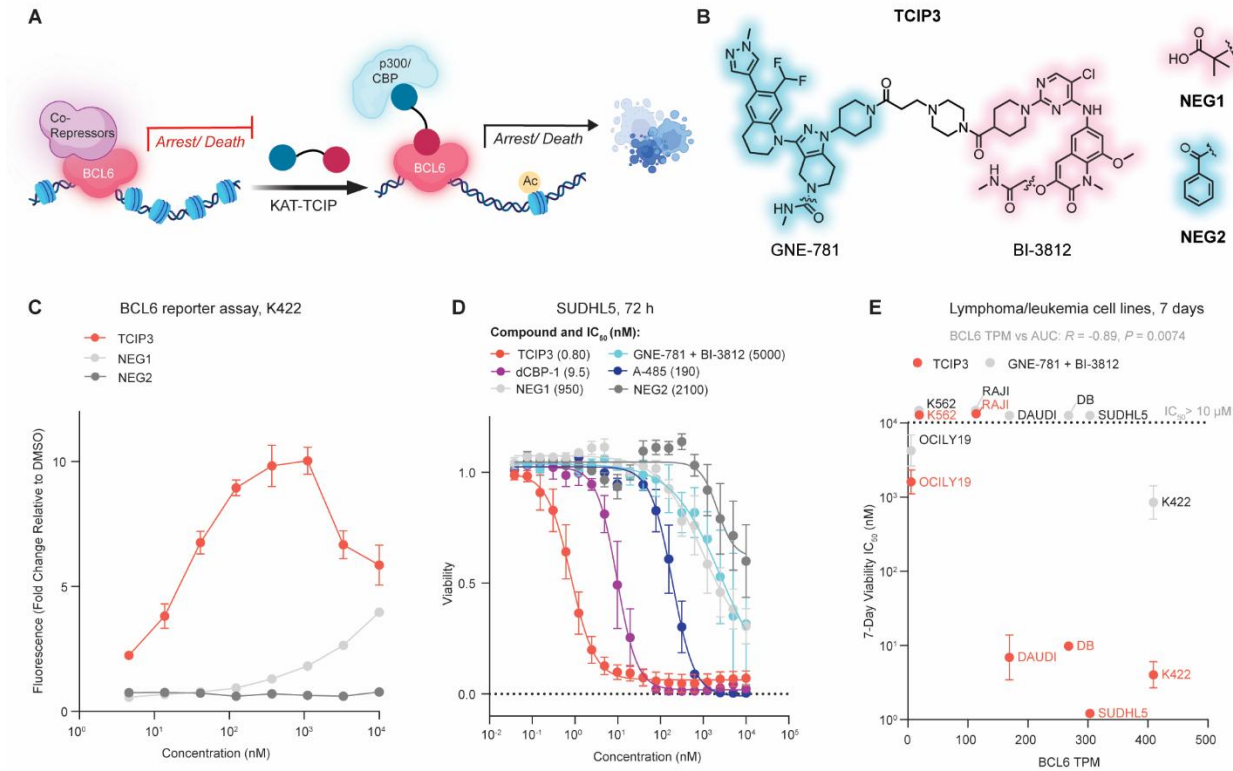
601 KAT-TCIPs killed DLBCL cells by redirecting p300/CBP activity in a mechanism that
602 depended on the oncogenic driver BCL6. The consequences of this on chromatin,
603 transcription, and protein expression in the cell unexpectedly resembled changes induced
604 by p300/CBP degradation. Three observations distinguish KAT-TCIPs from simple
605 inhibitors or degraders. First, while the p300/CBP degrader dCBP-1 depletes both histone
606 acetylation genome-wide and p300/CBP protein levels³⁰, **TCIP3** selectively targeted
607 DLBCL-specific super-enhancers and stabilized p300/CBP, indicating that it is not simply
608 a super-inhibitor. Second, **TCIP3** activated apoptotic protein signaling. Elevated PUMA,
609 a BH3-only protein sufficient for intrinsic apoptosis⁶⁸⁻⁷⁰, exemplifies this characteristic.
610 Third, acute treatment produced rapid and durable repression of c-MYC in a manner
611 dependent on chemically induced proximity to BCL6. All three molecular effects combined
612 to elicit more potent cell killing than p300/CBP PROTACs, KAT inhibitors, or bromodomain
613 inhibitors and BTB domain inhibitors of BCL6 (Fig. 1). The fact that c-MYC replacement
614 could reverse cell cycle arrest but not death (Fig. 5) strongly suggests that anti-cancer
615 activity is the product of multiple gain-of-function effects. Our results demonstrate the
616 potential of redirecting epigenetic regulators via CIP to produce cancer cell killing.
617

618 The redistribution mechanism suggests that cells particularly vulnerable to disruption of
619 p300/CBP that also have high BCL6 activity may be sensitive to **TCIP3**. In addition to
620 DLBCL, follicular lymphoma, an incurable subtype of non-Hodgkin's lymphoma,
621 represents a potentially responsive disease. Patients exhibit both a high frequency of
622 inactivating *CREBBP* mutations (65%) that lead to a loss of BCL6 antagonism and
623 unchecked BCL6 activity^{58,89,90,91}. Moreover, while BCL6-expressing lymphomas provide
624 a compelling model to explore the therapeutic potential of the BCL6-targeting KAT-TCIPs
625 described here, the widespread expression of p300/CBP across various cancers
626 suggests the broader applicability of CIPs that redirect p300/CBP to pro-apoptotic TFs.
627

628 The combinatorial nature of transcription led us to hypothesize that recruiting
629 acetyltransferases to BCL6 would reprogram gene networks distinct from those induced
630 by the recruitment of other co-activators, despite localization to the same TF. We
631 previously developed TCIP1 and CDK-TCIP1, molecules that redirect the positive
632 transcription elongation factors BRD4 and CDK9, respectively, to activate BCL6-target
633 genes^{39,40}. **TCIP3** provoked substantially different gene expression changes and cell
634 arrest/death phenotypes relative to these TCIPs (Fig. 4 and Supplemental Fig. 7).
635 Differential activity is consistent with the complex multistep nature of transcriptional
636 activation. While the elongation factors BRD4 and CDK9 work in concert to release
637 promoter-proximal paused RNA Polymerase II, facilitating active transcription along the
638 gene body⁹², p300/CBP promotes chromatin accessibility and TF binding, enabling the
639 core transcriptional machinery to assemble^{93,94}. Thus, we speculate that BRD4 and
640 CDK9-based TCIPs may be more effective at inducing transcription of BCL6 sites where
641 RNA Pol II is already in the vicinity of transcriptional start sites, while p300/CBP KAT-
642 TCIPs may exhibit the most influential activity at BCL6 sites lacking RNA Pol II.

643 Consequently, transcriptional output and cell fate would be different. The modular
644 pharmacology of TCIPs stands in contrast to targeted protein degraders, which result in
645 target depletion-mediated effects regardless of the E3 ubiquitin ligase recruited. Our
646 studies suggest TCIPs targeting the same transcription factor but recruiting different
647 transcriptional/epigenetic modifiers could be used sequentially to overcome mechanism-
648 based resistance.
649

650 **MAIN FIGURES**



651

Figure 1. Design and Activity of KAT-TCIPs

652
653

(A) KAT-TCIPs targeting p300/CBP are designed to de-repress cell death and cell cycle arrest pathways controlled by the transcription factor BCL6 in DLBCL cells.

654
655
656

(B) Structure of **TCIP3**, **NEG1**, which retains binding to p300/CBP, and **NEG2**, which retains binding to BCL6.

657
658

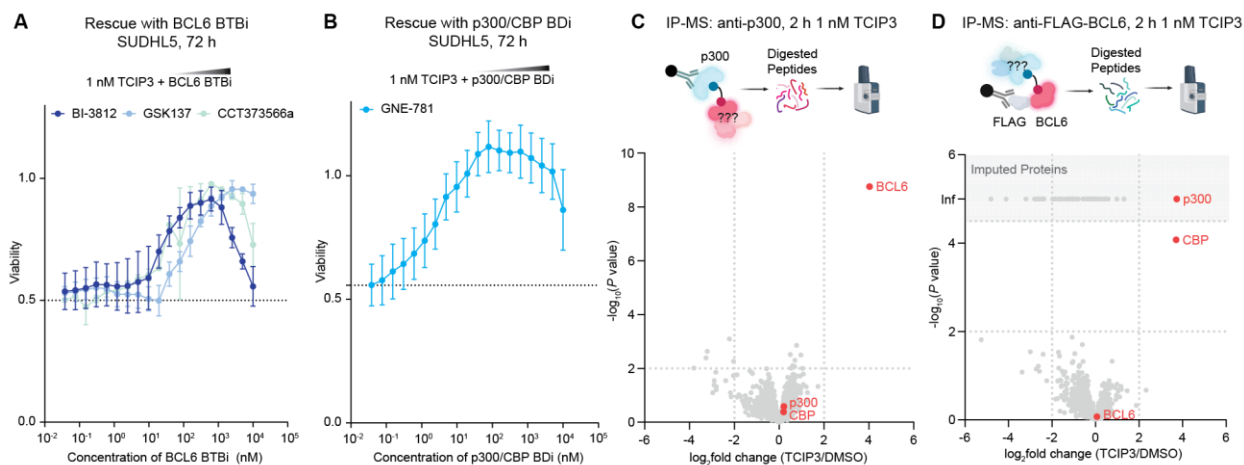
(C) Activation of a BCL6-repressed GFP reporter construct integrated into K422 cells after compound treatment for 24 h; 3 biological replicates, mean \pm s.e.m.

659
660

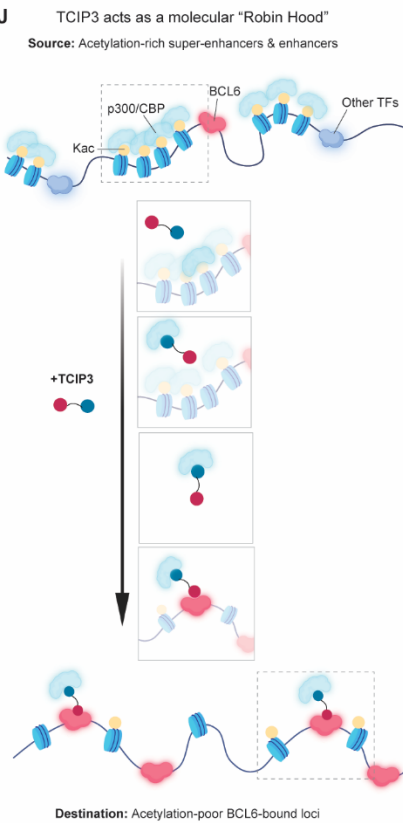
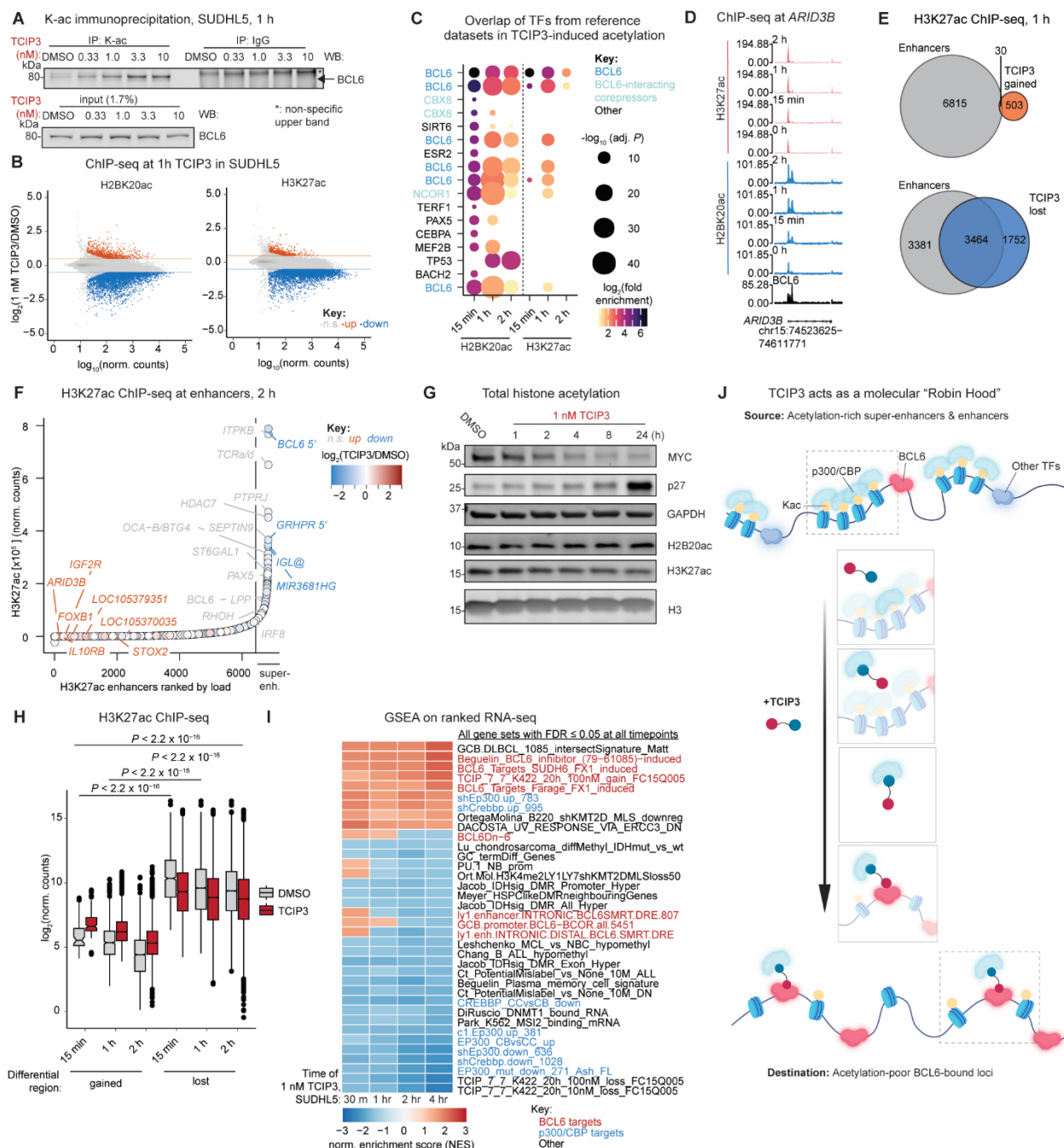
(D) Cell-killing potencies of compounds after 72 h of treatment in SUDHL5 cells; 3-5 biological replicates, mean \pm s.e.m.

661
662
663
664

(E) IC₅₀ values (nM) of antiproliferation after 7 days of compound treatment in DLBCL and leukemia cells plotted against *BCL6* expression in transcripts/million (TPM)⁹⁵; 3-4 biological replicates, mean \pm s.d.; *R* of *BCL6* TPM vs AUC computed by Pearson's correlation and *P*-value computed by two-sided Student's t-test.



665
666 **Figure 2. TCIP3 Kills Cells Via Chemically Induced Proximity (CIP)**
667 (A) Measurement of cell viability after competitive titration of constant 1 nM **TCIP3** with
668 BCL6^{BTB} domain inhibitors (BI-3812⁴⁸, GSK137⁴⁹, or CCT373566a⁴⁶), or (B) the
669 p300/CBP bromodomain inhibitor GNE-781⁵⁰; cells were treated simultaneously with
670 **TCIP3** and the inhibitor or DMSO for 72 h; 3 biological replicates, mean \pm s.e.m.
671 (C) p300 immunoprecipitation-mass spectrometry (IP-MS) from SUDHL5 cells treated for
672 2 h with 1 nM **TCIP3**; plotted with cutoffs of $\log_2(\text{fold change}) \geq 2$ and $P \leq 0.01$; 3 biological
673 replicates. For (C) and (D), P -values computed by a moderated t-test.
674 (D) FLAG IP-MS from genomic knock-in FLAG-tagged *BCL6* SUDHL5 cells treated with
675 1 nM **TCIP3** for 2 h plotted with cutoffs of $\log_2(\text{fold change}) \geq 2$ and $P \leq 0.01$. Proteins
676 that did not contain peptides for DMSO but contained peptides upon **TCIP3** treatment
677 were imputed; 3 biological replicates.
678



679

Figure 3. TCIP3 Redistributions p300/CBP Activity to BCL6 and Proximal Chromatin

680 **(A)** Acetylated lysine (K-ac)- IP and western blot (WB) for BCL6 after 1 h of **TCIP3** in
681 SUDHL5 cells; representative of three biological replicates.

682 **(B)** Changes in histone 3 lysine 27 and histone 2B lysine 20 acetylation (H3K27ac and
683 H2BK20ac) as measured by chromatin immunoprecipitation sequencing (ChIP-seq) after
684 1 h of 1 nM **TCIP3** in SUDHL5 cells; significant: adj. $P \leq 0.05$ and up, $\log_2(\text{fold change})$
685 ≥ 0.5 ; down, $\log_2(\text{fold change}) \leq -0.5$; 2 biological replicates, P -values computed by two-
686 sided Wald test and adjusted by multiple comparisons by Benjamini-Hochberg.

687 **(C)** Enrichment of predicted transcription factor (TF) binding in gained H3K27ac and
688 H2BK20ac peaks calculated by overlap with public ChIP-seq datasets from blood-lineage
689

690 cells; full enrichment data in Supplemental Table 2; *P*-values computed by two-sided
691 Fisher's exact test and adjusted for multiple comparisons by Benjamini-Hochberg.
692 **(D)** Induction of H2BK20ac and H3K27ac with time at the promoter of the BCL6 target
693 gene *ARID3B*; BCL6 track is CUT&RUN in untreated SUDHL5 cells, tracks merged from
694 two biological replicates and sequence-depth normalized and, for histone acetylation
695 ChIP-seq, also input-subtracted.
696 **(E)** Overlap of gained and lost H3K27ac peaks after 1 h of 1 nM **TCIP3** with annotated
697 enhancers and super-enhancers in SUDHL5 cells.
698 **(F)** Changes in H3K27ac at annotated enhancers and super-enhancers after 2 h of 1 nM
699 **TCIP3**; significant: adj. $P \leq 0.05$ and up, $\log_2(\text{fold change}) \geq 0.5$; down, $\log_2(\text{fold change})$
700 ≤ -0.5 ; 2 biological replicates, *P*-values computed by two-sided Wald test and adjusted by
701 multiple comparisons by Benjamini-Hochberg.
702 **(G)** Western blot of SUDHL5 cells treated with 1 nM **TCIP3** for the indicated time periods;
703 representative of 3 biological replicates.
704 **(H)** Comparison of H3K27ac loading at differential regions at 15 min, 1 h, and 2 h of 1 nM
705 **TCIP3**; differential regions defined as in **(A)**, *P*-values adjusted by Tukey's test after type
706 II analysis of variance (ANOVA).
707 **(I)** Gene set enrichment analysis of ranked $\log_2(\text{fold change})$ in gene expression
708 measured by RNA-sequencing (RNA-seq) after 1 nM **TCIP3** in SUDHL5 cells; only all
709 gene sets adj. $P \leq 0.05$ at all timepoints displayed, positive normalized enrichment scores
710 (NES) indicate gene sets enriched in **TCIP3**- induced genes while negative NES scores
711 indicate sets enriched in decreased genes, *P*-values computed by permutation and
712 adjusted for multiple comparisons by Benjamini-Hochberg.
713 **(J)** Model of how **TCIP3** redistributes p300/CBP from super-enhancers to BCL6.
714

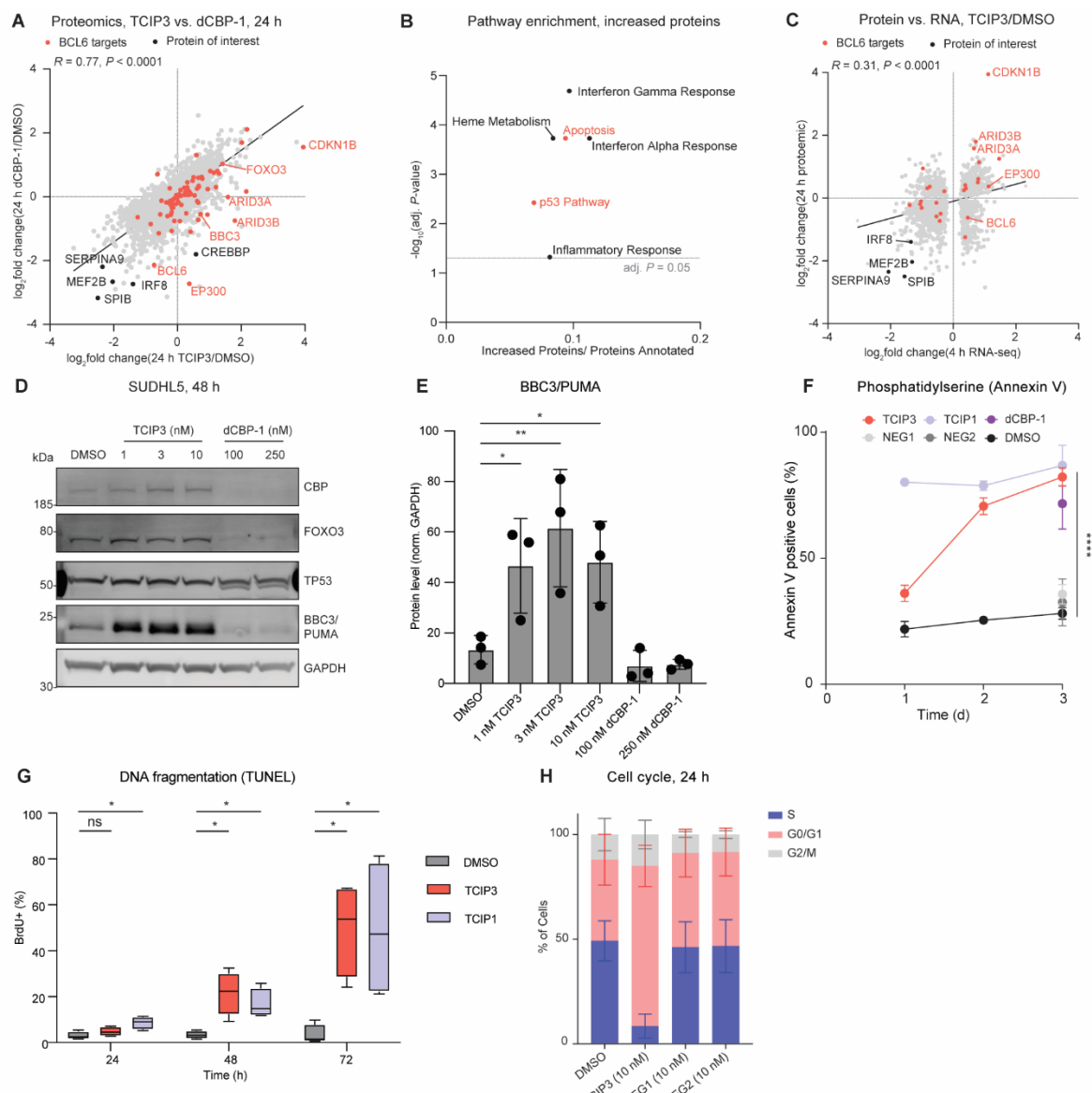


Figure 4. Activation of Apoptotic Signaling by TCIP3

(A) Comparison of whole-proteome profiling of SUDHL5 cells treated with 10 nM TCIP3 or 250 nM of the p300/CBP degrader dCBP-1³⁰ for 24 h; proteins labeled change statistically significantly (adj. $P \leq 0.05$); 3 biological replicates; P -values computed using a moderated t-test and adjusted by Benjamini-Hochberg; R computed by Pearson's correlation and P -value computed by two-sided Student's t-test.
 (B) Signaling pathways (MSigDB Hallmark 2020) enriched in significantly increased proteins (adj. $P < 0.05$, $\log_2(\text{foldchange}) > 1$) after 24 h treatment of 10 nM TCIP3 in SUDHL5.
 (C) Correlation of whole-proteome profiling of SUDHL5 cells treated with 10 nM TCIP3 for 24 h to bulk transcriptomics (RNA-seq) performed on SUDHL5 cells treated with 1 nM TCIP3 for 4 h; only genes whose transcripts that change significantly (adj. $P \leq 0.05$) were analyzed; 3 biological replicates; P -value for RNA-seq computed by two-sided Wald test

729 and adjusted by Benjamini-Hochberg; R computed by Pearson's correlation and P -value
730 for Pearson's correlation computed by two-sided Student's t-test.

731 **(D)** Western blot of pro-apoptotic proteins in SUDHL5 cells treated with indicated
732 compounds and doses after 48 h; representative of 3 biological replicates.

733 **(E)** Quantification of BBC3/PUMA protein levels from **(D)**; P -values computed by Fisher's
734 LSD test after ANOVA; **: $P < 0.01$, *: $P < 0.05$; only the comparisons to DMSO were
735 computed. 3 biological replicates, mean \pm s.d.

736 **(F)** Quantification of Annexin V-positive SUDHL5 cells treated with indicated compounds
737 and doses at 24, 48, or 72 h; P -values adjusted by Tukey's test after ANOVA. The
738 following comparisons were significantly different from each other at 72 h (****: adj. $P <$
739 0.0001): 10 nM **TCIP3** vs DMSO, 10 nM **NEG1**, and 10 nM **NEG2** 72 h; 10 nM **TCIP1**³⁹
740 vs DMSO, 10 nM NEG1, and 10 nM NEG2; 250 nM dCBP1 vs DMSO, 10 nm NEG1 (adj.
741 $P = 0.0023$), and 10 nM NEG2 (adj. $P = 0.0008$). The following comparisons were
742 significant at 48 h (****: adj. $P < 0.0001$): 10 nM **TCIP3** vs DMSO, 10 nM **TCIP1** vs DMSO.
743 The following comparisons were significant at 24 h: 10 nM **TCIP3** vs DMSO (****: adj. P
744 < 0.0001), 10 nM **TCIP1** vs DMSO (****: adj. $P < 0.0001$), 10 nM **TCIP3** vs 10 nM **TCIP1**
745 (*: adj. $P = 0.0187$). There were no significant differences between any other comparisons
746 (adj. $P \geq 0.05$). 3-12 biological replicates, mean \pm s.e.m.

747 **(G)** Concurrent analysis of apoptosis and cell cycle effects of TCIPs by terminal
748 deoxynucleotidyl transferase dUTP nick end labeling (TUNEL) and total DNA content co-
749 staining of SUDHL5 cells treated with DMSO, 10 nM **TCIP1**, or 10 nM **TCIP3** for 24, 48,
750 or 72 h; mean \pm s.e.m; 4 biological replicates; P -values computed by Fisher's LSD test
751 after analysis of variance (ANOVA); *: $P < 0.05$; ns: not significant, $P > 0.05$; only the
752 comparisons to DMSO at each timepoint were computed.

753 **(H)** Quantification of percentage of fixed SUDHL5 cells in G1, S Phase, or G2/M phase
754 after 24 h treatment with indicated compounds; 3 biological replicates, mean \pm s.e.m; P -
755 values adjusted by Tukey's test after analysis of variance (ANOVA) on cells in either S,
756 G0/G1, or G2/M phase. For G2/M cells, there were no significant differences (adj. $P \geq$
757 0.05); for S and G0/G1 phase cells, **TCIP3** was significantly different from all other
758 treatments (adj. $P < 0.05$). No other comparisons were significant.

759

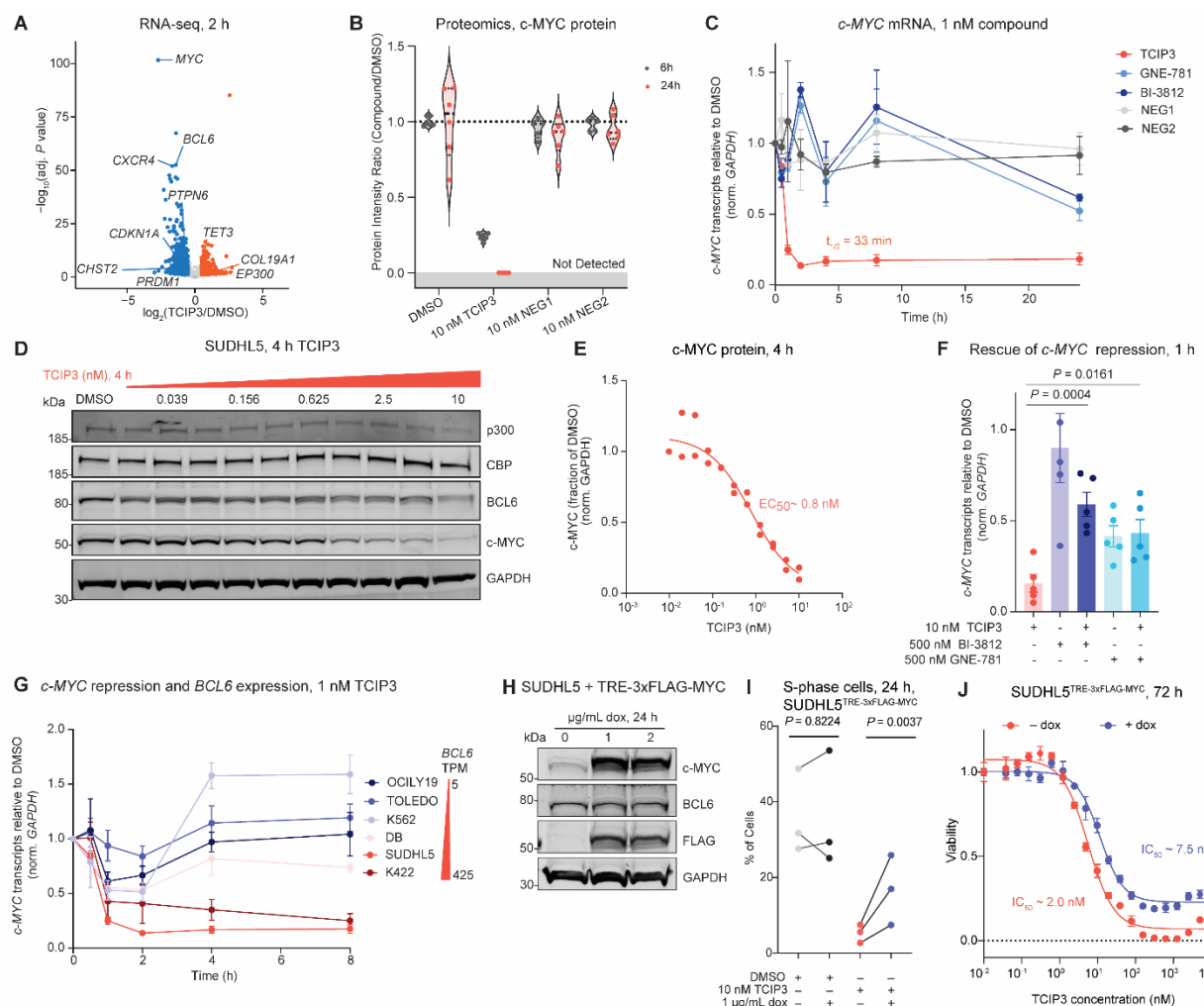


Figure 5. Rapid and Potent Reduction in c-MYC is Sufficient for Cell Cycle Arrest

(A) RNA-seq of SUDHL5 cells treated with 1 nM **TCIP3** for 2 h; colored are differential genes defined by adj. $P \leq 0.05$ and $|\log_2(\text{fold change})| \geq 0.5$, P -values computed by two-sided Wald test and adjusted for multiple comparisons by Benjamini-Hochberg; 3 biological replicates.

(B) All peptides of c-MYC detected by global proteomics after 10 nM **TCIP3**, **NEG1**, and **NEG2** treatment of SUDHL5 cells treated for 24 h; intensities are mean of 3 biological replicates. Lines represent median and interquartile range.

(C) Time-course of c-MYC transcripts in SUDHL5 cells treated with 1 nM of compounds normalized to *GAPDH* and DMSO treatment as quantified through reverse transcription quantitative PCR (RT-qPCR); 3 biological replicates, mean \pm s.e.m.

(D) Western blot of c-MYC protein in SUDHL5 cells treated with **TCIP3** for 4 h; blot representative of 2 biological replicates.

(E) Quantification of c-MYC protein normalized to GAPDH and DMSO levels from **(C)**.

(F) Measurement of c-MYC mRNA in SUDHL5 cells (normalized to *GAPDH* and DMSO treatment) by RT-qPCR after competitive titration of constant 10 nM **TCIP3** with 500 nM of the *BCL6*^{BTB} domain inhibitor **BI-3812**⁴⁸ or 500 nM of the p300/CBP bromodomain inhibitor **GNE-781**⁵⁰; cells were treated simultaneously with **TCIP3** and the inhibitor or DMSO for 1 h; effects of co-treatment of DMSO and inhibitors shown for comparison; 3

780 biological replicates, mean \pm s.e.m.; *P*-values adjusted by Tukey's test after analysis of
781 variance (ANOVA). Only comparisons of co-treatments to **TCIP3** were computed.

782 **(G)** c-MYC transcripts in DLBCL and leukemia cells with varying *BCL6* expression⁹⁵
783 (TPM: transcripts/million) treated with 1 nM of **TCIP3** normalized to *GAPDH* and DMSO
784 treatment as quantified through RT-qPCR; 3 biological replicates, mean \pm s.e.m. SUDHL5
785 data is from panel **B**.

786 **(H)** Doxycycline-inducible overexpression of c-MYC in SUDHL5 cells.

787 **(I)** S phase cells of SUDHL5^{TRE-3xFLAG-MYC} cells treated with or without 1 μ g/mL doxycycline
788 dissolved in ethanol or vehicle 24 h prior to 24 h treatment with 10 nM **TCIP3** or DMSO;
789 3 biological replicates, *P*-values computed by two-tailed ratio paired Students' t-test.

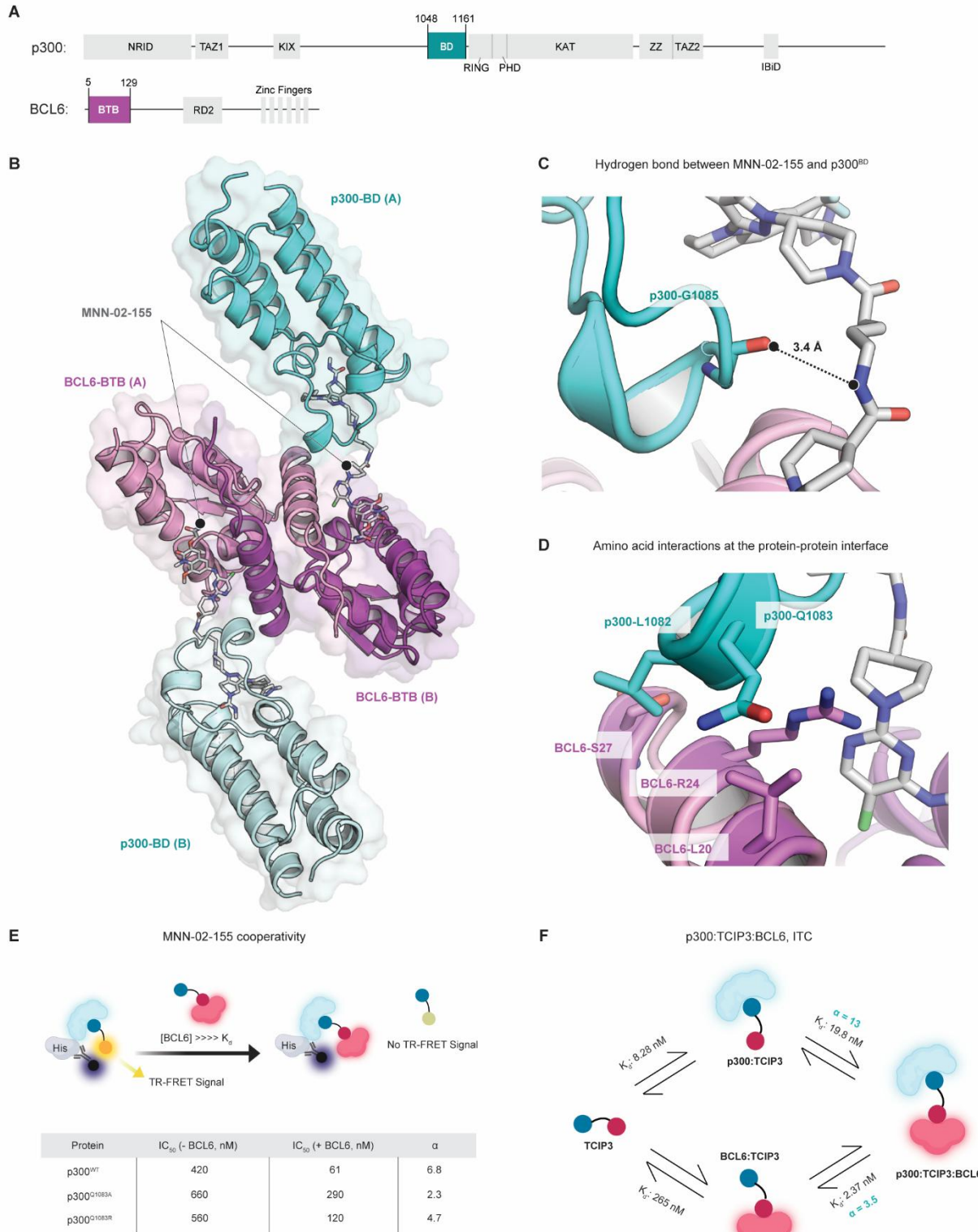
790 **(J)** Viability of SUDHL5^{TRE-3xFLAG-MYC} cells treated with 1 μ g/mL doxycycline dissolved in
791 ethanol or vehicle 24 h prior to 72 h treatment with **TCIP3**; mean \pm s.e.m., 3 biological
792 replicates.

793

794

795

796



797
798
799
800
801

Figure 6. The Crystal Structure and Cooperativity of the Ternary Complex
(A) Domain structure of full-length p300/CBP and BCL6. The highlighted p300 bromodomain (BD) and BCL6 BTB domain (BTB) were crystallized in complex with **MNN-02-155**.

802 **(B)** Co-crystal structure of the ternary complex formed by **MNN-02-155**, BCL6^{BTB}, and
803 p300^{BD}. One dimer of BCL6 is bound to two molecules of MNN-02-155, each of which
804 engages one protomer of p300^{BD}.
805 **(C)** Neo-hydrogen bond formed between **MNN-02-155** and the backbone of P300G¹⁰⁸⁵.
806 **(D)** Neo-protein-protein interactions formed at the interface of p300^{BD} and BCL6^{BTB}
807 mediated by **MNN-02-155** binding.
808 **(E)** Binary TR-FRET displacement assay assessing the binding of 6x-His-P300^{BD} to **MNN-02-155**. **MNN-02-155** was titrated into a biochemical complex of terbium-labeled 6x-His-p300^{BD} pre-incubated with **MNN-06-112**. Parallel experiments were performed by preincubating with BCL6 at concentrations exceeding its dissociation constant ($>> K_d$). Binding affinities of p300^{WT}, p300^{Q1083A}, and p300^{Q1083R} to **MNN-02-155** were evaluated in the absence and presence of BCL6 and a cooperativity constant was calculated ($\alpha = K_d \text{ binary}/K_d \text{ ternary}$). $n = 3$ independent experiments, mean.
815 **(F)** K_d calculations for each binding event, based on $n = 2-3$ independent experiments, mean \pm s.e.m. α was calculated for both p300 and BCL6 ($\alpha = K_d \text{ binary}/K_d \text{ ternary}$).
817
818
819
820
821
822
823
824
825
826
827
828
829
830
831
832
833
834
835
836
837
838
839
840
841
842
843
844
845
846
847

848 **SUPPLEMENTAL FIGURES**

849

850

851

852

853

854

855

856

857

858

859

860

861

862

863

864

865

866

867

868

869

870

871

872

873

874

875

876

877

878

879

880

881

882

883

884

885

886

887

888

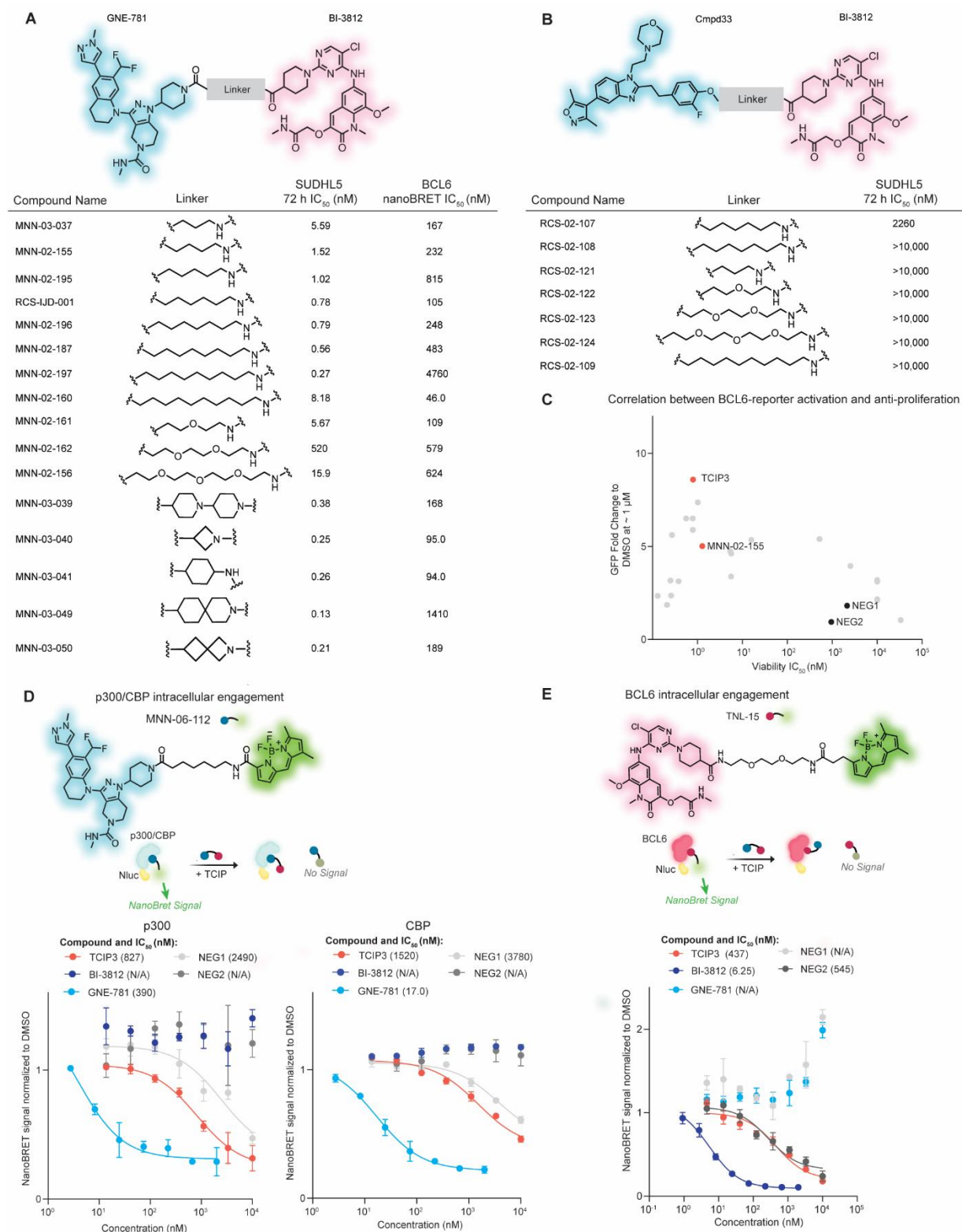
889

890

891

892

893



(A) Design of GNE-781 and **(B)** Cmpd33-based KAT-TCIP libraries and corresponding IC₅₀ values of cell viability after 72 h treatment in SUDHL5 and BCL6^{BTB} intracellular

899 probe-displacement (nanoBRET: nano-bioluminescence resonance energy transfer) in
900 HEK293T cells; for cell viability, mean of 1-4 biological replicates; for nanoBRET, mean
901 of 3 technical replicates.

902 **(C)** Reporter transactivation (fold change of BCL6-repressed GFP) after 24 h of treatment
903 in K422 reporter cells versus IC₅₀ values of cell viability after 72 h treatment in SUDHL5
904 for all KAT-TCIP compounds; for cell viability, mean of 1-4 biological replicates.

905 **(D)** Assessment of compounds and corresponding IC₅₀ values of p300 and CBP
906 intracellular probe-displacement in 293T cells; the probe **MNN-06-112** is shown; Nluc:
907 nano-luciferase.

908 **(E)** Assessment of compounds and corresponding IC₅₀ values in BCL6 nanoBRET in
909 HEK293T cells; the probe **TNL-15** is shown. For **(D)**, **(E)**, mean ± s.e.m of 3 technical
910 replicates.

911

912

913

914

915

916

917

918

919

920

921

922

923

924

925

926

927

928

929

930

931

932

933

934

935

936

937

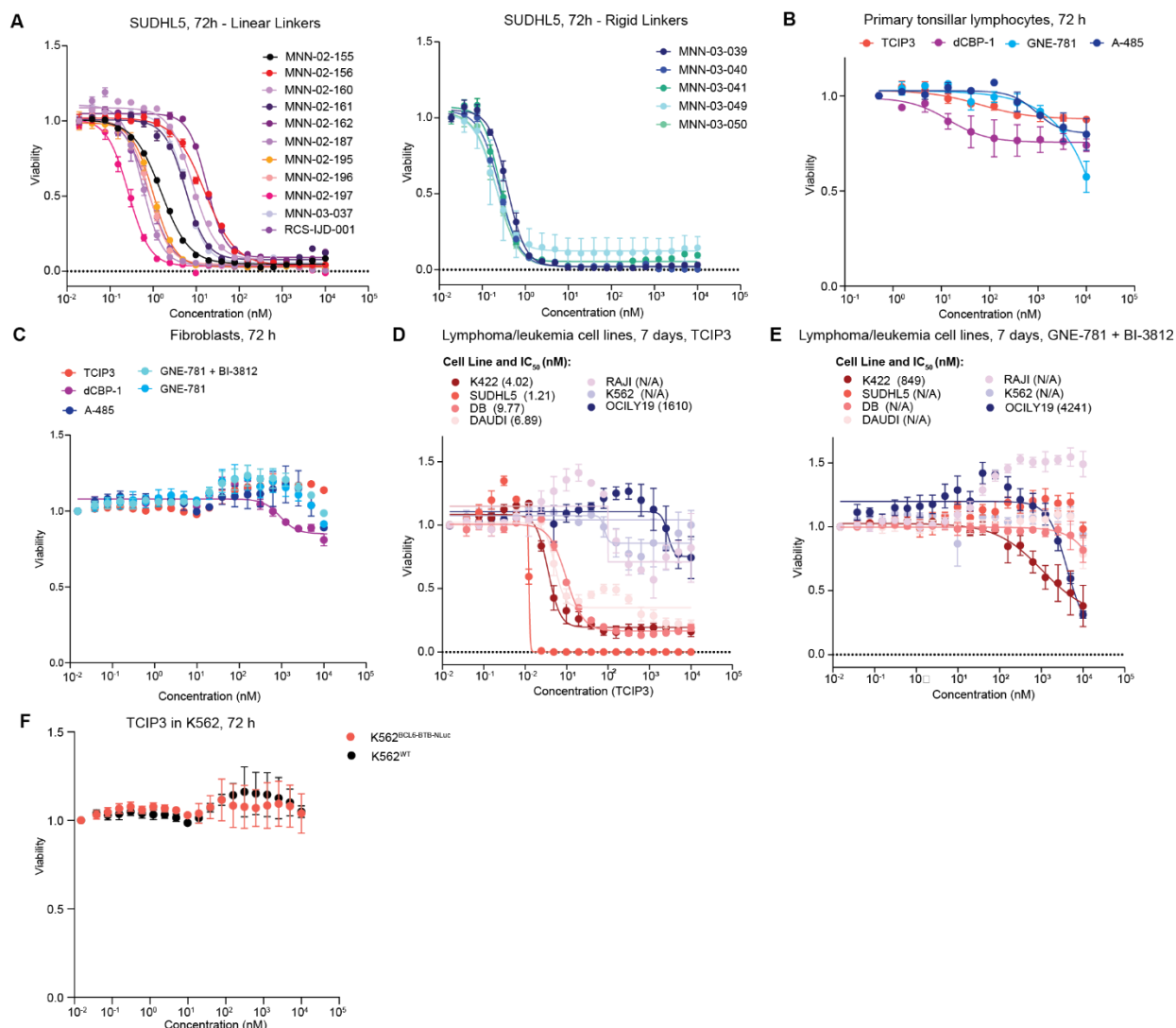
938

939

940

941

942



943

944 Supplemental Figure 2. Assessment of KAT-TCIP Toxicity in Primary and DLBCL 945 Cells

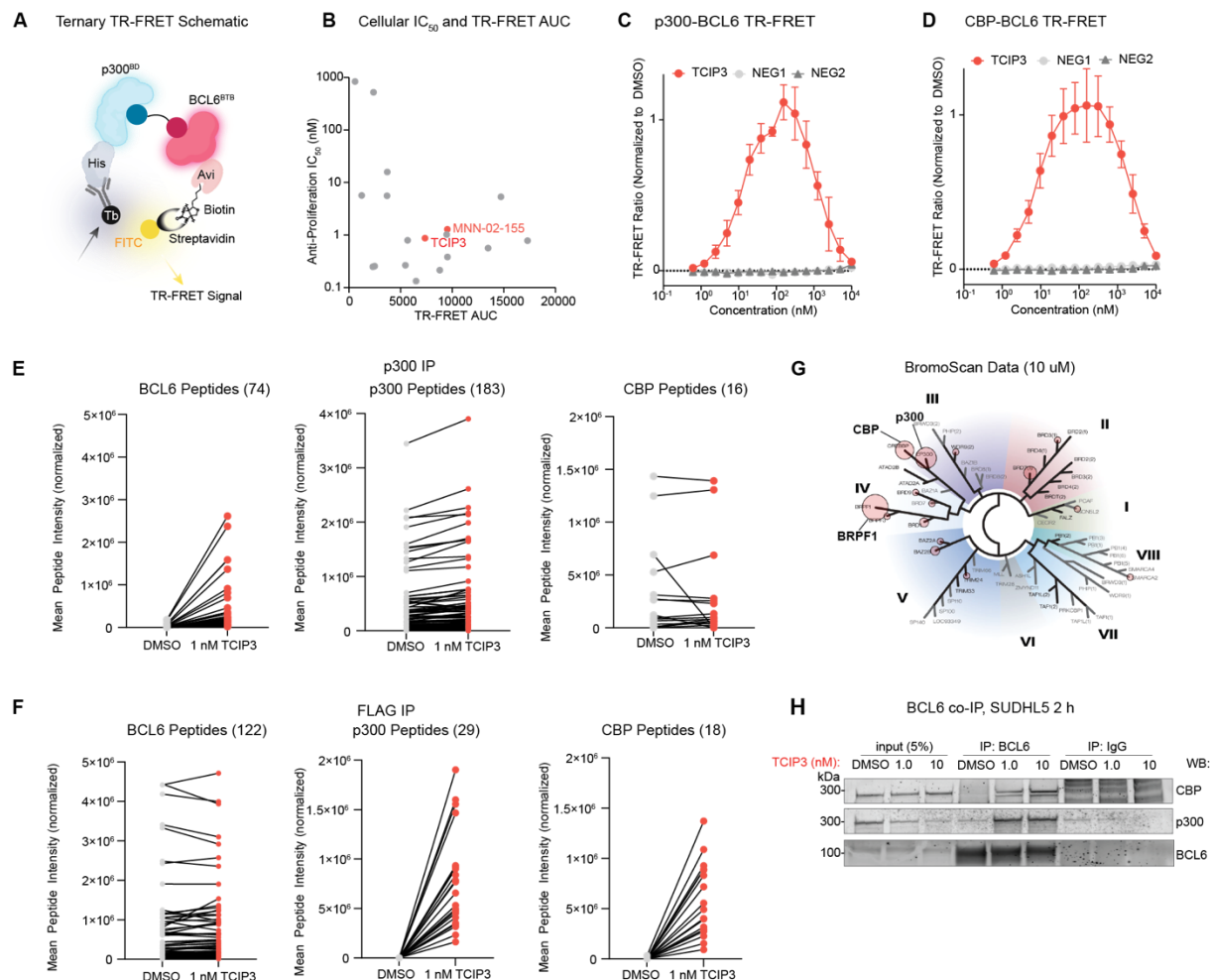
946 (A) Cell viability curves of GNE-781-based KAT-TCIPs containing either linear or rigid
947 linkers after 72 h treatment in SUDHL5 cells; corresponds to summary data in
948 Supplemental Fig. 1A; mean \pm s.e.m. of 2-3 biological replicates or 3 technical replicates.
949 (B) Viability effects of **TCIP3** and known p300/CBP targeting agents in primary tonsillar
950 lymphocytes from two independent donors (Methods) after treatment for 72 h; mean \pm
951 s.e.m.

952 (C) Viability effects of **TCIP3** and known p300/CBP targeting agents in human fibroblasts
953 after treatment for 72 h; 2 biological replicates; mean \pm s.e.m.

954 (D) Viability effects of 7 days of **TCIP3** treatment in DLBCL and leukemia cell lines; 3-4
955 biological replicates; mean \pm s.e.m.

956 (E) Viability effects of 7 days of BI-3812 and GNE-781 co-treatment in DLBCL and
957 leukemia cell lines; 3-4 biological replicates; mean \pm s.e.m.

958 (F) Viability effects after 72 h of **TCIP3** treatment in K562 cells overexpressing NLuc-
959 BCL6^{BTB}; 3 biological replicates; mean \pm s.e.m.



960
961 **Supplemental Figure 3. Biochemical and Cellular Engagement of BCL6 and**
962 **p300/CBP**

963 **(A)** Design of ternary TR-FRET assay using recombinant 6x-His-p300^{BD} or 6x-His-CBP^{BD}
964 and biotinylated BCL6^{BTB}-Avi to measure ternary complex formation.

965 **(B)** Antiproliferation IC₅₀ (nM) vs TR-FRET curve (AUC) for KAT-TCIPs synthesized from
966 GNE-781; for TR-FRET, mean of 3 biological replicates each with 3 technical replicates;
967 for cell viability IC₅₀s, mean of 1-4 biological replicates.

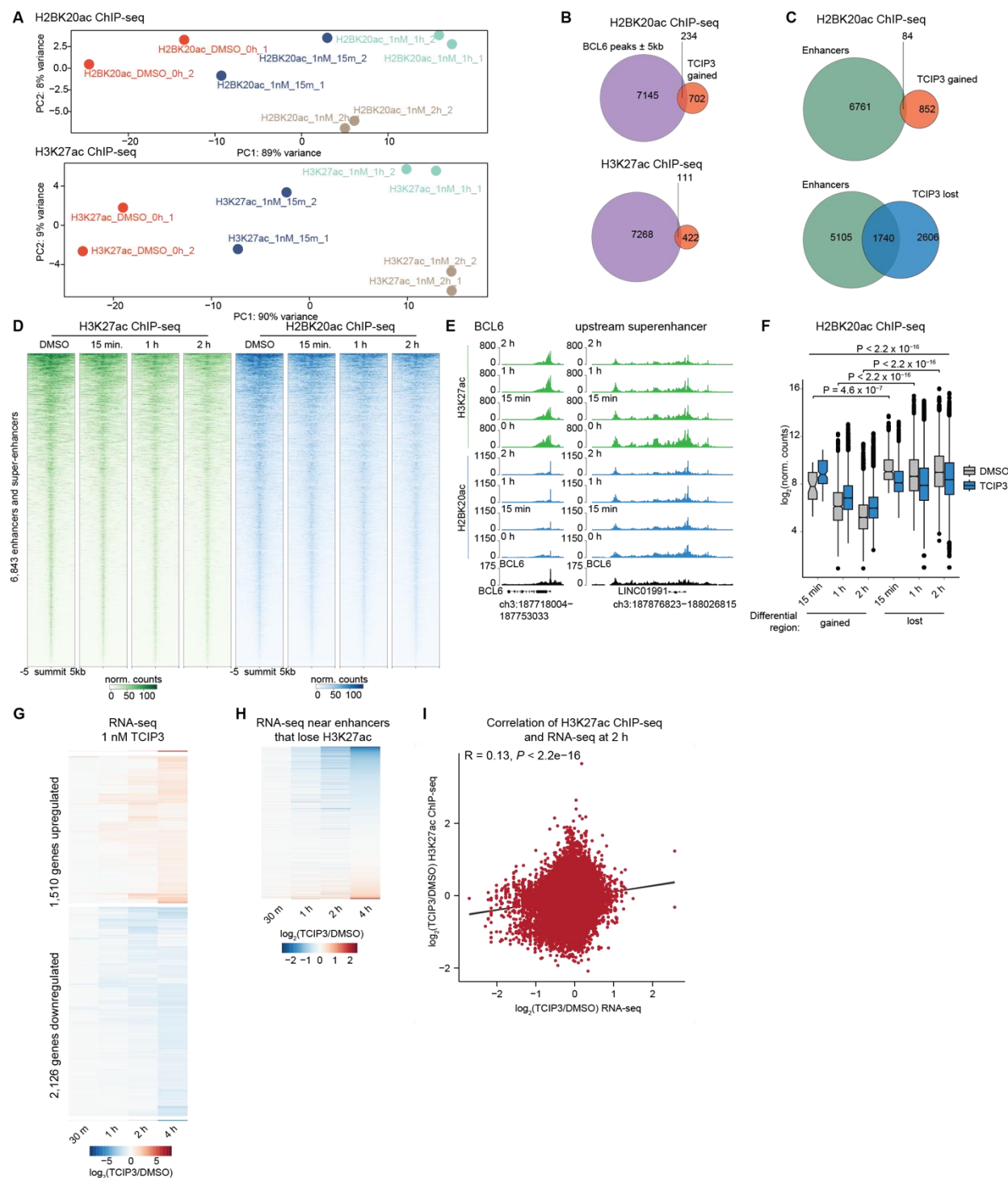
968 **(C)** p300-BCL6 or **(D)** CBP-BCL6 TR-FRET assay of **TCIP3**, **NEG1**, or **NEG2**; mean \pm
969 s.e.m. of 3 technical replicates.

970 **(E)** Mean peptide intensities of BCL6, p300, or CBP matched between DMSO or **TCIP3**
971 treatments in SUDHL5 cells treated for 2 h for p300 IP-MS shown in Figure 2C.

972 **(F)** Mean peptide intensities of BCL6, p300, or CBP matched between DMSO or **TCIP3**
973 treatments in FLAG-tagged *BCL6* SUDHL5 cells treated for 2 h for FLAG IP-MS shown
974 in Figure 2D. For **E** and **F**, total number of unique, proteotypic peptides across all
975 conditions provided in heading parentheses.

976 **(G)** Selectivity of binding to 40 recombinant human bromodomains (BROMOscan) with
977 **TCIP3** (10 μ M).

978 **(H)** BCL6 IP from SUDHL5 cells treated with the indicated doses of **TCIP3** for 2 h;
979 representative of 3 biological replicates.



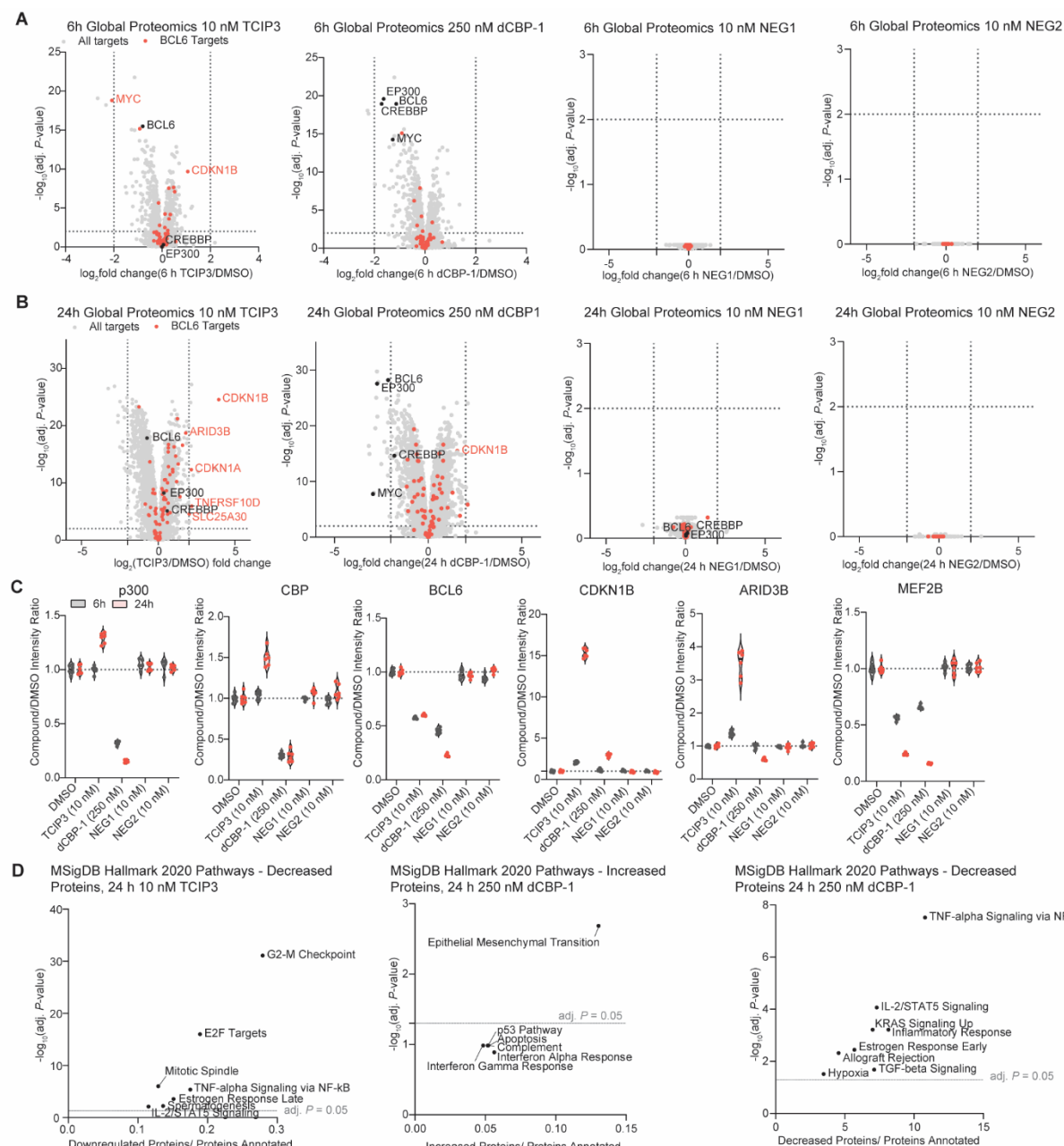
980

981 Supplemental Figure 4. Reprogramming of Histone Lysine Acetylation and Gene 982 Expression

983 **(A)** Principal component analysis of biological replicates for H3K27ac (2 per timepoint)
984 and H2BK20ac (2 per timepoint) ChIP-seq experiments.

985 **(B)** Overlap of gained H2BK20ac and H3K27ac peaks after 1 h of 1 nM TCIP3 with BCL6
986 summits \pm 5 kilobases (kb) in SUDHL5 cells as measured by BCL6 CUT&RUN.

987 **(C)** Overlap of gained and lost H2BK20ac peaks after 1 h of 1 nM **TCIP3** with annotated
988 enhancers and super-enhancers in SUDHL5 cells.; differential regions defined as in **Fig.**
989 **3A.**
990 **(D)** H3K27ac and H2BK20ac at all enhancers and super-enhancers for the indicated
991 timepoints of **TCIP3** treatment; merged from 2 biological replicates and sequence-depth
992 normalized and input-subtracted.
993 **(E)** Induction of H2BK20ac and H3K27ac with time at the promoter of *BCL6* concomitant
994 with loss at the *BCL6* upstream super-enhancer; *BCL6* track is CUT&RUN in untreated
995 SUDHL5 cells, tracks merged from two biological replicates and sequence-depth
996 normalized and, for histone acetylation ChIP-seq, also input-subtracted.
997 **(F)** Comparison of H2BK20ac loading at differential regions at 15 min, 1 h, and 2 h of 1
998 nM **TCIP3**; *P*-values adjusted by Tukey's test after type II analysis of variance (ANOVA).
999 **(G)** Time-dependent changes in gene expression; plotted are differential genes defined
1000 by adj. *P* ≤ 0.05 and |log₂(fold change)| ≥ 0.5, *P*-values computed by two-sided Wald test
1001 and adjusted for multiple comparisons by Benjamini-Hochberg.
1002 **(H)** Changes in gene expression at genes near enhancers and super-enhancers that had
1003 statistically significant (adj. *P* ≤ 0.05 and log₂(fold change) ≤ -0.5) losses in H3K27ac as
1004 measured by ChIP-seq **Fig. 3E**.
1005 **(I)** Correlation of changes at all H3K27ac peaks (66,995) after 2 h of 1 nM **TCIP3**
1006 treatment with changes in gene expression of nearest gene to peak; *R* computed by
1007 Pearson's correlation and *P*-value computed by two-sided Student's t-test.
1008
1009
1010
1011
1012
1013
1014
1015
1016
1017
1018
1019
1020
1021
1022
1023
1024
1025
1026
1027
1028
1029
1030



1031

1032 **Supplemental Figure 5. Proteomic Effects of TCIP3, dCBP1, NEG1, and NEG2**

1033 **(A)** Whole-proteome profiling of SUDHL5 cells treated with 10 nM **TCIP3**, 250 nM dCBP1,
1034 10 nM **NEG1**, or 10 nM **NEG2** for 24 h plotted with cutoffs of $\log_2(\text{fold change}) \geq 2$ and
1035 $\text{adj. } P \leq 0.05$.

1036 **(B)** Whole-proteome profiling of SUDHL5 cells treated with 10 nM **TCIP3**, 250 nM dCBP1,
1037 10 nM **NEG1**, or 10 nM **NEG2** for 6 h plotted with cutoffs of $\log_2(\text{fold change}) \geq 2$ and $\text{adj. } P \leq 0.05$. For **(A)**, **(B)**: 3 biological replicates; P -values computed using a moderated t-test and adjusted by Benjamini-Hochberg.

1040 **(C)** Quantification of individual peptides of interest from global proteomics of all
1041 treatments and timepoints matched across treatments. Lines represent median and
1042 interquartile range.

1043 (D) Signaling pathways (MSigDB Hallmark 2020) enriched after 24 h treatment of
1044 indicated compounds in SUDHL5 in significantly decreased (adj. $P < 0.05$,
1045 $\log_2(\text{foldchange}) < -1$) or significantly increased (adj. $P < 0.05$, $\log_2(\text{foldchange}) > 1$)
1046 proteins.

1047

1048

1049

1050

1051

1052

1053

1054

1055

1056

1057

1058

1059

1060

1061

1062

1063

1064

1065

1066

1067

1068

1069

1070

1071

1072

1073

1074

1075

1076

1077

1078

1079

1080

1081

1082

1083

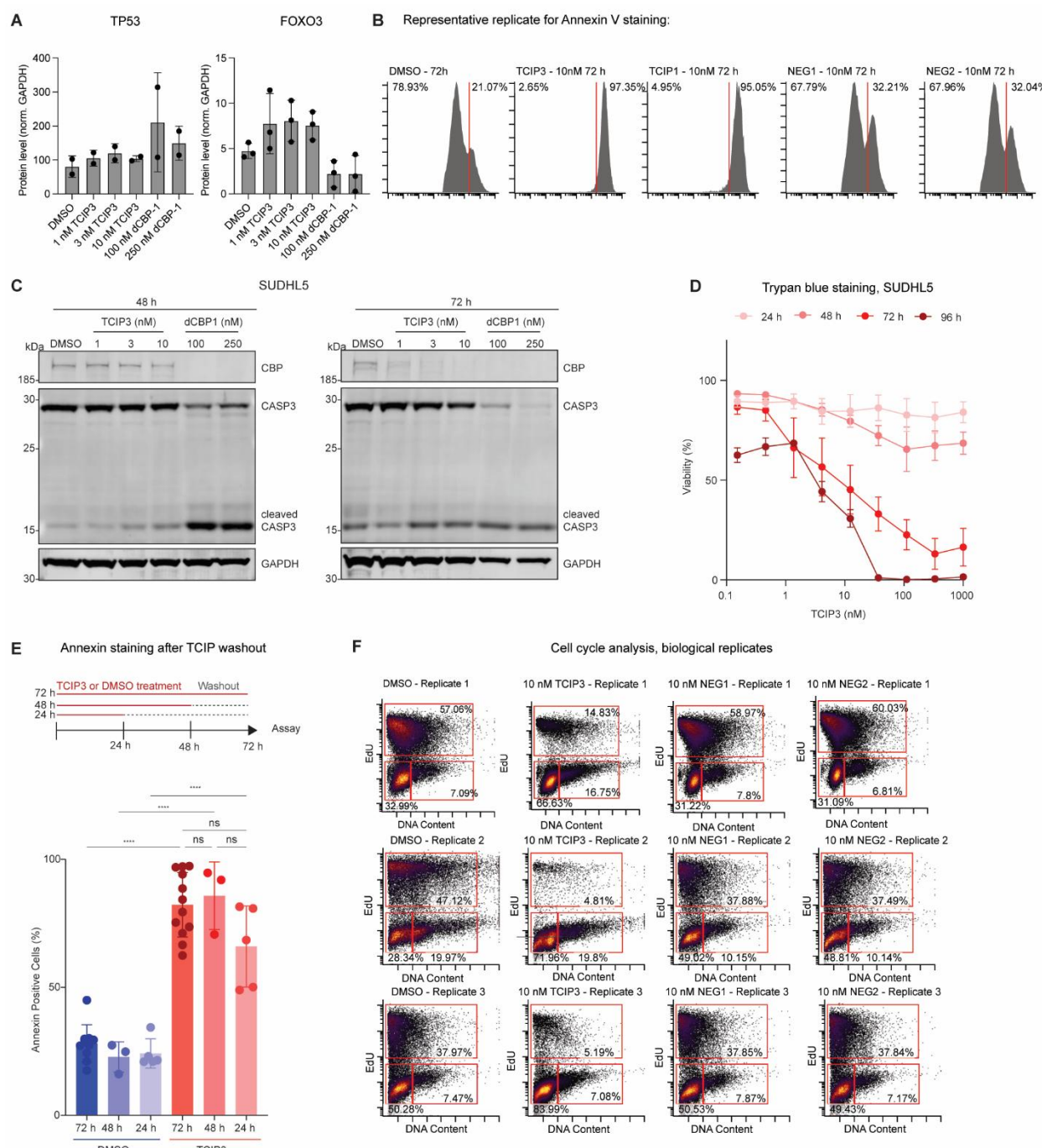
1084

1085

1086

1087

1088



1089

1090

Supplemental Figure 6. Characterization of Apoptosis and Cell Cycle Arrest

1091

1092

1093

1094

1095

1096

1097

(A) Quantification of TP53 and FOXO3 protein levels from Fig. 4D; *P*-values computed by Fisher's LSD test after ANOVA; only the comparisons to DMSO were computed; no comparisons were significant.

(B) Representative (of 3-12 biological replicates) Annexin V staining replicate of SUDHL5 cells treated with **TCIP3**, **NEG1**, **NEG2**, or DMSO for 72 h.

(C) Western blot of caspase 3 in SUDHL5 cells treated with indicated compounds and doses after 48 and 72 h; representative of 3 biological replicates.

1098 (D) Percent of cells alive after Trypan blue staining (Trypan blue negative); SUDHL5 cells
1099 treated with **TCIP3** for indicated timepoints and doses. 3 biological replicates; mean \pm
1100 sem.

1101 (E) Quantification of Annexin V positive SUDHL5 cells treated with DMSO or 10 nM **TCIP3**
1102 for 24, 48, or 72 h and then washed with PBS and replaced with media for 48, 24, or 0 h,
1103 respectively; *P*-values adjusted by Tukey's test after analysis of variance (ANOVA); ****:
1104 adj. *P* < 0.0001; all unlabeled comparisons were not significant. 72 h data corresponds to
1105 Fig. 4F.

1106 (F) Individual cell cycle analysis biological replicates corresponding to Fig. 4H.

1107

1108

1109

1110

1111

1112

1113

1114

1115

1116

1117

1118

1119

1120

1121

1122

1123

1124

1125

1126

1127

1128

1129

1130

1131

1132

1133

1134

1135

1136

1137

1138

1139

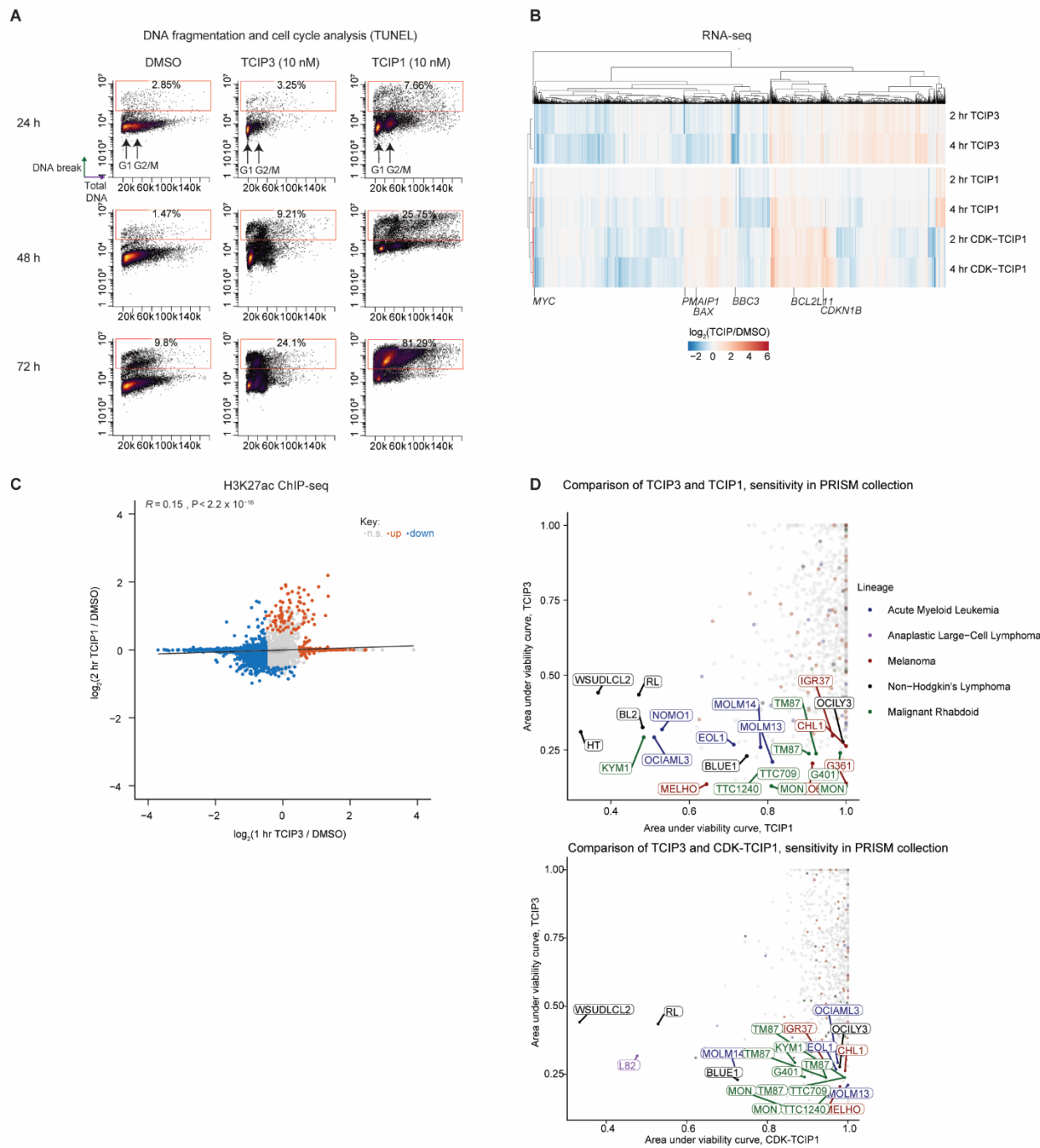
1140

1141

1142

1143

1144



1145
1146
1147
1148
1149
1150
1151

Supplemental Figure 7. Comparison of BCL6-targeting TCIPs

(A) Concurrent analysis of apoptosis and cell cycle effects of TCIPs by terminal deoxynucleotidyl transferase dUTP nick end labeling (TUNEL) and total DNA content co-staining of SUDHL5 cells treated with DMSO, 10 nM TCIP1, or 10 nM **TCIP3** for 24, 48, or 72 h; corresponds to Fig. 4G; representative of 4 biological replicates; cell cycle phases labeled.

1152 **(B)** Unbiased clustering of differential gene expression caused by **TCIP3**, **TCIP1**³⁹, and
1153 **CDK-TCIP1**⁴⁰; differential genes were defined by adj. $P \leq 0.05$ and $|\log_2(\text{fold change})| \geq 0.5$, P -values computed by two-sided Wald test and adjusted for multiple comparisons
1154 by Benjamini-Hochberg; 3-4 biological replicates.

1155 **(C)** Correlation of changes at all H3K27ac peaks (86,087) between **TCIP1** and **TCIP3**
1156 treatment; colored are peaks that change significantly for either treatment, significance
1157 defined by adj. $P \leq 0.05$ and $|\log_2(\text{fold change})| \geq 0.5$, P -values computed by two-sided
1158 Wald test and adjusted for multiple comparisons by Benjamini-Hochberg; 2 biological
1159 replicates; R computed by Pearson's correlation and P -value computed by two-sided
1160 Student's t-test.

1161 **(D)** Comparison of sensitivity of cell line to **TCIP3** with sensitivity to **TCIP1**³⁹ and **CDK-TCIP1**⁴⁰ in ~900 cancer cell lines in PRISM^{55,96}; labeled are top-ranked (most sensitive)
1162 lines colored by lineage.

1163

1164

1165

1166

1167

1168

1169

1170

1171

1172

1173

1174

1175

1176

1177

1178

1179

1180

1181

1182

1183

1184

1185

1186

1187

1188

1189

1190

1191

1192

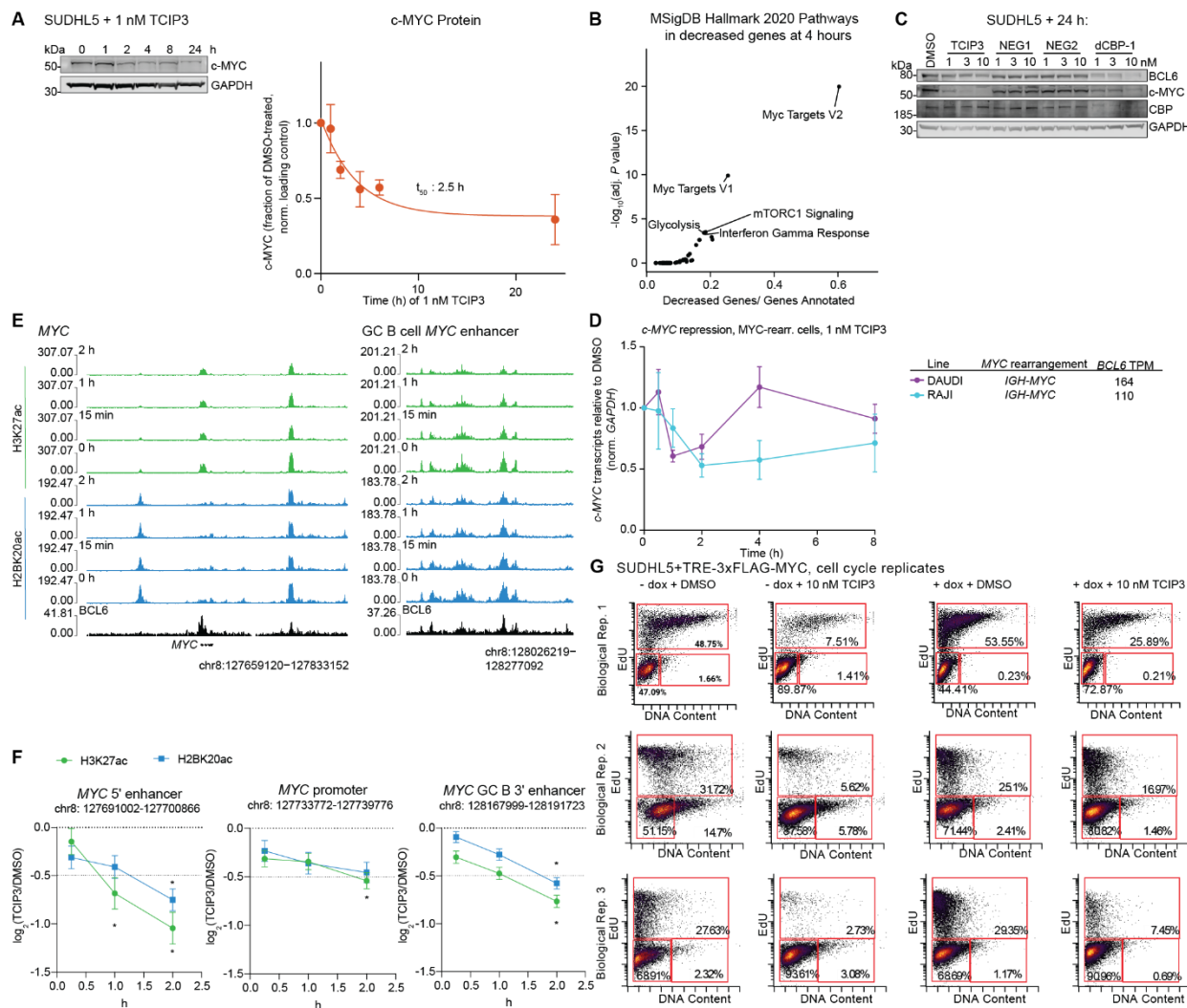
1193

1194

1195

1196

1197



1215 (F) Quantification of changes in H2BK20ac and H3K27ac differential peaks around the *c-*
1216 *MYC* locus; *: adj. $P \leq 0.05$ and $\log_2(\text{fold change}) \leq -0.5$; 2 biological replicates, mean \pm
1217 s.e.m.; P -values computed by two-sided Wald test and adjusted by multiple comparisons
1218 by Benjamini-Hochberg.

1219 (G) Individual biological replicates of cell cycle analysis of SUDHL5^{TRE-3xFLAG-MYC} cells
1220 treated with or without 1 $\mu\text{g/mL}$ doxycycline dissolved in ethanol or vehicle 24 h prior to
1221 24 h treatment with 10 nM **TCIP3** or DMSO.

1222

1223

1224

1225

1226

1227

1228

1229

1230

1231

1232

1233

1234

1235

1236

1237

1238

1239

1240

1241

1242

1243

1244

1245

1246

1247

1248

1249

1250

1251

1252

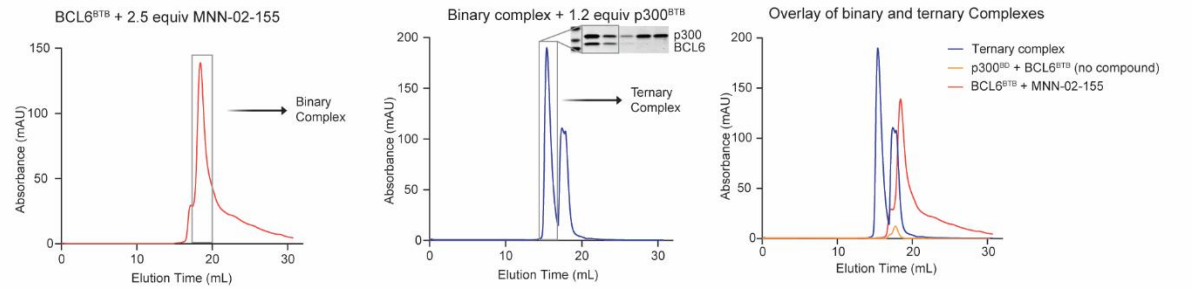
1253

1254

1255

1256

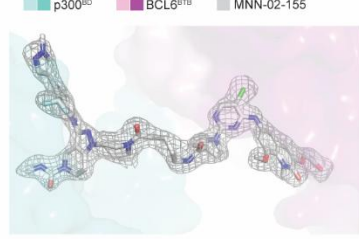
A Sequence of ternary complex formation



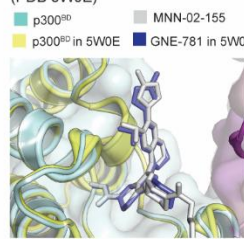
B Representative crystals



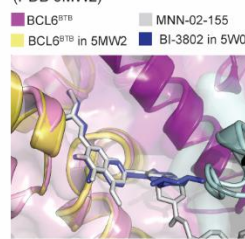
C F_o-F_c omit map (2 sigma; docked naive models)



D Overlay of GNE-781 bound to CBP^{BD} (PDB 5W0E)



E Overlay of BI-3802 bound to BCL6^{BTB} (PDB 5MW2)



1257

Supplemental Figure 9. Structural Analyses of KAT-TCIPs

1259 (A) Schematic of biochemical formation of a ternary complex between **MNN-02-155**,
1260 P300^{BD}, and BCL6^{BTB} domains. Binary and ternary complexes were purified by size-
1261 exclusion and concentrated to desired concentrations.

1262 (B) Representative images of crystals containing the ternary complex.

1263 (C) F_o-F_c map of **MNN-02-155** in the co-crystal structure with p300^{BD} and BCL6^{BTB}
1264 domains.

1265 (D) Overlay of the co-crystal structure with the published structure of GNE-781 bound to
1266 CBP (PDB: 5W0E).

1267 (E) Overlay of the co-crystal structure with the published structure of BI-3812 bound to
1268 BCL6 (PDB: 5MW2).

1269

1270

1271

1272

1273

1274

1275

1276

1277

1278

1279

1280

1281

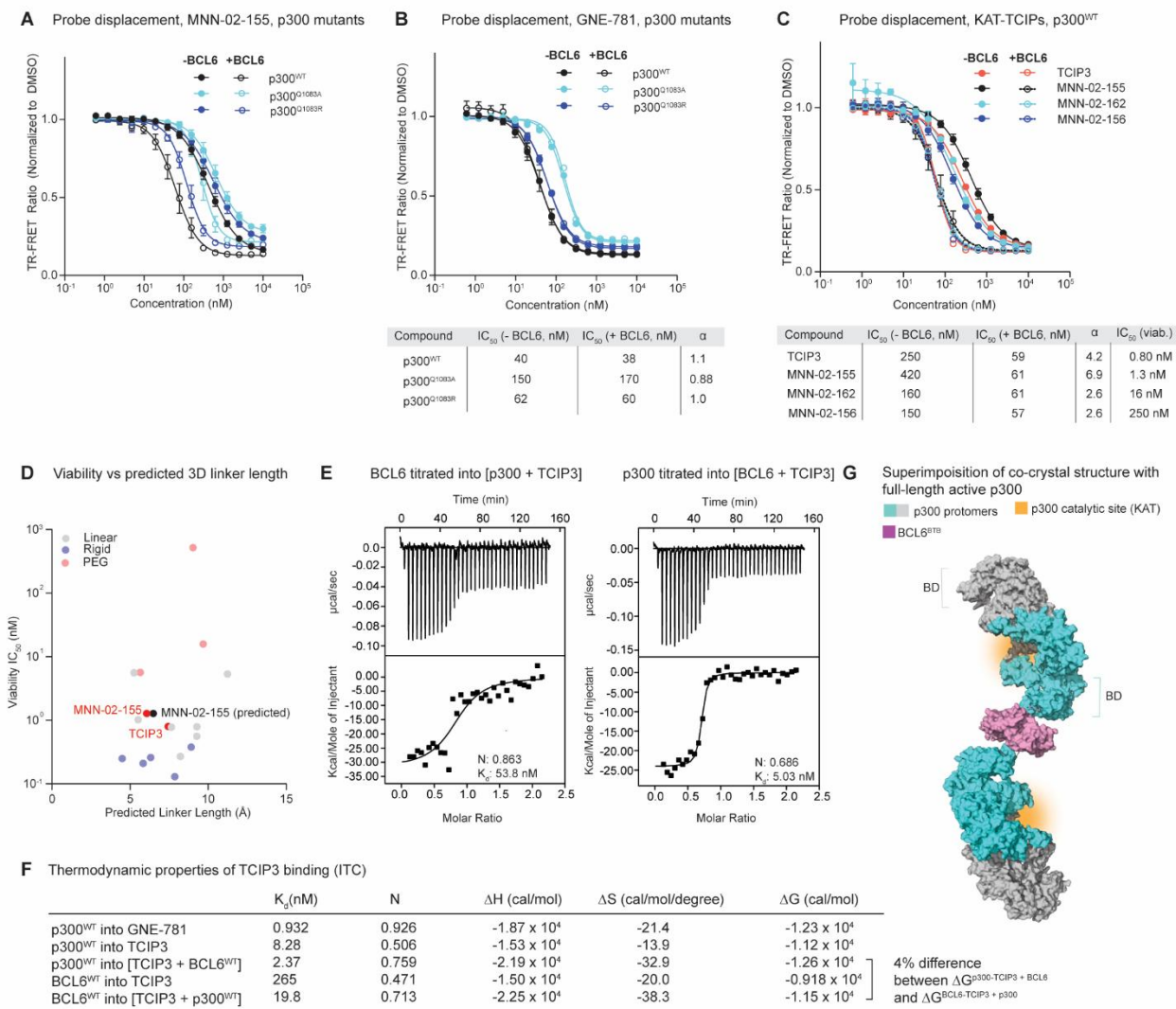
1282

1283

1284

1285

1286



1287

1288 Supplemental Figure 10. Biophysical Analyses of KAT-TCIPs

1289

(A) Binary TR-FRET displacement curves of **MNN-02-155** corresponding to Fig. 7D.

1290

(B) Binary TR-FRET displacement assay and cooperativity analysis evaluating the inhibition of GNE-781 against p300^{WT}, p300^{1083A}, p300^{1083R} in the absence or presence of BCL6 (>> K_d). n = 2-3 biological replicates; mean ± s.e.m.

1291

(C) Binary TR-FRET displacement assay and cooperativity analysis evaluating the inhibition of **TCIP3**, **MNN-02-155**, **MNN-02-162**, or **MNN-02-156** against p300^{WT} in the absence or presence of BCL6 (>> K_d); cell viability IC₅₀ after 72 h treatment in SUDHL5 (Supplemental Fig. 1) labeled in table. n = 2-3 biological replicates; mean ± s.e.m.

1292

(D) IC₅₀s (nM) of KAT-TCIPs synthesized from GNE-781 treated for 72 h in SUDHL5 (from Supplemental Fig. 1A, 2A) plotted against predicted lowest-energy-conformation linker lengths (average of the 2-3 lowest energy conformations).

1293

(E) ITC traces of binding events to form a ternary complex, including BCL6^{BTB} (10 μ M) titrated into p300^{BD} (20 μ M) and **TCIP3** (1 μ M), or p300^{BD} (20 μ M) titrated into BCL6^{BTB} (40 μ M) and **TCIP3** (2 μ M), and respective N and K_d values; corresponds to Fig. 6E; representative of 3 biological replicates.

1304 (F) Thermodynamic parameters of binding measured from ITC. All measurements
1305 represent the mean of 2-3 biological replicates.

1306 (G) Superimposition of the co-crystal structure of **MNN-02-155** engaged with p300^{BD} and
1307 BCL6^{BTB} with the active p300 core, containing two p300 protomers, one teal and one gray
1308 (PDB: 6GYR).

1309

1310

1311

1312

1313

1314

1315

1316

1317

1318

1319

1320

1321

1322

1323

1324

1325

1326

1327

1328

1329

1330

1331

1332

1333

1334

1335

1336

1337

1338

1339

1340

1341

1342

1343

1344

1345

1346

1347

1348

1349

1350 **Supplemental Figure 11. Full Scans of Western Blots.**

1351

1352 **Supplemental Figure 12. Flow Gating Strategies.**

1353

1354 **Supplemental Table 1. Enriched proteins after p300 IP-MS in SUDHL5 cells, FLAG**
1355 **IP-MS in FLAG-tagged *BCL6* SUDHL5 cells, or after global proteome profiling after**
1356 **TCIP3, dCBP-1, NEG1, and NEG2 treatment in SUDHL5 cells.**

1357

1358 **Supplemental Table 2. Full results of enrichment of histone acetylation peaks in**
1359 **public transcription factor ChIP-seq datasets in blood-lineage cells (ChIP-atlas).**

1360 Contains all significantly enriched TFs in H3K27ac and H2BK20ac differential peaks.

1361 Legend is on Sheet 1 of the Table.

1362

1363 **Supplemental Table 3: Crystallographic data collection and refinement statistics.**

1364

1365 **Supplemental File 1: Chemical Synthesis and Characterization.**

1366

1367 **Supplemental Video 1: Co-Crystal Structure of MNN-02-155 in complex with p300^{BD}**
1368 **and BCL6^{BTB}.**

1369

1370 **LIMITATIONS OF THE STUDY**

1371 KAT-TCIPs recruit the acetyltransferases p300/CBP to the master transcriptional
1372 repressor BCL6 to activate cell death in DLBCL cells. We primarily assessed our lead
1373 KAT-CIP molecule **TCIP3** in DLBCL cell lines with either high or low BCL6 expression,
1374 and the extent to which **TCIP3**'s pharmacology can be generalized across other DLBCL
1375 subtypes and other cancers remains to be explored. Additionally, we only incorporated
1376 two p300/CBP bromodomain-containing ligands and one BCL6-binding ligand into our
1377 KAT-TCIP designs. Other ligands may demonstrate different potencies and
1378 pharmacology. Although we investigated KAT-TCIP mediated acetylation of BCL6 and
1379 histone proteins, we did not comprehensively assess the possibility of other protein
1380 substrates. We did not investigate the *in vivo* efficacy of **TCIP3** in mouse models of
1381 DLBCL. **TCIP3** should be considered a tool molecule to manipulate cancer cell signaling
1382 and not a therapeutic candidate.

1383

1384 **ACKNOWLEDGEMENTS**

1385 We thank members of the Crabtree and Gray laboratories for constructive comments. We
1386 thank Dr. Anja Deutzmann and Dr. Jesse Engreitz for discussions about KAT-TCIP
1387 induced *c-MYC* repression, and Dr. Caitlin Mills for her suggestions regarding cell death
1388 studies. We thank members of the Weis laboratory for allowing us to use their ITC
1389 instrument. This work was supported by the Howard Hughes Medical Institute (G.R.C.);
1390 the National Institutes of Health (grants CA276167, CA163915, and MH126720-01 to
1391 G.R.C.); High-End Instrumentation Grant S10OD028697-01 to Stanford Chemistry,
1392 Engineering & Medicine for Human Health; R01CA201380 to MRG); the Mary Kay
1393 Foundation; and the Schweitzer Family Fund. Use of the Stanford Synchrotron Radiation
1394 Lightsource, SLAC National Accelerator Laboratory, is supported by the U.S. Department
1395 of Energy, Office of Science, Office of Basic Energy Sciences under Contract No. DE-

1396 AC02-76SF00515. The SSRL Structural Molecular Biology Program is supported by the
1397 DOE Office of Biological and Environmental Research, and by the National Institutes of
1398 Health, National Institute of General Medical Sciences (P30GM133894). The contents of
1399 this publication are solely the responsibility of the authors and do not necessarily
1400 represent the official views of NIGMS or NIH. M.N.N. was supported by the David L. Sze
1401 and Kathleen Donahue Interdisciplinary Fellowship. H.Y. was supported by a Leukemia
1402 and Lymphoma Society Special Fellow Award. N.S.G. was supported by funds from the
1403 Department of Chemical and Systems Biology and the Stanford Cancer Institute, both at
1404 Stanford University. M.R.G. was supported by a Leukemia & Lymphoma Society Scholar
1405 award, the MD Anderson B-cell Lymphoma Moonshot Program and the Schweitzer
1406 Family Fund. The Gray lab also receives or has received research funding from Novartis,
1407 Takeda, Astellas, Taiho, Jansen, Kinogen, Arbella, Deerfield, Springworks, Interline, and
1408 Sanofi.

1409

1410 MATERIALS AND DATA AVAILABILITY

1411 The mass spectrometry proteomics data have been deposited to the ProteomeXchange
1412 Consortium via the PRIDE⁹⁷ partner repository with the dataset identifier PXD059919.
1413 Genomic sequencing data has been deposited to GSE287542 and GSE287543. The X-
1414 ray co-crystal structure of MNN-02-155 in complex with p300^{BD} and BCL6^{BTB} has been
1415 deposited to the Protein Data Bank (PDB: 9MZA). All other materials are available from
1416 the authors upon request.

1417

1418 AUTHOR CONTRIBUTIONS

1419 G.R.C., N.S.G., M.N.N., R.C.S., and S.G. conceived the project. S.G. and M.N.N.
1420 conducted cell biological, biochemical, and genomic studies and contributed equally to
1421 this work. M.N.N. and R.C.S. designed and conducted chemical syntheses. S.G. and
1422 S.A.N. conducted ChIP-seq studies with help from M.N.N. S.A.N. made the FLAG-BCL6
1423 line and S.A.N. and B.G.D. performed IP-MS experiments. S.M.H, M.N.N., M.M., D.F.,
1424 and S.G. conducted structural and biochemical studies. B.G.D. performed proteomic
1425 experiments. H.A., M.M, B.R., J.M.S., C.L., and H.M.J. performed experiments designed
1426 by G.R.C., S.G., N.S.G., M.N.N., B.G.D., and S.M.H. M.M. conducted NanoBRET studies.
1427 H.A performed Western Blots and generated lentiviruses. Y.W. assisted with studies of
1428 cell death. H.Y. and M.R.G. conducted BCL6 CUT&RUN studies and contributed gene
1429 set enrichment analyses relevant to DLBCL. T.L. synthesized the BI3812-BODIPY probe.
1430 A.K. and T.Z. contributed to TCIP biological application and chemical synthesis,
1431 respectively. L.C. and M.M.D. contributed to cytotoxicity testing in primary lymphocytes.
1432 G.R.C., M.N.N., S.G., S.M.H, and N.S.G. wrote the manuscript with input from all authors.

1433

1434 DECLARATION OF INTERESTS

1435 G.R.C. is a founder and scientific adviser for Foghorn Therapeutics and Shenandoah
1436 Therapeutics. N.S.G. is a founder, science advisory board member, and equity holder in
1437 Syros, C4, Allorion, Lighthorse, Voronoi, Inception, Matchpoint, CobroVentures, GSK,
1438 Shenandoah (board member), Larkspur (board member), and Soltego (board member).
1439 T.Z. is a scientific founder, equity holder, and consultant for Matchpoint and an equity
1440 holder in Shenandoah. The Gray lab receives or has received research funding from
1441 Novartis, Takeda, Astellas, Taiho, Jansen, Kinogen, Arbella, Deerfield, Springworks,

1442 Interline, and Sanofi. M.R.G. reports research funding from Sanofi, Kite/Gilead, Abbvie,
1443 and Allogene; consulting for Abbvie, Allogene, Johnson & Johnson, Arvinas and Bristol
1444 Myers Squibb; honoraria from Esai and MD Education; and stock ownership of KDAc
1445 Therapeutics. Shenandoah has a license from Stanford for the TCIP technology that was
1446 invented by G.R.C., S.G., A.K., R.C.S., M.N.N., N.S.G., and T.Z. The remaining authors
1447 declare no competing interests.

1448

1449 METHODS

1450

1451 Cell Culture

1452 Lymphoma and leukemia cells were grown in RPMI-1640 medium (ATCC 30-2001)
1453 supplemented with 10% fetal bovine serum (FBS) and 1% 100X Penicillin-Streptomycin
1454 (Gibco, 15140122) in incubators at 37°C with 5% carbon dioxide. KARPAS422 cells were
1455 obtained from Sigma (06101702) and DB and SUDHL5 were obtained from the American
1456 Tissue Culture Collection (ATCC). The Daudi cell line, originally from ATCC, was
1457 generously provided by R. Levy's laboratory at Stanford University. Raji cells, also from
1458 ATCC, were a gift from J. Cochran's laboratory at Stanford University. TOLEDO and K562
1459 cells were originally obtained from ATCC and were kindly shared by A. Alizadeh's
1460 laboratory at Stanford University. Primary human tonsillar lymphocytes were from two
1461 separate donors (male, 6 years old; male, 44 years old) from the laboratory of M. M. Davis
1462 under IRB protocol numbers IRB-60741 (adult tonsils) and IRB-30837 (pediatric tonsils).
1463 BJ CRL-2522 human fibroblasts were obtained from ATCC and grown in DMEM media
1464 (ThermoFisher 11965118) supplemented with 10% fetal bovine serum (FBS) and 1%
1465 100X Penicillin-Streptomycin (Gibco, 15140122) in incubators at 37°C with 5% carbon
1466 dioxide. Cells were routinely checked for mycoplasma and immediately checked upon
1467 suspicion. No cultures tested positive.

1468

1469 Cell Viability Measurements

1470 *Compound treatment for 72 hours:* Thirty thousand cells were seeded in 100 µl of media
1471 per well of a 96-well plate and treated with drug for the indicated times and doses. A
1472 resazurin-based indicator of cell health (PrestoBlue; P50200, Thermo Fisher) was added
1473 for 1.5 h at 37°C, at which point the fluorescence ratio at 560/590 nm was recorded (Tecan
1474 Spark). The background fluorescence was subtracted, and the signal was normalized to
1475 DMSO-treated cells. IC₅₀ measurements on cell lines were calculated using at least three
1476 biological replicates (separate cell passages). Fit of dose–response curves to data and
1477 statistical analysis was performed using GraphPad PRISM using the four-parameter
1478 log(inhibitor) vs response function.

1479 *Compound treatment for 7 days:* Fifteen thousand cells were seeded in 100 µl of media
1480 per well of a U-bottom 96-well plate and treated with digitally dispensed drugs (Tecan
1481 D300e) for the indicated times and doses. After 96 hours, plates were centrifuged for 750
1482 rpm for 3 minutes, and old media was exchanged for 100 µl of fresh media. Drug
1483 treatment was then repeated at the indicated doses. 72 hours following media change,
1484 cells were transferred to 96 well flat-bottom opaque plates. Viability was measured by
1485 adding 25 µL Cell Titer-Glo reagent (Promega G7570) to each well and luminescence
1486 was measured (BMG Labtech Pherastar FS). The background luminescence was
1487 subtracted, and the signal was normalized to DMSO-treated cells. IC₅₀ measurements on

1488 cell lines were calculated using at least three biological replicates by separate cell
1489 passages. Fit of dose-response curves to data and statistical analysis was performed
1490 using GraphPad PRISM using the four-parameter log(inhibitor) vs response function.
1491

1492 **Trypan Blue Cell Counting Assay**

1493 Thirty thousand cells were seeded into a 96-well plate and treated with digitally dispensed
1494 drugs (Tecan D300e) for the indicated times and doses. At either 24, 48, 72, or 96 hours,
1495 cells were transferred to a U-bottom well, centrifuged for 4 minutes at 500g, then
1496 aspirated. 10 μ L phosphate-buffered saline (PBS) pH 7.4 and 10 μ L Trypan Blue
1497 (Invitrogen T10282) were added to the well and mixed, at which point 10 μ L of the mixture
1498 was transferred to a cell counting slide and the percentage of cells alive was recorded.
1499

1500 **PRISM Cell Proliferation Assay**

1501 The PRISM cell proliferation assay was carried out as previously described⁹⁸. Briefly, up
1502 to 859 barcoded cell lines in pools of 20-25 were thawed and plated into 384-well plates
1503 (1250 cells/well for adherent cells, 2000 cells/well for suspension or mixed
1504 suspension/adherent pools). Cells were treated with an 8-point dose curve starting at 10
1505 μ M with threefold dilutions in triplicate and incubated for 120 hours, then lysed. Each cell's
1506 barcode was read out by mRNA-based Luminex detection as described previously⁵⁵ and
1507 input to a standardized R pipeline
1508 (https://github.com/broadinstitute/prism_data_processing) to generate viability estimates
1509 relative to vehicle treatment and fit dose-response curves. The area under the dose-
1510 response-curve (AUC), which is correlated with drug potency, was used as a metric of
1511 drug potency in a cell line, and correlated (Pearson's) with dependency of the cell line to
1512 gene knockout⁹⁶.
1513

1514 **Protein Expression and Purification**

1515 The bacterial expression vectors for 6xHis-p300^{BD} and 6xHis-CBP^{BD} used for isothermal
1516 calorimetry, crystallography, and TR-FRET assays were generous gifts from Nicola
1517 Burgess-Brown (p300: Addgene plasmid 746580; <http://n2t.net/addgene:74658>;
1518 RRID:Addgene_74658; CBP: Addgene plasmid 38977; <http://n2t.net/addgene:38977>;
1519 RRID:Addgene_38977). Mutations in p300 (Uniprot: Q09472) were introduced by site-
1520 directed mutagenesis (NEB E0554). The bacterial expression vector for BCL6^{BTB} used
1521 for isothermal calorimetry and crystallography (renamed pSG219C) was created as
1522 follows: codon-optimized coding sequences for human BCL6 (residues 5-129; Uniprot:
1523 P41182) and were synthesized and cloned into pET-48b(+) (Novagen). The open reading
1524 frame codes for N-terminal Trx and 6xHis tags as well as a 3C cleavage site. The bacterial
1525 expression vector for BCL6^{BTB} used for TR-FRET assays (renamed pSG233) included a
1526 C-terminal GS linker and AviTag (GLNDIFEAQKIEWHE) used for biotinylation.
1527 Both vectors coded for the following BCL6 mutations: C8Q, C67R, C84N⁹⁹. These
1528 enhance stability but do not affect the affinity for BI3812 or for SMRT.
1529

1530 Protein expression was carried out for 18 hours in Rosetta(DE3) cells (Novagen 70954)
1531 at 18°C before pelleting cells by centrifugation. Cell pellets were resuspended in ~2 mL
1532 per liter buffer D800 (20 mM HEPES, pH 7.5; 800 mM NaCl; 10 mM imidazole, pH 8.0;
1533 2 mM beta-mercaptoethanol; 10 % glycerol (v:v)) supplemented with protease inhibitors

1534 (1 mM PMSF, 1 mM benzamidine, ~20 µg/ml pepstatin, aprotinin, and leupeptin), and
1535 stored at -80 °C.

1536
1537 To purify 6xHis-CBP^{BD} and 6xHis-p300^{BD}, cell pellets were thawed in warm water. All
1538 subsequent steps were carried out at 4 °C or on ice. Cells were lysed by sonication before
1539 centrifugation at 3,214 g for 1 hour. Clarified lysate was mixed with ~0.5 mL/L of culture
1540 cobalt resin (GoldBio) for one hour. Beads were washed by low-speed centrifugation and
1541 subsequently by gravity flow with ~25 column volumes of buffer D800 (followed by ~10
1542 column volumes of buffer B50 (D800 but with 50 mM NaCl). Protein was eluted with 50
1543 mL C50 (B50 with 400 mM imidazole), and the eluate was applied to a 5 mL anion
1544 exchange column (Q HP, Cytiva) and eluted via salt gradient (8 CV; B50 to D800). Peak
1545 fractions were concentrated by ultrafiltration before application to a 24 ml gel filtration
1546 column (S200 increase, Cytiva) charged with GF150 buffer (20 mM Tris-HCl, pH 8.5,
1547 150 mM NaCl, 1 mM tris(2-carboxyethyl)phosphine (TCEP)). Peak fractions were again
1548 concentrated by ultrafiltration, supplemented with 5% glycerol by volume (final), and
1549 aliquoted and frozen at -80 °C. Individual aliquots were thawed and stored for no more
1550 than 24 hours at 4 °C or on ice before use or disposal.

1551
1552 Purification of BCL6^{BTB} for crystallography and isothermal calorimetry followed the same
1553 procedure as 6xHis-CBP^{BD} and 6xHis- p300^{BD} with the following modifications: 6xHis-3C
1554 (homemade, produced with pET-NT*-HRV3CP, a kind gift from Gottfried Otting
1555 (Addgene plasmid 162795; <http://n2t.net/addgene:162795>; RRID:Addgene_162795))
1556 was added to the eluate from the anion exchange column for 18 hours at 4 °C under slow
1557 rotation. Imidazole concentration was adjusted to 50 mM and the mixture was applied to
1558 a 5 mL nickel column (HisTrap FF Crude, Cytiva) and the flow-through captured. Flow-
1559 through was concentrated by ultrafiltration before application to a gel filtration column and
1560 peak fractions were concentrated and stored as written above.

1561
1562 Purification of biotinylated BCL6^{BTB}-AviTag for TR-FRET assays followed the same
1563 procedure as BCL6^{BTB} with the following modification: following cleavage of the tag with
1564 6xHis-3C, the mixture was charged with 14xHis-BirA (homemade; produced with pTP264,
1565 a kind gift from Dirk Görlich (Addgene plasmid 149334 ; <http://n2t.net/addgene:149334> ;
1566 RRID:Addgene_149334)) with 0.01 mM D-biotin (Sigma 2031), 10mM MgCl₂, and 10mM
1567 ATP and nutated for 1 hour 30 °C. The sample was applied to a 5 mL nickel column
1568 (HisTrap FF Crude, Cytiva) and the flow-through captured. Flow-through was
1569 concentrated by ultrafiltration before application to a gel filtration column and peak
1570 fractions were concentrated and stored as written above. Biotinylation efficiency was
1571 confirmed to be almost 100% by incubation of a small sample with streptavidin beads and
1572 monitoring of the flowthrough by SDS-PAGE.

1573
1574 **TR-FRET Ternary Assay**
1575 10 µL reactions containing 10 nM 6x-His- p300^{BD} or 6x-His-CBP^{BD}, 200 nM Biotinylated-
1576 Avi-BCL6^{BTB}, 20 nM streptavidin-FITC (SA1001, Thermo), and 1:400 anti-6x-His-terbium
1577 (PerkinElmer 61HI2TLF) in buffer containing 20 mM HEPES pH 7.5, 150 mM NaCl, 0.1%
1578 BSA, 0.1% NP-40, and 1 mM TCEP were plated in low-volume 384 well plates. Drugs
1579 were digitally dispensed (Tecan D300e) into protein-containing wells, and the plate was

1580 allowed to incubate in the dark for 1 hour at room temperature. Emission at 490 nm
1581 (terbium) and 520 nm (FITC) was measured on a PHERAstar FS plate reader (BMG
1582 Labtech) upon excitation with 337 nm. The ratio of signal at 520 nm to 490 nm was
1583 calculated and normalized to DMSO-treated protein.

1584

1585 **TR-FRET Binary Assay**

1586 10 μ L reactions containing 25 nM 6x-His-p300^{BD} or 6x-His-CBP^{BD}, 50 nM MNN-06-112,
1587 1:400 anti-6x-His-terbium (PerkinElmer 61HI2TLF), and with or without 10 μ M BCL6^{BTB}
1588 in buffer containing 20 mM HEPES pH 7.5, 150 mM NaCl, 0.1% BSA, 0.1% NP-40, and
1589 1 mM TCEP were plated in low-volume 384 well plates. Drugs were digitally dispensed
1590 (Tecan D300e) into protein-containing wells, and the plate was allowed to incubate in the
1591 dark for 1 hour at room temperature. Emission at 490 nm (terbium) and 520 nm (FITC)
1592 was measured on a PHERAstar FS plate reader (BMG Labtech) upon excitation with 337
1593 nm. The ratio of signal at 520 nm to 490 nm was calculated and normalized to DMSO-
1594 treated protein.

1595

1596 **Crystallography**

1597 In GF150 buffer, 1 mg of BCL6^{BTB} protein was incubated for 1 hour on ice with 2.5
1598 equivalents of MNN-02-155 that was diluted 10-fold from a 10 mM DMSO stock in GF150
1599 prior to mixing. The mixture was then purified by size-exclusion chromatography as
1600 above. The centermost peaks were collected, concentrated by ultrafiltration, and then
1601 incubated with 1.2 equivalents of 6x-His-p300^{BD} on ice for 1 hour. This mixture was
1602 purified by size-exclusion chromatography, which resulted in two distinct peaks. Fractions
1603 from the early-eluting peak were collected and concentrated to approximately 4.5 mg/mL
1604 in a 3k Amicon Ultra-4 Centrifugal filter. The sample was used immediately for
1605 crystallization by the sitting drop vapor diffusion method. Rectangular plate-like crystals
1606 grew within 48 hours in multiple conditions. Crystals were cryoprotected in a solution
1607 containing the crystallization solution supplemented with 25% glycerol before cryo-
1608 cooling by dipping the crystal in liquid nitrogen. Data was collected at Stanford SSRL
1609 experimental beamline 9-2. The best diffraction dataset came from crystals grown in 0.15
1610 M DL-Malic acid pH 7.0, 20 % PEG 3,350. Data were integrated and scaled in the
1611 P212121 space group using Aimless and data quality analyzed using Ctruncate^{100,101}. We
1612 used data to a minimum Bragg spacing of 2.1 \AA according to the CC1/2 cutoff suggested
1613 by Ctruncate. The L-test indicated twinning was not present in the crystal.

1614

1615 Initial phases were determined by molecular replacement using MOLREP [PMID
1616 20057045] as implemented in CCP4¹⁰². We used as search models crystal structures of
1617 the BCL6 BTB domain (6CQ1) and the p300 bromodomain (5BT3) with the small
1618 molecule ligands removed¹⁰³. The resolution cutoff for molecular placement was 3 \AA , and
1619 we specified a multicopy search for hetero-multimers. This operation successfully placed
1620 individual copies of BCL6 and p300. Initial refinement using REFMAC¹⁰⁴ and analysis of
1621 the overall Matthews Coefficient indicated the likely presence of two copies each for BCL6
1622 and p300. Thus, these initial coordinates were used as an input for PHASER¹⁰⁵, which
1623 placed two copies of the starting model in the unit cell. Refinement of this model using
1624 REFMAC converged rapidly and produced unambiguous extra density corresponding to
1625 the compound included in crystallography experiments. In later rounds of refinement, we

1626 added this compound, generating restraints using AceDRG¹⁰⁶. We also added water
1627 molecules in later refinement rounds. Manual model adjustments were done in Coot¹⁰⁷.
1628

1629 We note that, while the L-test indicated no twinning, the presence of multiple screw axes
1630 in the space group, as well as the existence of non-crystallographic symmetry within the
1631 biologically relevant protomer (2 BCL6:2 p300:2 TCIP) could potentially complicate data
1632 reduction and analysis. Specifically, we explored the possibility of translational non-
1633 crystallographic symmetry resulting in the averaging of non-equivalent protomers along a
1634 screw axis, which would result in higher-than-expected intensity statistics at low
1635 resolutions and would thus complicate L-tests for twinning. Unaccounted-for tNCS may
1636 also explain the relatively high Rfree value in the final refined model. However, the
1637 Phaser-MR solution was superior given the P212121 space group versus other
1638 orthorhombic possibilities (PHASER Refined LLG = 2749.7 versus 701.5 for the next best
1639 space group, P21221). Additionally, refinement produced features of the small molecule,
1640 which was not present in the molecular replacement models, indicative of high quality and
1641 unbiased maps. We note the presence of similar cases of potential unresolved tNCS in
1642 the literature with similar statistics. See¹⁰⁸ and references therein. The final refined model
1643 has Rwork/Rfree values of .217/.281. There are no Ramachandran outliers, and the
1644 overall clashscore is 9.
1645

1646 Isothermal Calorimetry

1647 12 hours prior to performing ITC, frozen stocks of 6xHis-p300^{BD} and BCL6^{BTB} were
1648 dialyzed for two hours in ITC buffer at 4°C (50 mM HEPES pH 7.4, 100 µM TCEP, 150
1649 mM NaCl), followed by dialysis in fresh ITC buffer overnight at 4°C to remove glycerol
1650 and equalize protein mixtures. Samples were centrifuged at 10,000g for 10 min to remove
1651 any precipitate. In all titrations, DMSO was added to protein mixtures to match the DMSO
1652 concentration of ligand dissolved in ITC buffer. For binary assays with TCIP3, dialyzed
1653 6xHis-p300^{BD} or BCL6^{BTB} were titrated from the syringe into a cell containing TCIP3
1654 dissolved in ITC buffer. For p300 titrations, 50 µM or 25 µM protein was titrated into 5 µM
1655 or 2.5 µM, respectively, of TCIP3. For BCL6 titrations, 70 µM or 40 µM protein was titrated
1656 into 7 µM or 5 µM, respectively, of TCIP3. For ternary titrations, 20x 6xHis-p300^{BD} was
1657 incubated with 1x TCIP3 in the cell to drive saturation of the binary complex, followed by
1658 a titration of 10x BCL6^{BTB} from the syringe, at 310 rpm stirring at 25°C. The following
1659 concentrations were used in each run: 15 µM BCL6^{BTB}, 30 µM p300, and 1.5 µM TCIP3;
1660 18 µM BCL6^{BTB}, 36 µM 6xHis-p300^{BD}, and 1.8 µM TCIP3; or 10 µM BCL6^{BTB}, 20 µM
1661 6xHis-p300^{BD}, and 1 µM TCIP3. Alternatively, 20x BCL6^{BTB} was incubated with 1x TCIP3
1662 in the cell to drive saturation of the binary complex, followed by a titration of 10x 6xHis-
1663 p300^{BD} from the syringe, at 310 rpm stirring at 25°C. The following concentrations were
1664 used in each run: 30 µM BCL6, 15 µM 6xHis-p300^{BD}, and 1.5 µM TCIP3; 20 µM BCL6
1665 ^{BTB}, 10 µM 6xHis-p300^{BD}, and 1 µM TCIP3; or 40 µM BCL6^{BTB}, 20 µM 6xHis-p300^{BD}, and
1666 2 µM TCIP3. The first one or two injections and outliers from instrument noise were
1667 routinely excluded. Data were fit to a one-site model using MicroCal LLC Origin software.
1668 The following injection parameters were used for each run: (Total injection number: 35;
1669 Cell temp: 25 °C; Ref power: 10; Initial delay: 250 s; stirring speed: 310; Feedback mode:
1670 High; volume: 8 µL; Duration: 13.7 s; Filter period: 2; initial injection volume: 2 µL).
1671

1672 **nanoBRET**

1673 *BCL6^{BTB} nanoBRET*: The construct for NanoLuciferase(NanoLuc)-tagged BCL6^{BTB} was
1674 created as follows in a lentiviral construct: an N-terminal NanoLuc (subcloned from
1675 pNLSF-1, Promega N1351) was fused to the BTB domain of human BCL6 (Uniprot:
1676 P41182; aa1-129) with an internal GSG linker followed by a V5 tag. HEK293T cells were
1677 plated at a density of 6x10⁵ cells/mL in 2 mL of DMEM/well in a tissue culture treated 6-
1678 well plate and were allowed to incubate overnight at 37 °C. The next day, each well of
1679 cells was transfected with 2 ug of NanoLuc-BCL6^{BTB} (renamed pNSG218) using
1680 Lipofectamine 2000. The transfected cells were allowed to incubate overnight at 37 °C.
1681 The following day, the transfected cells were trypsinized, washed with PBS, counted with
1682 Trypan Blue, and brought to a final concentration of 1.25x10⁵ cells/mL in Fluorobrite
1683 DMEM (Gibco A1896701) supplemented with 10% FBS. 1 uM TNL-15 probe was added
1684 to the cells before plating 5000 cells per well in a volume of 40 uL per well in a 384-well
1685 plate. Control wells without the inclusion of TNL-15 probe were plated before its addition
1686 to the cells to be used as a negative control for data analysis. The plated cells were
1687 allowed to incubate overnight at 37 °C. The next day, the cells were treated with test
1688 compounds using a Tecan D300e Digital drug dispenser, normalized with DMSO, and
1689 allowed to incubate at 37 °C for 1 hour. After 1 h, 5 uL of NanoBRET NanoGlo Substrate
1690 plus Extracellular NanoLuc Inhibitor was added to each well (Promega N1661) and mixed
1691 on an orbital shaker at 200 g for 30 seconds. Data was then obtained using a PheraStar
1692 FS plate reader (BMG Labtech) measuring luminescence with 520-BP and 450-BP filters.
1693 Wells were normalized to treatment with DMSO.

1694

1695 *p300^{BD} and CBP^{BD} nanoBRET*: The constructs for NanoLuc-tagged p300^{BD} and CBP^{BD}
1696 were subcloned in pNLF-1 (Promega N1351) and created as follows: an N-terminal
1697 NanoLuc was fused to the bromodomains(BD) of human p300(Uniprot: Q09472; aa1040-
1698 1161) or human CBP (Uniprot: Q92793; aa1081-1197) with an internal GSSG linker.
1699 HEK293T cells were plated at a density of 6x10⁵ cells/mL in 2 mL of DMEM/well in a
1700 tissue culture treated 6-well plate and were allowed to incubate overnight at 37 °C. The
1701 next day, each well of cells was transfected with 2 ug of NanoLuc-p300^{BD} and NanoLuc-
1702 CBP^{BD} using Lipofectamine 2000. The transfected cells were allowed to incubate
1703 overnight at 37 °C. The following day, the transfected cells were trypsinized, washed with
1704 PBS, counted with Trypan Blue, and brought to a final concentration of 1.25x10⁵ cells/mL
1705 in Fluorobrite DMEM supplemented with 10% FBS. 100 nM of MNN-05-112 probe was
1706 added to the cells before plating 5000 cells per well in a volume of 40 uL per well in a
1707 384-well plate. Control wells without the inclusion of MNN-05-112 probe were plated
1708 before its addition to the cells as a negative control for data analysis. The plated cells
1709 were allowed to incubate overnight at 37 °C. The next day, the cells were treated with test
1710 compounds using a Tecan D300e Digital drug dispenser, normalized with DMSO, and
1711 allowed to incubate at 37 °C for 1 hour. After 1 h, 5 uL of NanoBRET NanoGlo Substrate
1712 plus Extracellular NanoLuc Inhibitor was added to each well and mixed on an orbital
1713 shaker at 200 g for 30 seconds. Data was then obtained using a PheraStarFS plate
1714 reader (BMG Labtech) measuring luminescence with 520-BP and 450-BP filters. Wells
1715 were normalized to treatment with DMSO.

1716

1717 For all NanoBRET assays, a dose-response curve with 3 technical replicates was
1718 constructed for each compound, and corrected BRET ratios were calculated according to
1719 manufacturer assay protocol (Promega TM439). Data was fit using a standard four
1720 parameter log-logistic function using the R package drc or using GraphPad Prism.
1721

1722 **Annexin V staining**

1723 25,000 cells were plated in 200 μ L of media in 96 well U-bottom plates and treated with
1724 compound. 72 hours later, the plate was spun at 500g for 4 minutes at 4°C, at which point
1725 cells were washed in 100 μ L cold 2.5% FBS in PBS. Centrifugation and washing was
1726 repeated once more. Cells were then resuspended in 50 μ L cold binding buffer (10 mM
1727 HEPES pH 7.4, 140 mM NaCl, 2.5 mM CaCl₂) and 2.5 μ L FITC-Annexin-V (Biolegend
1728 640922). A no-stain control was also included to draw gates. The plate was allowed to
1729 incubate for 15 minutes at room temperature, at which point 100 μ L of 2.5% FBS in PBS
1730 was added to each well. The plate was gently agitated through shaking, and samples
1731 were analyzed by flow cytometry on a BD Accuri. At least 50k events were collected per
1732 sample.
1733

1734 **Cell Cycle Analysis**

1735 2 million SUDHL5 cells were plated in 4 mL of media in 6-well plates and treated with 10
1736 nM of drug. After 22 hours, cells were dosed with 10 μ M 5-ethynyl-2'-deoxyuridine (EdU)
1737 and allowed to incubate for an additional 2 hours, at which point cells were harvested and
1738 collected by centrifuging at 300g for 4 minutes at 4°C. Cells were washed once with 1%
1739 BSA in PBS. 1.1 million cells in 1% BSA/PBS were then transferred to flow cytometry
1740 polypropylene tubes and centrifuged at 300g for 4 minutes at 4°C. Supernatant was
1741 removed, and cells were fixed for 15 minutes in the dark at room temperature with 100
1742 μ L of 4% PFA in PBS, in which gentle flicking was used to resuspend cells. Cells were
1743 then washed with 1 mL of 1% BSA/PBS and permeabilized with 100 μ L of 0.1% Triton-X
1744 for 30 minutes at room temperature in the dark. Cells were washed with 3 mL 1%
1745 BSA/PBS, then incubated in the dark for 30 minutes with a cocktail of AlexaFluor-488-
1746 Azide (438 μ L PBS, 10 μ L 100 mM CuSO₄, 2 μ L 488-azide, and 50 μ L of 1x EdU Reaction
1747 Buffer dissolved in water) (Invitrogen C10337). Cells were washed with 1 mL 1% BSA in
1748 PBS, then incubated with a reaction cocktail of 7-AAD/RNAseA for 30 minutes in the dark
1749 (500 μ L 1% BSA/PBS, 2 μ L 7-AAD (BD 559925), 5 μ L RNAseA (Invitrogen 12091021)).
1750 Cells were washed with 1 mL 1% BSA/PBS centrifuged a final time, then resuspended in
1751 500 μ L 1% BSA/PBS. Cells were gently agitated by shaking, then analyzed through flow
1752 cytometry on a BD Accuri. At least 100k events were collected per sample. Gates were
1753 drawn from single-stain and no-stain controls.
1754

1755 **TUNEL Analysis of DNA Fragmentation**

1756 1 million SUDHL5 cells were plated in 6 mL of media in 6-well plates and treated with
1757 compound for indicated timepoints and doses. 1.2 million total cells were counted,
1758 washed in PBS, fixed in 4% paraformaldehyde/PBS at a concentration of 10M/mL for 15
1759 minutes at room temperature in the dark, washed in PBS, and stored in 70% ethanol at -
1760 20°C until ready for processing (at least 24 hours). DNA breaks in fixed cells were labeled
1761 with bromolated deoxyuridine (Br-dUTP or BrdU) by incubation with deoxynucleotidyl
1762 transferase (TdT) for 60 min at 37°C, washed, and stained with FITC-labeled anti-BrdU

1763 antibodies for 30 min at room temperature in the dark (BD 556405). Cells were
1764 resuspended in 1% BSA/PBS with 1:100 RNaseA (Invitrogen 12091021) and co-stained
1765 with 7-AAD for 30 min at room temperature in the dark (BD 559925). The suspension was
1766 gently agitated by shaking and analyzed by flow cytometry within 1 hour (BD Accuri).
1767

1768 **BCL6 Reporter Assay**

1769 KARPAS422 cells were lentivirally transduced with a construct containing the reporter.
1770 Description of the reporter construct has been published previously³⁹. After selection,
1771 cells were plated and treated with indicated amount of compound for 24 hours. Cells were
1772 washed in 2.5% FBS/PBS, stained with 1:250 v/v of 7-AAD (BD 559925) to distinguish
1773 live from dead cells, and harvested for flow cytometry on a BD Accuri. Given the polyclonal
1774 population after transduction, the area under the curve of the histogram representing
1775 FITC signal across all live cells was calculated as an integrative measure of total GFP
1776 signal. A GFP-positive gate two standard deviations from the mean was drawn from non-
1777 transduced cells and the area past a constant threshold was calculated and normalized
1778 to the signal from cells treated with DMSO.
1779

1780 **Lentivirus Production and Overexpression**

1781 *c-MYC overexpression*: An N-terminal fusion of 3xFLAG followed by a GGSGS linker
1782 fused to the coding sequence of human *c-MYC* (NM_002467.6) was subcloned into
1783 pCW57-MCS1-2A-MCS2 (a gift from Adam Karpf (Addgene plasmid 71782 ;
1784 <http://n2t.net/addgene:71782> ; RRID:Addgene_71782)).

1785 *NanoLuc-BCL6^{BTB} overexpression*: This construct is the same used for BCL6 nanoBRET
1786 studies above. Lentivirus was produced from HEK293T cells via polyethylenimine
1787 transfection. Briefly, cells were transfected using 2nd-generation packaging plasmids and
1788 media replaced after 24 hours. Media containing virus 72 h after transfection was
1789 harvested, filtered, and used immediately or concentrated in PBS by ultracentrifugation
1790 (2 hours, 20,000 rpm, Beckman-Coulter Optima XE), flash-frozen, and stored at -80°C.
1791 Cells were lentivirally transduced with the overexpression construct by spinfection of virus
1792 (1000 g for 1 hour at 30°C) and selected using puromycin. Cells were maintained under
1793 antibiotic selection throughout experimental procedures.
1794

1795 **RNA Extraction, qPCR, and Sequencing Library Preparation**

1796 Cells were plated at 1M/mL and harvested in TRIsure (Bioline 38033). RNA was extracted
1797 using Direct-zol RNA MicroPrep columns (Zymo R2062) treated with DNaseI. cDNA was
1798 prepared (Meridian Bioscience BIO-65054) and used for qPCR (Meridian Bioscience BIO-
1799 94050) using an AppliedBiosystems QuantStudio 6Pro. Primer sequences were the
1800 following:

1801 *c-MYC* fwd: CCTTCTCTCCGTCCTCGGAT;
1802 *c-MYC* rev: CTTCTTGTTCCTCCTCAGAGTCG;
1803 *GAPDH* fwd: GCCAGCCGAGGCCACAT;
1804 *GAPDH* rev: CTTTACCAAGAGTTAAAGCAGCCC.

1805 For sequencing library preparation, rRNA was depleted (NEB E7400) and total RNA
1806 prepared into paired-end libraries (NEB E7765) and indexed (NEB E7335). Library size
1807 distributions were confirmed using an Agilent Bioanalyzer and High Sensitivity DNA

1808 reagents (Agilent 5067) and concentrations determined by qPCR. Equimolar pooled
1809 libraries were sequenced on an Illumina NovaSeq with 2 x 150 bp cycles.

1810

1811 **Acetyl-lysine and BCL6 Immunoprecipitation for Immunoblotting**

1812 Cells were plated at 1M/mL and treated with compound or DMSO at indicated timepoints
1813 and doses. Cells were harvested on ice, counted, normalized by count, and washed 1X
1814 in PBS containing compound or DMSO. For only BCL6 immunoprecipitation, compound
1815 or DMSO was maintained in nuclear preparation buffers at identical concentration to cell
1816 treatment throughout. Nuclei were prepared by incubation in Buffer A (25 mM HEPES pH
1817 7.5, 25 mM KCl, 0.05 mM EDTA, 1mM MgCl₂, 10% glycerol, 0.1% NP-40) supplemented
1818 with protease inhibitors (1 mM PMSF, ~20 mg/ml pepstatin, aprotinin, and leupeptin) at 4
1819 °C for 7 mins. Nuclear preparation was confirmed by Trypan blue staining and nuclei were
1820 pelleted by centrifugation for 5 min at 500g at 4 °C. Pelleted nuclei were resuspended in
1821 IP Buffer (25 mM HEPES pH 7.5, 150mM KCl, 0.05 mM EDTA, 1 mM MgCl₂, 10% glycerol,
1822 0.1% NP-40) supplemented with protease inhibitors and 1 µL/250 units benzonase
1823 (Sigma E1014). Chromatin was removed by incubation with rotation for 30 min and nuclei
1824 sheared using a 27-gauge needle exactly five times. Insoluble material was pelleted by
1825 centrifugation at 21,000g for 10 min at 4 °C and the supernatant containing soluble
1826 nuclear protein preserved. Extracts were normalized by total protein concentration
1827 (Bradford) and identical amounts of total protein and concentrations were used for
1828 immunoprecipitation. 1 µg acetylated-lysine antibodies (Cell Signaling 9441), anti-BCL6
1829 antibodies (Cell Signaling D65C10), or normal rabbit IgG (Cell Signaling 2729) and
1830 paramagnetic beads conjugated to Protein G (Thermo 10003D) were added to samples
1831 and incubated with rotation at 4 °C for 18 hours. Samples were washed five times with 1
1832 mL IP Buffer supplemented with protease inhibitors and eluted by denaturation in 1X
1833 NuPage LDS/RIPA sample buffer (Thermo NP0008) supplemented with beta-
1834 mercaptoethanol by incubation at 95 °C for 5 mins.

1835

1836 **Western Blots**

1837 Cells were plated at 1M/mL and treated with drug at indicated timepoints and doses. Cells
1838 were harvested on ice in RIPA buffer (50mM Tris-HCl pH 8, 150mM NaCl, 1% NP-40,
1839 0.1% DOC, 1% SDS, protease inhibitor cocktail (~20 mg/ml pepstatin, aprotinin, and
1840 leupeptin), 1mM DTT) and 1:200 benzonase (Sigma E1014) was added and incubated
1841 for 20 mins. After 10 min centrifugation at 14,000g and 4 °C, the supernatant was
1842 collected and protein concentration was measured by Bradford. SDS-PAGE analysis was
1843 carried out in either 4-12% or 12% Bis-Tris PAGE gels (Thermo NW04120 and
1844 NW04127). Antibodies used for immunoblots were: BCL6 (1:1000 v:v, Cell Signaling
1845 D65C10), p300 (1:250, Santa Cruz F-4 sc-48343), CBP (1:1000, Cell Signaling D6C5),
1846 c-MYC (1:1000, Cell Signaling D84C12), Caspase-3 (1:1000, Cell Signaling 9662),
1847 GAPDH (1:2000, Santa Cruz 6C5 sc-32233), BBC3/PUMA (1:1000, Cell Signaling
1848 E2P7G), FOXO3 (1:1000, Cell Signaling 75D8), H3K27ac (1:1000, abcam ab4729),
1849 H2BK20ac (1:1000, Cell Signaling D709W), H3 (1:10,000, Cell Signaling 1B1B2), H2B
1850 (1:10,000, Cell Signaling D2H6), p27/CDKN1B (1:1000, Cell Signaling D69C12), and
1851 TP53 (1:1000, Santa Cruz DO-1). ImageStudio (Licor) was used for blot imaging and
1852 quantification.

1853

1854 **Quantitative Global Proteome Profiling via LC-MS/MS**
1855 *Cell Treatment.* SUDHL5 cells (6M cells in 6 mL RPMI-1640 media supplemented with
1856 10% FBS and 1x pen-strep) were treated with 0.1% DMSO, 10 nM TCIP3, 10 nM Neg1,
1857 10 nM Neg2, or 250 nM dCBP1 (1000x stocks in DMSO for final 0.1% DMSO
1858 concentration) in 3 biologically independent replicates. The cells were washed twice with
1859 TBS (50 mM Tris, pH 8.5, and 150 mM NaCl) and then stored at -80 °C until use.
1860
1861 *Lysis & Digestion.* Lysis was performed by first thermally denaturing the samples in
1862 residual wash buffer for 5 min at 95 °C. Fresh Lysis Buffer (8 M urea, 150 mM NaCl, and
1863 100 mM HEPES, pH 8.0, in MS-grade water) was then added, and the lysates were
1864 homogenized using needle ultrasonication and then normalized to 30 µg of 2 mg/mL by
1865 diluting with Lysis Buffer via a Bradford protein concentration assay (Bio-Rad 5000006)
1866 in technical duplicates. The samples were then reduced and alkylated simultaneously by
1867 adding final concentrations of freshly prepared 10 mM tris(2-carboxyethyl)phosphine
1868 hydrochloride (TCEP; Sigma Aldrich C4706) and 40 mM chloroacetamide (CAM; Sigma
1869 Aldrich C0267) in 100 mM HEPES, pH 8.0, and shaking for 30-60 min. The samples were
1870 then diluted with 120 µL of 20 mM HEPES, pH 8.0, and CaCl₂ (Sigma Aldrich C4901) for
1871 final concentrations of ~1.3 M urea and 1 mM CaCl₂. Digestion using 1:100 (w/w)
1872 protease to protein lysate with MS-grade Trypsin/Lys-C Protease Mix (Thermo A40009)
1873 was then performed by mixing overnight at 37 °C. The samples were then acidified by
1874 adding trifluoroacetic acid (TFA) until the sample reached pH ≤ 3, as confirmed by pH
1875 paper.
1876
1877 *SPE Desalting.* Samples were then desalted using SOLA^μ SPE HRP Peptide Desalting
1878 columns (Thermo 60209-001) with a Positive Pressure Manifold and all MS-grade
1879 reagents. The desalting cartridges were activated with 200 µL of acetonitrile and then
1880 equilibrated with two washes of 200 µL Wash Buffer (2% ACN + 0.2% TFA in water). After
1881 loading samples into the cartridges, the samples were washed three times with 200 µL
1882 Wash Buffer and then eluted using 100 µL 50% acetonitrile with 0.1% formic acid (FA) in
1883 water. The desalted peptides were then immediately dried on a centrifugal vacuum
1884 concentrator (Thermo SPD120-115). The samples were then reconstituted in 0.1% FA in
1885 water and then analyzed by LC-MS/MS (see below).
1886
1887 **Generation of FLAG-BCL6 knock-in SUDHL5 cell lines**
1888 Construction of FLAG-BCL6 knock-in cell lines were adapted from previously described
1889 procedures (Savic et al. 2015, Meadows et al. 2020). Plasmid expressing wildtype Cas9
1890 under the control of chicken β-actin (CBA) and a human U6 promoter-driven gRNAs to
1891 direct were obtained from Addgene (PX458_BCL6_iso1_1 and PX458_BCL6_iso1_2
1892 were a gift from Eric Mendenhall & Richard M. Myers (plasmids #104046 and #104047;
1893 <http://n2t.net/addgene:104046> and <http://n2t.net/addgene:104047>;
1894 RRID:Addgene_104046 and 104047, respectively). gRNAs were designed to direct Cas9
1895 nuclease activity near the stop codon of *BCL6*. The donor plasmid contained a 3x FLAG
1896 epitope tag, P2A linker, and a Neomycin resistance gene, flanked by regions homologous
1897 to the C-terminus of the *BCL6* gene.
1898

1899 SUDHL5 cells were electroporated with donor and gRNA plasmids in a cuvette using the
1900 Amaxa™ Cell Line Nucleofector™ Kit V (Lonza, VVCA-1003) and Amaxa™
1901 Nucleofector™ II transfection machine. 2 million cells were resuspended in Nucleofector
1902 solution containing supplement with 10 µg pooled plasmid (5 µg donor plasmid and 2.5
1903 µg of each gRNA). This was done in biological triplicate (i.e. three separate
1904 electroporations performed), with cells from each electroporation maintained
1905 independently thereafter. Immediately after electroporation, cells were transferred to
1906 culture flask containing pre-warmed culture media. 24 hours post-transfection, cells were
1907 selected with G418 (Geneticin) at a concentration of 800 µg/mL. Selection was performed
1908 for 7 days. Cells were maintained under selection as a polyclonal pool for the generation
1909 of cell stocks. Subsequently, single clones were isolated by limiting dilution. To validate
1910 homologous recombination, genomic DNA from FLAG-BCL6 SUDHL5 cells was isolated
1911 using DNeasy Blood and Tissue kit (Qiagen, 69504). The C-terminus of the BCL6 gene
1912 was amplified using Q5 Hot Start High Fidelity 2X Master Mix (NEB M0494) with primers
1913 that bind internal to the 3x Flag tag and external to the homologous arms. The PCR
1914 product was purified using QIAquick PCR Purification Kit (Qiagen) and submitted for
1915 Sanger sequencing.
1916

1917 **FLAG and p300 Immunoprecipitation**

1918 50 million FLAG-BCL6 knock-in SUDHL5 cells were treated compound or DMSO (0.1%)
1919 at indicated doses for 2 hours. Cells were lysed in NE10 buffer (20 mM HEPES (pH 7.5),
1920 10 mM KCl, 1 mM MgCl₂, 0.1% Triton X-100 (v/v), protease inhibitors (Roche), 15 mM β-
1921 mercaptoethanol), dounced 15 times and pelleted 5 min at 500 g. Nuclei were washed in
1922 NE10 buffer and then digested with 250 units benzonase (Millipore) for 30 min rotating at
1923 25°C. Nuclei were resuspended in NE150 buffer (NE10 supplemented with 150mM NaCl)
1924 and incubated for 20 min. Lysates were pelleted at 16,000 g for 20 min at 4°C and
1925 supernatants were immunoprecipitated by incubating with 2.5 µg FLAG M2 antibody
1926 (F1804, Millipore-Sigma) or 2.5 µg p300 (A300-358A, Bethyl Laboratories) antibody with
1927 Dynabeads Protein G (Thermo Fisher) overnight at 4°C. The IP fraction was recovered
1928 by magnetic separation followed by three washes with NE10 buffer containing 150mM–
1929 300mM NaCl but without Triton-X. For mass spectrometry analysis, the IP was then eluted
1930 from the beads with Ammonium Hydroxide, pH 11-12; 3% v/v.
1931

1932 **Immunoprecipitation-Mass Spectrometry (IP-MS)**

1933 Immunoprecipitation was performed as described above for FLAG-BCL6 and p300 in
1934 three biologically independent replicates. Enriched proteins were eluted three times with
1935 150 µL of 3% v/v ammonium hydroxide (pH 11-12) for 15 min with gentle agitation. The
1936 collected eluate was then dried using a centrifugal vacuum concentrator (Thermo
1937 SPD120-115). The samples were reconstituted in 50 µL of reduction-alkylation buffer
1938 containing 8 M urea, 10 mM TCEP, 40 mM chloroacetamide, 4.4 mM CaCl₂, and 100 mM
1939 HEPES, pH 8.0 and then incubated for at least 30 min while shaking. The samples were
1940 then diluted with 160 µL of 20 mM HEPES, pH 8.0, and then digested overnight at 37 °C
1941 with 500 ng of MS-grade Trypsin/Lys-C Protease Mix (50 ng/µL). The samples were then
1942 acidified by adding trifluoroacetic acid (TFA) until the sample reached pH ≤ 3, as
1943 confirmed by pH paper.
1944

1945 **LC-MS/MS diaPASEF Acquisition & Statistical Analysis**

1946 *diaPASEF LC-MS/MS Analysis.* The reconstituted desalted peptides were then analyzed
1947 using a nanoElute 2 UHPLC (Bruker Daltonics, Bremen, Germany) coupled to a timsTOF
1948 HT (Bruker Daltonics, Bremen, Germany) via a CaptiveSpray nano-electrospray source.
1949 The peptides were separated in the UHPLC using an Aurora Ultimate nanoflow UHPLC
1950 column with CSI fitting (25 cm x 75 μ m ID, 1.7 μ m C18; IonOptics AUR3-25075C18-CSI)
1951 over a 70 min gradient shown in the table below at a flow rate of 400 nL/min with column
1952 temperature maintained at 50 °C using Mobile Phase A (MPA; 3% acetonitrile + 0.1% FA
1953 in water) and Mobile Phase B (MPB; 0.1% FA in ACN).

Time (min)	Composition % (v/v)
0	6
40	17
55	25
64	34
65	85
70	92

1954

1955

1956 The TIMS elution voltages were calibrated linearly with three points (Agilent ESI-L Tuning
1957 Mix Ions; 622, 922, 1,222 m/z) to determine the reduced ion mobility coefficients (1/K₀).
1958 diaPASEF was performed using the MS settings 100 m/z for Scan Begin and 1700 m/z
1959 for Scan End in positive mode, the TIMS settings 0.70 V·s/cm² for 1/K₀ start, 1.30 V·s/cm²
1960 for 1/K₀ end, ramp time of 120.0 ms, 100% duty cycle, ramp rate of 7.93 Hz, and the
1961 capillary voltage set to 1600 V. diaPASEF windows from mass range 226.8 Da to 1226.8
1962 Da and mobility range 0.70 1/K₀ to 1.30 1/K₀ were designed to provide 25 Da windows
1963 covering doubly and triply charged peptides as confirmed by DDA-PASEF scans,
1964 whereas singly charged peptides were excluded from the acquisition due to their position
1965 in the m/z-ion mobility plane.

1966

1967 *Raw data processing.* The raw diaPASEF files were processed using library-free analysis
1968 in FragPipe 22.0. DIA spectrum deconvolution was performed using diaTracer 1.1.5 with
1969 the following default settings: (i) “Delta Apex IM” to 0.01, (ii) “Delta Apex RT” to 3, (iii) “RF
1970 max” to 500, (iv) “Corr threshold” to 0.3, and (v) mass defect filter enabled with offset set
1971 to 0.1. The reviewed Homo sapiens protein sequence database was obtained from
1972 UniProt (07/13/2024; 20,468 entities) with decoys and common contaminants. In the MS
1973 Fragger 4.1 database search, the following settings were used: (i) initial precursor and
1974 fragment mass tolerances of 10 ppm and 20 ppm, respectively, (ii) enabled spectrum
1975 deisotoping, mass calibration, and parameter optimization, and (iii) isotope error set to
1976 “0/1/2”. For protein digestion, “stricttrypsin” for fully tryptic peptides was enabled with up
1977 to 1 missed cleavage, peptide length from 7 to 50, and peptide mass range from 500 to
1978 5,000 Da. For modifications, methionine oxidation (2 max occurrences) and N-terminal
1979 acetylation (1 max occurrence) were set as variable modifications (maximum up to 3),
1980 while cysteine carbamidomethylation was set as a fixed modification. For validation,
1981 MSBooster (DIA-NN model) and Percolator were used for RT and MS/MS spectra
1982 prediction and PSM rescoring, while ProteinProphet (--maxppmdiff 2000000) was used

1983 for protein inference with FDR filtering (--picked --prot 0.01). The spectral library was then
1984 generated by EasyPQP 0.1.49 using default settings. Peptides were then quantified using
1985 DIA-NN 1.9.1 with 0.1% FDR and QuantUMS high accuracy settings. The DIA-NN
1986 parquet report containing peptide quantification and scoring was then analyzed in R.
1987

1988 *Statistical Analysis.* DIA-NN quantified peptides were then further filtered including (i)
1989 common contaminants and reverse sequences, (ii) 1% FDR filtering at the global.q.value
1990 (precursor Q value across all samples) and pg.q.value (protein group Q value in single
1991 injection), (iii) quantification of a given peptide in at least two replicates in one condition,
1992 and (iv) removal of singly charged peptides and non-proteotypic (unique) peptides.
1993 Protein intensities were then re-calculated using the MaxLFQ method¹⁰⁹ provided in the
1994 DIA-NN R package. Differential statistics was then performed using the DEqMS¹¹⁰ R
1995 package, which performs a LIMMA-moderated t-test with an adjustment for number of
1996 detected peptides per protein, to determine the p-value, fold change, and Benjamini-
1997 Hochberg adjusted p-value. For the mean peptide intensity plots, the arithmetic mean
1998 was calculated for unique peptide precursors across conditions imputing a value of 1 unit
1999 for replicates where a peptide was not detected. For protein-level imputation in IP-MS,
2000 proteins were selected for imputation if (i) a fold change using DEqMS differential
2001 statistics could not be calculated and (ii) the protein was not detected in DMSO condition
2002 at all but detected in at least all but one replicate in the compound-treated condition.
2003 Selected proteins had imputed 15th percentile MaxLFQ protein intensities for the DMSO
2004 condition and the subsequent fold changes between DMSO and compound conditions
2005 were recalculated.
2006

2007 **RNA-seq Analysis**

2008 Raw reads were checked for quality using fastqc
2009 (<https://www.bioinformatics.babraham.ac.uk/projects/fastqc/>) and trimmed from adapters
2010 using cutadapt¹¹¹ using parameters cutadapt -a
2011 AGATCGGAAGAGCACACGTCTGAAGTCAGTCA -b
2012 AGATCGGAAGAGCGTCGTAGGGAAAGAGTGT --nextseq-trim=20 --minimum-
2013 length 1. Transcripts were quantified using kallisto¹¹² against the human Gencode v33
2014 indexed transcriptome and annotations. Transcript isoforms were collapsed to genes and
2015 differential gene analysis was performed using DESeq2¹¹³ using aperglm¹¹⁴ to shrink fold
2016 changes. Pathway analyses were performed using Enrichr¹¹⁵ on genes defined by
2017 significance cutoffs as detailed in figure legends. GSEA analysis was performed using
2018 fgsea¹¹⁶ on differential genes ranked by log₂(fold change) with an in-house dataset
2019 consisting of LymphDB (L. Staudt, NIH, <https://lymphochip.nih.gov/signaturedb/>),
2020 MSigDB pathways, and an internal dataset generated at MD Anderson of lymphoma-
2021 specific signaling. Correlation analyses with ChIP-seq used only genes with normalized
2022 (using DESeq2¹¹³, relative log expression (RLE)) mean expression ≥ 32 ; this number was
2023 chosen by automatic independent filtering for outlier and low mean counts¹¹³. Unbiased
2024 clustering analyses with TCIP1³⁹ and CDK-TCIP1⁴⁰ were performed using pheatmap¹¹⁷
2025 using parameters cutree_cols = 6, cutree_rows=2 including only significantly changed
2026 genes in any of the treatment conditions ($|\log_2(\text{fold change})| \geq 0.5$ and adj. $P \leq 0.05$; P -
2027 values computed by two-sided Wald test and adjusted by Benjamini-Hochberg). Re-
2028 processed published datasets from the Sequence Read Archive (SRA) were the following:

2029 TCIP1 – SRX20228454, SRX20228455, SRX20228456, SRX20228457,
2030 SRX20228458, SRX20228459, SRX20228448, SRX20228449, SRX20228450; CDK-
2031 TCIP1 – SRX22117221, SRX22117222, SRX22117223, SRX22117224, SRX22117225,
2032 SRX22117226, SRX22117227, SRX22117228, SRX22117229).

2033

2034 ChIP-seq Experiment and Library Preparation

2035 25-30 million cells were treated with TCIP3 or DMSO for indicated timepoints. Cells were
2036 washed in PBS containing TCIP3 or DMSO and crosslinked for 11 min in CiA Fix Buffer
2037 (50 mM HEPES pH 8.0, 1 mM EDTA, 0.5 mM EGTA, 100 mM NaCl) with addition of
2038 formaldehyde to a final concentration of 1%. The crosslinking reaction was quenched by
2039 glycine added at 0.125 M final concentration. Crosslinked cells were centrifuged at 1,000
2040 x g for 5 min. Nuclei were prepared by 10 min incubation of resuspended pellet in CiA
2041 NP-Rinse 1 buffer (50 mM HEPES pH 8.0, 140 mM NaCl, 1 mM EDTA, 10% glycerol,
2042 0.5% IPEGAL CA-630, 0.25% Triton X100) followed by wash in CiA NP-Rinse 2 buffer
2043 (10 mM Tris pH 8.0, 1 mM EDTA, 0.5 mM EGTA, 200 mM NaCl). The pellet was
2044 resuspended in CiA Covaris Shearing Buffer (0.1% SDS, 1 mM EDTA pH 8.0, 10 mM Tris
2045 HCl pH 8.0) with protease inhibitors and sonicated for 20 min with a Covaris E220
2046 sonicator (Peak Power 140, Duty Factor 5.0, Cycles/Burst 200). The distribution of
2047 fragments was confirmed with D1000 Tapestation or by agarose gel electrophoresis. 20
2048 µg of chromatin per ChIP was used with anti-H3K27ac antibodies (abcam ab4729) and
2049 anti-H2Bk20ac antibodies (Cell Signaling D709W), with 40 ng Drosophila chromatin
2050 (53083, ActiveMotif) spiked in. After overnight incubation at 4 °C in IP buffer (50 mM
2051 HEPES pH 7.5, 300mM NaCl, 1mM EDTA, 1% Triton X100, 0.1% sodium deoxycholic
2052 acid salt (DOC), 0.1% SDS), IPs were washed twice with IP buffer, once with DOC buffer
2053 (10 mM Tris pH 8, 0.25 M LiCl, 0.5% IPEGAL CA-630, 0.5% sodium deoxycholic acid salt
2054 (DOC), 1mM EDTA), and once with 10 mM Tris/1 mM EDTA buffer (TE) pH 8. IPs and
2055 inputs were reverse-crosslinked in TE/0.5% SDS/0.5 µg/µL proteinase K for 55 °C /3
2056 hours then 65 °C /18 hours, then DNA was purified using a PCR cleanup spin column
2057 (Takara #74609). Paired-end sequencing libraries were constructed using an NEBNext
2058 Ultra II DNA kit (E7645S) and indexed (NEB E7335). Library size distributions were
2059 confirmed using an Agilent Bioanalyzer and High Sensitivity DNA reagents (Agilent 5067)
2060 and concentrations determined by qPCR. Equimolar pooled libraries were sequenced on
2061 an Illumina NovaSeq XPlus with 2 x 150 bp cycles.

2062

2063 CUT&RUN Experiment and Library Preparation

2064 CUT&RUN was performed as previously described^{118,119} with minor modifications. Briefly,
2065 cells were collected and washed by PBS. After final wash, nuclei were isolated using
2066 nuclei extraction buffer (20mM HEPES pH 7.9, 10 mM KCl, 0.1% Triton X-100, 20%
2067 glycerol, 1x cOmplete protease inhibitors (Roche 11836153001), 0.5mM spermidine) and
2068 then washed twice with wash buffer (20mM HEPES pH 7.5, 150mM NaCl, 0.5mM
2069 Spermidine, 1x cOmplete protease inhibitor). Five-hundred thousand nuclei were counted
2070 and incubated with activated Concanavalin A coated beads (EpiCypher 21-1411) and
2071 subsequently mixed with BCL6 antibodies (Cell Signaling D65C10) in antibody buffer
2072 (wash buffer + 0.01% digitonin + 2 mM EDTA) for overnight incubation on nutator in a
2073 cold room. IgG controls (normal rabbit IgG, Cell Signaling 2729) were set in parallel for
2074 antibody enrichment and specificity validation. Nuclei were then washed three times with

2075 digitonin buffer (wash buffer + 0.01% digitonin) and incubated with pAG-MNase
2076 (EpiCypher 15-1116) for 10 minutes at room temperature. After 10 minutes of incubation,
2077 nuclei were washed three times again with digitonin buffer and resuspended with
2078 prechilled low-salt, high-Ca²⁺ buffer (20 mM HEPES pH 7.5, 0.5mM spermidine, 1x
2079 cComplete protease inhibitor, 10mM CaCl₂) to initiate 1-hour digestion at 0°C using an ice
2080 block. The reaction was terminated by switching into stop buffer (340 mM NaCl, 20mM
2081 EDTA, 4 mM EGTA, 50 µg/mL RNaseA, 50 µg/mL glycogen) and incubating at 37°C for
2082 10 minutes to release digested DNA from the nuclei. DNA was then purified with Ampure
2083 beads (Beckman A63882), subjected to two-sided size selection(0.5X to remove large
2084 fragment and 2X to recover desired nucleosomal DNA fragments). Sequencing libraries
2085 were generated with KAPA Hyper Prep Kits (Roche KK8502) using 14 cycles of PCR
2086 amplification. Libraries were validated on a Tapestation 4200 (Agilent G2991BA),
2087 quantified by Qubit High Sensitivity dsDNA Kit (Life Technologies Q32854), multiplexed
2088 and sequenced on a NovaSeq6000 using 2x 100 bp cycles.
2089

2090 ChIP-seq and CUT&RUN Analysis

2091 The data quality was checked using fastq
2092 (<https://www.bioinformatics.babraham.ac.uk/projects/fastqc/>). The raw reads were
2093 trimmed from adapters with cutadapt (parameters: -a
2094 AGATCGGAAGAGCACACGTCTGAAGTCCAGTCA -A
2095 AGATCGGAAGAGCGTCGTAGGGAAAGAGTGT) and raw reads were aligned to
2096 hg38 human genome assembly using bowtie2 (parameters: --local --maxins 1000). Low
2097 quality reads, duplicated reads and reads with multiple alignments were removed using
2098 samtools¹²⁰ and Picard (<https://broadinstitute.github.io/picard/>). macs2¹²¹ was used to
2099 map position of peaks with FDR cutoff of 0.05. Bedtools¹²² was used to find a consensus
2100 set of peaks by merging peaks across multiple conditions (bedtools merge), count number
2101 of reads in peaks (bedtools intersect -c) and generate genome coverage (bedtools
2102 genomecov -bga). deepTools¹²³ was used to generate coverage densities across multiple
2103 experimental conditions (deeptools computeMatrix and deeptools plotProfile) and to
2104 generate bigwig files (deeptools bamCoverage), where reads mapping to ENCODE
2105 blacklist regions were excluded¹²⁴. All browser tracks and metaprofiles shown were
2106 calculated with sequence-depth-normalized, replicate-merged (bigWigMerge¹²⁵) and, for
2107 ChIP-seq, input-subtracted data (deeptools bigWigCompare). Tracks were plotted using
2108 trackplot¹²⁶. Peak differential analysis and PCA analysis was performed using DESeq2¹¹³
2109 using apeglm¹¹⁴ to shrink fold changes across relevant peaksets. Overlap analyses were
2110 performed using valr¹²⁷. Enhancers were annotated using ROSE¹¹ by stitching together
2111 H3K27ac peaks in untreated cells within 12.5 kb but excluding regions within 2 kb of a
2112 transcription start site unless within a larger H3K27ac domain. For analyses of differential
2113 changes at enhancers, only read counts across annotated enhancers were considered in
2114 the peakset input to DESeq2. Peaks and enhancers were assigned first to their nearest
2115 gene by simple linear distance and manually annotated as needed from literature.
2116

2117 Predicting KAT-TCIP Linker Length:

2118 LigPrep (Shrodinger Maestro 13.8) was performed on all KAT-TCIPs. The following
2119 settings were used: Force Field OPLS4, Ionization (Generate possible states at target
2120 pH: 7.00 ± 2.00), Epik Classic, Desalt, Generate Tautomers, Retain Specific Chiralities,

2121 Generate at Most 32 poses per ligand. The distance between the carbons within the
2122 amide bonds of each linker was measured. The average of the two or three lowest energy
2123 conformations was recorded.

2124

2125 **Chemical Synthesis:** See **Supplemental File 1**, Chemical Synthesis and
2126 Characterization.

2127

2128

2129

2130

2131

2132

2133

2134

2135

2136

2137

2138

2139

2140

2141

2142

2143

2144

2145

2146

2147

2148

2149

2150

2151

2152

2153

2154

2155

2156

2157

2158

2159

2160

2161

2162

2163

2164

2165

2166

2167 REFERENCES

- 2168
- 2169 1. Shaima, N. (1997). The p300/CBP family: integrating signals with transcription
2170 factors and chromatin. *Trends Cell Biol* 7, 230-236. 10.1016/S0962-
2171 8924(97)01048-9.
- 2172 2. Merika, M., Williams, A.J., Chen, G., Collins, T., and Thanos, D. (1998).
2173 Recruitment of CBP/p300 by the IFN beta enhanceosome is required for
2174 synergistic activation of transcription. *Mol Cell* 1, 277-287. 10.1016/s1097-
2175 2765(00)80028-3.
- 2176 3. Wang, Z., Zang, C., Cui, K., Schones, D.E., Barski, A., Peng, W., and Zhao, K.
2177 (2009). Genome-wide mapping of HATs and HDACs reveals distinct functions in
2178 active and inactive genes. *Cell* 138, 1019-1031. 10.1016/j.cell.2009.06.049.
- 2179 4. Bannister, A.J., and Kouzarides, T. (1996). The CBP co-activator is a histone
2180 acetyltransferase. *Nature* 384, 641-643.
- 2181 5. Ogryzko, V.V., Schiltz, R.L., Russanova, V., Howard, B.H., and Nakatani, Y.
2182 (1996). The transcriptional coactivators p300 and CBP are histone
2183 acetyltransferases. *Cell* 87, 953-959.
- 2184 6. Weinert, B.T., Narita, T., Satpathy, S., Srinivasan, B., Hansen, B.K., Scholz, C.,
2185 Hamilton, W.B., Zucconi, B.E., Wang, W.W., Liu, W.R., et al. (2018). Time-
2186 Resolved Analysis Reveals Rapid Dynamics and Broad Scope of the CBP/p300
2187 Acetylome. *Cell* 174, 231-244 e212. 10.1016/j.cell.2018.04.033.
- 2188 7. Dancy, B.M., and Cole, P.A. (2015). Protein lysine acetylation by p300/CBP.
2189 *Chem Rev* 115, 2419-2452. 10.1021/cr500452k.
- 2190 8. Iyer, N.G., Ozdag, H., and Caldas, C. (2004). p300/CBP and cancer. *Oncogene*
2191 23, 4225-4231. 10.1038/sj.onc.1207118.
- 2192 9. Tsang, F.H., Law, C.T., Tang, T.C., Cheng, C.L., Chin, D.W., Tam, W.V., Wei, L.,
2193 Wong, C.C., Ng, I.O., and Wong, C.M. (2019). Aberrant Super-Enhancer
2194 Landscape in Human Hepatocellular Carcinoma. *Hepatology* 69, 2502-2517.
2195 10.1002/hep.30544.
- 2196 10. Loven, J., Hoke, H.A., Lin, C.Y., Lau, A., Orlando, D.A., Vakoc, C.R., Bradner,
2197 J.E., Lee, T.I., and Young, R.A. (2013). Selective inhibition of tumor oncogenes
2198 by disruption of super-enhancers. *Cell* 153, 320-334. 10.1016/j.cell.2013.03.036.
- 2199 11. Whyte, W.A., Orlando, D.A., Hnisz, D., Abraham, B.J., Lin, C.Y., Kagey, M.H.,
2200 Rahl, P.B., Lee, T.I., and Young, R.A. (2013). Master transcription factors and
2201 mediator establish super-enhancers at key cell identity genes. *Cell* 153, 307-319.
2202 10.1016/j.cell.2013.03.035.
- 2203 12. Giotopoulos, G., Chan, W.I., Horton, S.J., Ruau, D., Gallipoli, P., Fowler, A.,
2204 Crawley, C., Papaemmanuil, E., Campbell, P.J., Gottgens, B., et al. (2016). The
2205 epigenetic regulators CBP and p300 facilitate leukemogenesis and represent
2206 therapeutic targets in acute myeloid leukemia. *Oncogene* 35, 279-289.
2207 10.1038/onc.2015.92.
- 2208 13. Waddell, A.R., Huang, H., and Liao, D. (2021). CBP/p300: Critical Co-Activators
2209 for Nuclear Steroid Hormone Receptors and Emerging Therapeutic Targets in
2210 Prostate and Breast Cancers. *Cancers (Basel)* 13. 10.3390/cancers13122872.
- 2211 14. Zhao, D., Fukuyama, S., Sakai-Tagawa, Y., Takashita, E., Shoemaker, J.E., and
2212 Kawaoka, Y. (2015). C646, a Novel p300/CREB-Binding Protein-Specific Inhibitor

- 2213 of Histone Acetyltransferase, Attenuates Influenza A Virus Infection. *Antimicrob*
2214 *Agents Chemother* 60, 1902-1906. 10.1128/AAC.02055-15.
- 2215 15. Lasko, L.M., Jakob, C.G., Edalji, R.P., Qiu, W., Montgomery, D., Digiammarino,
2216 E.L., Hansen, T.M., Risi, R.M., Frey, R., Manaves, V., et al. (2017). Discovery of a
2217 selective catalytic p300/CBP inhibitor that targets lineage-specific tumours.
2218 *Nature* 550, 128-132. 10.1038/nature24028.
- 2219 16. Armstrong, A.J., Gordon, M.S., Reimers, M.A., Sedkov, A., Lipford, K., Snavely-
2220 Merhaut, J., Kumar, S., Guichard, S.M., and Shore, N. (2021). The Courage
2221 study: A first-in-human phase 1 study of the CBP/p300 inhibitor FT-7051 in men
2222 with metastatic castration-resistant prostate cancer. *Journal of Clinical Oncology*
2223 39. 10.1200/JCO.2021.39.15_suppl.TPS5085.
- 2224 17. Joy, S.T., Henley, M.J., De Salle, S.N., Beyersdorf, M.S., Vock, I.W., Huldin,
2225 A.J.L., and Mapp, A.K. (2021). A Dual-Site Inhibitor of CBP/p300 KIX is a
2226 Selective and Effective Modulator of Myb. *J Am Chem Soc* 143, 15056-15062.
2227 10.1021/jacs.1c04432.
- 2228 18. Wilson, J.E., Patel, G., Patel, C., Brucelle, F., Huhn, A., Gardberg, A.S., Poy, F.,
2229 Cantone, N., Bommi-Reddy, A., Sims, R.J., 3rd, et al. (2020). Discovery of CPI-
2230 1612: A Potent, Selective, and Orally Bioavailable EP300/CBP Histone
2231 Acetyltransferase Inhibitor. *ACS Med Chem Lett* 11, 1324-1329.
2232 10.1021/acsmedchemlett.0c00155.
- 2233 19. Stanton, B.Z., Chory, E.J., and Crabtree, G.R. (2018). Chemically induced
2234 proximity in biology and medicine. *Science* 359. 10.1126/science.aa05902.
- 2235 20. Nalawansha, D.A., and Crews, C.M. (2020). PROTACs: An Emerging
2236 Therapeutic Modality in Precision Medicine. *Cell Chem Biol* 27, 998-1014.
2237 10.1016/j.chembiol.2020.07.020.
- 2238 21. Ho, S., Clipstone, N., Timmermann, L., Northrop, J., Graef, I., Fiorentino, D.,
2239 Nourse, J., and Crabtree, G.R. (1996). The mechanism of action of cyclosporin A
2240 and FK506. *Clin Immunol Immunopathol* 80, S40-45. 10.1006/clin.1996.0140.
- 2241 22. Liu, J., Farmer, J.D., Jr., Lane, W.S., Friedman, J., Weissman, I., and Schreiber,
2242 S.L. (1991). Calcineurin is a common target of cyclophilin-cyclosporin A and
2243 FKBP-FK506 complexes. *Cell* 66, 807-815.
- 2244 23. Schreiber, S.L. (2021). The Rise of Molecular Glues. *Cell* 184, 3-9.
2245 10.1016/j.cell.2020.12.020.
- 2246 24. Choi, J., Chen, J., Schreiber, S.L., and Clardy, J. (1996). Structure of the
2247 FKBP12-Rapamycin Complex Interacting with the Binding Domain of Human
2248 FRAP. *Science* 273, 239-242.
- 2249 25. Banaszynski, L.A., Liu, C.W., and Wandless, T.J. (2005). Characterization of the
2250 FKBP.rapamycin.FRB ternary complex. *J Am Chem Soc* 127, 4715-4721.
2251 10.1021/ja043277y.
- 2252 26. Schreiber, S.L. (2024). Molecular glues and bifunctional compounds: Therapeutic
2253 modalities based on induced proximity. *Cell Chem Biol* 31, 1050-1063.
2254 10.1016/j.chembiol.2024.05.004.
- 2255 27. Luo, J., Chen, Z., Qiao, Y., Tien, J.C., Young, E., Mannan, R., Mahapatra, S., He,
2256 T., Eyunni, S., Zhang, Y., et al. (2024). p300/CBP degradation is required to
2257 disable the active AR enhanceosome in prostate cancer. *bioRxiv*.
2258 10.1101/2024.03.29.587346.

- 2259 28. Chen, Z., Wang, M., Wu, D., Zhao, L., Metwally, H., Jiang, W., Wang, Y., Bai, L.,
2260 McEachern, D., Luo, J., et al. (2024). Discovery of CBPD-409 as a Highly Potent,
2261 Selective, and Orally Efficacious CBP/p300 PROTAC Degrader for the Treatment
2262 of Advanced Prostate Cancer. *J Med Chem* 67, 5351-5372.
2263 10.1021/acs.jmedchem.3c01789.
- 2264 29. Thomas, J.E., 2nd, Wang, M., Jiang, W., Wang, M., Wang, L., Wen, B., Sun, D.,
2265 and Wang, S. (2023). Discovery of Exceptionally Potent, Selective, and
2266 Efficacious PROTAC Degraders of CBP and p300 Proteins. *J Med Chem* 66,
2267 8178-8199. 10.1021/acs.jmedchem.3c00492.
- 2268 30. Vannam, R., Sayilgan, J., Ojeda, S., Karakyriakou, B., Hu, E., Kreuzer, J., Morris,
2269 R., Herrera Lopez, X.I., Rai, S., Haas, W., et al. (2021). Targeted degradation of
2270 the enhancer lysine acetyltransferases CBP and p300. *Cell Chem Biol* 28, 503-
2271 514 e512. 10.1016/j.chembiol.2020.12.004.
- 2272 31. Chiarella, A.M., Butler, K.V., Gryder, B.E., Lu, D., Wang, T.A., Yu, X., Pomella, S.,
2273 Khan, J., Jin, J., and Hathaway, N.A. (2020). Dose-dependent activation of gene
2274 expression is achieved using CRISPR and small molecules that recruit
2275 endogenous chromatin machinery. *Nat Biotechnol* 38, 50-55. 10.1038/s41587-
2276 019-0296-7.
- 2277 32. Chen, L.Y., Singha Roy, S.J., Jadhav, A.M., Wang, W.W., Chen, P.H., Bishop, T.,
2278 Erb, M.A., and Parker, C.G. (2024). Functional Investigations of p53 Acetylation
2279 Enabled by Heterobifunctional Molecules. *ACS Chem Biol* 19, 1918-1929.
2280 10.1021/acschembio.4c00438.
- 2281 33. Chen, L.Y., Wang, W.W., Wozniak, J.M., and Parker, C.G. (2023). A
2282 heterobifunctional molecule system for targeted protein acetylation in cells.
2283 *Methods Enzymol* 681, 287-323. 10.1016/bs.mie.2022.08.014.
- 2284 34. Wang, W.W., Chen, L.Y., Wozniak, J.M., Jadhav, A.M., Anderson, H., Malone,
2285 T.E., and Parker, C.G. (2021). Targeted Protein Acetylation in Cells Using
2286 Heterobifunctional Molecules. *J Am Chem Soc* 143, 16700-16708.
2287 10.1021/jacs.1c07850.
- 2288 35. Taniguchi, J., Feng, Y., Pandian, G.N., Hashiya, F., Hidaka, T., Hashiya, K., Park,
2289 S., Bando, T., Ito, S., and Sugiyama, H. (2018). Biomimetic Artificial Epigenetic
2290 Code for Targeted Acetylation of Histones. *J Am Chem Soc* 140, 7108-7115.
2291 10.1021/jacs.8b01518.
- 2292 36. Kabir, M., Sun, N., Hu, X., Martin, T.C., Yi, J., Zhong, Y., Xiong, Y., Kaniskan,
2293 H.U., Gu, W., Parsons, R., and Jin, J. (2023). Acetylation Targeting Chimera
2294 Enables Acetylation of the Tumor Suppressor p53. *J Am Chem Soc* 145, 14932-
2295 14944. 10.1021/jacs.3c04640.
- 2296 37. Kabir, M., Hu, X., Martin, T.C., Pokushalov, D., Kim, Y.J., Chen, Y., Zhong, Y., Wu,
2297 Q., Chipuk, J.E., Shi, Y., et al. (2024). Harnessing the TAF1 Acetyltransferase for
2298 Targeted Acetylation of the Tumor Suppressor p53. *Adv Sci (Weinh)*, e2413377.
2299 10.1002/advs.202413377.
- 2300 38. Duffy, M.J., Tang, M., Rajaram, S., O'Grady, S., and Crown, J. (2022). Targeting
2301 Mutant p53 for Cancer Treatment: Moving Closer to Clinical Use? *Cancers*
2302 (Basel) 14. 10.3390/cancers14184499.
- 2303 39. Gourisankar, S., Krokhotin, A., Ji, W., Liu, X., Chang, C.Y., Kim, S.H., Li, Z.,
2304 Wenderski, W., Simanauskaitė, J.M., Yang, H., et al. (2023). Rewiring cancer

- 2305 drivers to activate apoptosis. *Nature* 620, 417-425. 10.1038/s41586-023-06348-
2306 2.
- 2307 40. Sarott, R.C., Gourisankar, S., Karim, B., Nettles, S., Yang, H., Dwyer, B.G.,
2308 Simanauskaitė, J.M., Tse, J., Abuzaid, H., Krokhotin, A., et al. (2024).
2309 Relocalizing transcriptional kinases to activate apoptosis. *Science* 386, eadl5361.
2310 10.1126/science.adl5361.
- 2311 41. Hatzi, K., and Melnick, A. (2014). Breaking bad in the germinal center: how
2312 deregulation of BCL6 contributes to lymphomagenesis. *Trends Mol Med* 20, 343-
2313 352. 10.1016/j.molmed.2014.03.001.
- 2314 42. Phan, R.T., and Dalla-Favera, R. (2004). The BCL6 proto-oncogene suppresses
2315 p53 expression in germinal-centre B cells. *Nature* 432, 635-639.
2316 10.1038/nature03147.
- 2317 43. Shaffer, A.L., Yu, X., He, Y., Boldrick, J., Chan, E.P., and Staudt, L.M. (2000).
2318 BCL-6 represses genes that function in lymphocyte differentiation, inflammation,
2319 and cell cycle control. *Immunity* 13, 199-212. 10.1016/s1074-7613(00)00020-0.
- 2320 44. Schmitz, R., Wright, G.W., Huang, D.W., Johnson, C.A., Phelan, J.D., Wang,
2321 J.Q., Roulland, S., Kasbekar, M., Young, R.M., Shaffer, A.L., et al. (2018).
2322 Genetics and Pathogenesis of Diffuse Large B-Cell Lymphoma. *N Engl J Med*
2323 378, 1396-1407. 10.1056/NEJMoa1801445.
- 2324 45. Bellenie, B.R., Cheung, K.J., Varela, A., Pierrat, O.A., Collie, G.W., Box, G.M.,
2325 Bright, M.D., Gowan, S., Hayes, A., Rodrigues, M.J., et al. (2020). Achieving In
2326 Vivo Target Depletion through the Discovery and Optimization of
2327 Benzimidazolone BCL6 Degraders. *J Med Chem* 63, 4047-4068.
2328 10.1021/acs.jmedchem.9b02076.
- 2329 46. Harnden, A.C., Davis, O.A., Box, G.M., Hayes, A., Johnson, L.D., Henley, A.T., de
2330 Haven Brandon, A.K., Valenti, M., Cheung, K.J., Brennan, A., et al. (2023).
2331 Discovery of an In Vivo Chemical Probe for BCL6 Inhibition by Optimization of
2332 Tricyclic Quinolinones. *J Med Chem* 66, 5892-5906.
2333 10.1021/acs.jmedchem.3c00155.
- 2334 47. Huckvale, R., Harnden, A.C., Cheung, K.J., Pierrat, O.A., Talbot, R., Box, G.M.,
2335 Henley, A.T., de Haven Brandon, A.K., Hallsworth, A.E., Bright, M.D., et al.
2336 (2022). Improved Binding Affinity and Pharmacokinetics Enable Sustained
2337 Degradation of BCL6 In Vivo. *J Med Chem* 65, 8191-8207.
2338 10.1021/acs.jmedchem.1c02175.
- 2339 48. Kerres, N., Steurer, S., Schlager, S., Bader, G., Berger, H., Caligiuri, M., Dank,
2340 C., Engen, J.R., Ettmayer, P., Fischerauer, B., et al. (2017). Chemically Induced
2341 Degradation of the Oncogenic Transcription Factor BCL6. *Cell Rep* 20, 2860-
2342 2875. 10.1016/j.celrep.2017.08.081.
- 2343 49. Pearce, A.C., Bamford, M.J., Barber, R., Bridges, A., Convery, M.A., Demetriou,
2344 C., Evans, S., Gobbi, T., Hirst, D.J., Holmes, D.S., et al. (2021). GSK137, a
2345 potent small-molecule BCL6 inhibitor with in vivo activity, suppresses antibody
2346 responses in mice. *J Biol Chem* 297, 100928. 10.1016/j.jbc.2021.100928.
- 2347 50. Romero, F.A., Murray, J., Lai, K.W., Tsui, V., Albrecht, B.K., An, L., Beresini, M.H.,
2348 de Leon Boenig, G., Bronner, S.M., Chan, E.W., et al. (2017). GNE-781, A Highly
2349 Advanced Potent and Selective Bromodomain Inhibitor of Cyclic Adenosine

- 2350 Monophosphate Response Element Binding Protein, Binding Protein (CBP). J
2351 Med Chem 60, 9162-9183. 10.1021/acs.jmedchem.7b00796.
2352 51. Hay, D.A., Fedorov, O., Martin, S., Singleton, D.C., Tallant, C., Wells, C., Picaud,
2353 S., Philpott, M., Monteiro, O.P., Rogers, C.M., et al. (2014). Discovery and
2354 optimization of small-molecule ligands for the CBP/p300 bromodomains. J Am
2355 Chem Soc 136, 9308-9319. 10.1021/ja412434f.
2356 52. Ho, S.N., Biggar, S.R., Spencer, D.M., Schreiber, S.L., and Crabtree, G.R.
2357 (1996). Dimeric ligands define a role for transcriptional activation domains in
2358 reinitiation. Nature 382, 822-826. 10.1038/382822a0.
2359 53. Spencer, D.M., Wandless, T.J., Schreiber, S.L., and Crabtree, G.R. (1993).
2360 Controlling signal transduction with synthetic ligands. Science 262, 1019-1024.
2361 10.1126/science.7694365.
2362 54. Machleidt, T., Woodroffe, C.C., Schwinn, M.K., Méndez, J., Robers, M.B.,
2363 Zimmerman, K., Otto, P., Daniels, D.L., Kirkland, T.A., and Wood, K.V. (2015).
2364 NanoBRET—A Novel BRET Platform for the Analysis of Protein–Protein
2365 Interactions. ACS Chemical Biology 10, 1797-1804.
2366 10.1021/acschembio.5b00143.
2367 55. Corsello, S.M., Nagari, R.T., Spangler, R.D., Rossen, J., Kocak, M., Bryan, J.G.,
2368 Humeidi, R., Peck, D., Wu, X., Tang, A.A., et al. (2020). Discovering the anti-
2369 cancer potential of non-oncology drugs by systematic viability profiling. Nat
2370 Cancer 1, 235-248. 10.1038/s43018-019-0018-6.
2371 56. Filippakopoulos, P., Picaud, S., Mangos, M., Keates, T., Lambert, J.P., Barsyte-
2372 Lovejoy, D., Felletar, I., Volkmer, R., Muller, S., Pawson, T., et al. (2012). Histone
2373 recognition and large-scale structural analysis of the human bromodomain family.
2374 Cell 149, 214-231. 10.1016/j.cell.2012.02.013.
2375 57. Stogios, P.J., Downs, G.S., Jauhal, J.J., Nandra, S.K., and Prive, G.G. (2005).
2376 Sequence and structural analysis of BTB domain proteins. Genome Biol 6, R82.
2377 10.1186/gb-2005-6-10-r82.
2378 58. Pasqualucci, L., Dominguez-Sola, D., Chiarenza, A., Fabbri, G., Grunn, A.,
2379 Trifonov, V., Kasper, L.H., Lerach, S., Tang, H., Ma, J., et al. (2011). Inactivating
2380 mutations of acetyltransferase genes in B-cell lymphoma. Nature 471, 189-195.
2381 10.1038/nature09730.
2382 59. Bereshchenko, O.R., Gu, W., and Dalla-Favera, R. (2002). Acetylation inactivates
2383 the transcriptional repressor BCL6. Nat Genet 32, 606-613. 10.1038/ng1018.
2384 60. Narita, T., Higashijima, Y., Kilic, S., Liebner, T., Walter, J., and Choudhary, C.
2385 (2023). Acetylation of histone H2B marks active enhancers and predicts
2386 CBP/p300 target genes. Nat Genet 55, 679-692. 10.1038/s41588-023-01348-4.
2387 61. Rada-Iglesias, A., Bajpai, R., Swigut, T., Brugmann, S.A., Flynn, R.A., and
2388 Wysocka, J. (2011). A unique chromatin signature uncovers early developmental
2389 enhancers in humans. Nature 470, 279-283. 10.1038/nature09692.
2390 62. Huang, C., Hatzi, K., and Melnick, A. (2013). Lineage-specific functions of Bcl-6
2391 in immunity and inflammation are mediated by distinct biochemical mechanisms.
2392 Nat Immunol 14, 380-388. 10.1038/ni.2543.
2393 63. Skene, P.J., and Henikoff, S. (2017). An efficient targeted nuclease strategy for
2394 high-resolution mapping of DNA binding sites. Elife 6. 10.7554/elife.21856.

- 2395 64. Hnisz, D., Abraham, B.J., Lee, T.I., Lau, A., Saint-Andre, V., Sigova, A.A., Hoke,
2396 H.A., and Young, R.A. (2013). Super-enhancers in the control of cell identity and
2397 disease. *Cell* **155**, 934-947. 10.1016/j.cell.2013.09.053.
- 2398 65. Bal, E., Kumar, R., Hadigol, M., Holmes, A.B., Hilton, L.K., Loh, J.W., Dreval, K.,
2399 Wong, J.C.H., Vlasevska, S., Corinaldesi, C., et al. (2022). Super-enhancer
2400 hypermutation alters oncogene expression in B cell lymphoma. *Nature* **607**, 808-
2401 815. 10.1038/s41586-022-04906-8.
- 2402 66. Martin, B.J.E., Brind'Amour, J., Kuzmin, A., Jensen, K.N., Liu, Z.C., Lorincz, M.,
2403 and Howe, L.J. (2021). Transcription shapes genome-wide histone acetylation
2404 patterns. *Nat Commun* **12**, 210. 10.1038/s41467-020-20543-z.
- 2405 67. Willis, S.N., Tellier, J., Liao, Y., Trezise, S., Light, A., O'Donnell, K., Garrett-Sinha,
2406 L.A., Shi, W., Tarlinton, D.M., and Nutt, S.L. (2017). Environmental sensing by
2407 mature B cells is controlled by the transcription factors PU.1 and SpiB. *Nat
2408 Commun* **8**, 1426. 10.1038/s41467-017-01605-1.
- 2409 68. Villunger, A., Michalak, E.M., Coulter, L., Mullauer, F., Bock, G., Ausserlechner,
2410 M.J., Adams, J.M., and Strasser, A. (2003). p53- and drug-induced apoptotic
2411 responses mediated by BH3-only proteins puma and noxa. *Science* **302**, 1036-
2412 1038. 10.1126/science.1090072.
- 2413 69. Marsden, V.S., and Strasser, A. (2003). CONTROL OF APOPTOSIS IN THE
2414 IMMUNE SYSTEM: Bcl-2, BH3-Only Proteins and More. *Annu Rev Immunol* **21**,
2415 71-105.
- 2416 70. Jeffers, J.R., Parganas, E., Lee, Y., Yang, C., Wang, J., Brennan, J., MacLean,
2417 K.H., Han, J., Chittenden, T., Ihle, J.N., et al. (2003). Puma is an essential
2418 mediator of p53-dependent and -independent apoptotic pathways. *Cancer Cell* **4**,
2419 321-328. 10.1016/s1535-6108(03)00244-7.
- 2420 71. You, H., Pellegrini, M., Tsuchihara, K., Yamamoto, K., Hacker, G., Erlacher, M.,
2421 Villunger, A., and Mak, T.W. (2006). FOXO3a-dependent regulation of Puma in
2422 response to cytokine/growth factor withdrawal. *J Exp Med* **203**, 1657-1663.
2423 10.1084/jem.20060353.
- 2424 72. Basso, K., and Dalla-Favera, R. (2015). Germinal centres and B cell
2425 lymphomagenesis. *Nat Rev Immunol* **15**, 172-184. 10.1038/nri3814.
- 2426 73. Brescia, P., Schneider, C., Holmes, A.B., Shen, Q., Hussein, S., Pasqualucci, L.,
2427 Basso, K., and Dalla-Favera, R. (2018). MEF2B Instructs Germinal Center
2428 Development and Acts as an Oncogene in B Cell Lymphomagenesis. *Cancer
2429 Cell* **34**, 453-465 e459. 10.1016/j.ccr.2018.08.006.
- 2430 74. Wang, H., Jain, S., Li, P., Lin, J.X., Oh, J., Qi, C., Gao, Y., Sun, J., Sakai, T.,
2431 Naghashfar, Z., et al. (2019). Transcription factors IRF8 and PU.1 are required
2432 for follicular B cell development and BCL6-driven germinal center responses.
2433 *Proc Natl Acad Sci U S A* **116**, 9511-9520. 10.1073/pnas.1901258116.
- 2434 75. Das, S.K., Lewis, B.A., and Levens, D. (2023). MYC: a complex problem. *Trends
2435 Cell Biol* **33**, 235-246. 10.1016/j.tcb.2022.07.006.
- 2436 76. Calado, D.P., Sasaki, Y., Godinho, S.A., Pellerin, A., Kochert, K., Sleckman, B.P.,
2437 de Alboran, I.M., Janz, M., Rodig, S., and Rajewsky, K. (2012). The cell-cycle
2438 regulator c-Myc is essential for the formation and maintenance of germinal
2439 centers. *Nat Immunol* **13**, 1092-1100. 10.1038/ni.2418.

- 2440 77. Dominguez-Sola, D., Victora, G.D., Ying, C.Y., Phan, R.T., Saito, M.,
2441 Nussenzweig, M.C., and Dalla-Favera, R. (2012). The proto-oncogene MYC is
2442 required for selection in the germinal center and cyclic reentry. *Nat Immunol* 13,
2443 1083-1091. 10.1038/ni.2428.
- 2444 78. Iyer, A.R., Gurumurthy, A., Kodgule, R., Aguilar, A.R., Saari, T., Ramzan, A.,
2445 Rausch, D., Gupta, J., Hall, C.N., Runge, J.S., et al. (2023). Selective Enhancer
2446 Dependencies in MYC -Intact and MYC -Rearranged Germinal Center B-cell
2447 Diffuse Large B-cell Lymphoma. *bioRxiv*. 10.1101/2023.05.02.538892.
- 2448 79. Hamlyn, P.H., and Rabbitts, T.H. (1983). Translocation joins c-myc and
2449 immunoglobulin gamma 1 genes in a Burkitt lymphoma revealing a third exon in
2450 the c-myc oncogene. *Nature* 304, 135-139.
- 2451 80. Haluska, F.G., Tsujimoto, Y., and Croce, C.M. (1987). The t(8;14) chromosome
2452 translocation of the Burkitt lymphoma cell line Daudi occurred during
2453 immunoglobulin gene rearrangement and involved the heavy chain diversity
2454 region. *Proc Natl Acad Sci U S A* 84, 6835-6839. 10.1073/pnas.84.19.6835.
- 2455 81. Ryan, R.J., Drier, Y., Whitton, H., Cotton, M.J., Kaur, J., Issner, R., Gillespie, S.,
2456 Epstein, C.B., Nardi, V., Sohani, A.R., et al. (2015). Detection of Enhancer-
2457 Associated Rearrangements Reveals Mechanisms of Oncogene Dysregulation in
2458 B-cell Lymphoma. *Cancer Discov* 5, 1058-1071. 10.1158/2159-8290.CD-15-
2459 0370.
- 2460 82. Gadd, M.S., Testa, A., Lucas, X., Chan, K.H., Chen, W., Lamont, D.J., Zengerle,
2461 M., and Ciulli, A. (2017). Structural basis of PROTAC cooperative recognition for
2462 selective protein degradation. *Nat Chem Biol* 13, 514-521.
10.1038/nchembio.2329.
- 2463 83. Ichikawa, S., Payne, N.C., Xu, W., Chang, C.F., Vallavoju, N., Frome, S.,
2464 Flaxman, H.A., Mazitschek, R., and Woo, C.M. (2024). The cyclimids: Degron-
2465 inspired cereblon binders for targeted protein degradation. *Cell Chem Biol* 31,
2466 1162-1175 e1110. 10.1016/j.chembiol.2024.01.003.
- 2467 84. Delvecchio, M., Gaucher, J., Aguilar-Gurrieri, C., Ortega, E., and Panne, D.
2468 (2013). Structure of the p300 catalytic core and implications for chromatin
2469 targeting and HAT regulation. *Nat Struct Mol Biol* 20, 1040-1046.
10.1038/nsmb.2642.
- 2470 85. Ortega, E., Rengachari, S., Ibrahim, Z., Houghoughi, N., Gaucher, J., Holehouse,
2471 A.S., Khochbin, S., and Panne, D. (2018). Transcription factor dimerization
2472 activates the p300 acetyltransferase. *Nature* 562, 538-544. 10.1038/s41586-018-
2473 0621-1.
- 2474 86. Thompson, P.R., Wang, D., Wang, L., Fulco, M., Pediconi, N., Zhang, D., An, W.,
2475 Ge, Q., Roeder, R.G., Wong, J., et al. (2004). Regulation of the p300 HAT
2476 domain via a novel activation loop. *Nat Struct Mol Biol* 11, 308-315.
10.1038/nsmb740.
- 2477 87. Ahmad, K.F., Melnick, A., Lax, S., Bouchard, D., Liu, J., Kiang, C.L., Mayer, S.,
2478 Takahashi, S., Licht, J.D., and Prive, G.G. (2003). Mechanism of SMRT
2479 corepressor recruitment by the BCL6 BTB domain. *Mol Cell* 12, 1551-1564.
10.1016/s1097-2765(03)00454-4.

- 2484 88. Ghetu, A.F., Corcoran, C.M., Cerchietti, L., Bardwell, V.J., Melnick, A., and Prive, G.G. (2008). Structure of a BCOR corepressor peptide in complex with the BCL6 BTB domain dimer. *Mol Cell* 29, 384-391. 10.1016/j.molcel.2007.12.026.
- 2485 89. Meyer, S.N., Scuoppo, C., Vlasevska, S., Bal, E., Holmes, A.B., Holloman, M., Garcia-Ibanez, L., Nataraj, S., Duval, R., Vantrimpont, T., et al. (2019). Unique and Shared Epigenetic Programs of the CREBBP and EP300 Acetyltransferases in Germinal Center B Cells Reveal Targetable Dependencies in Lymphoma. *Immunity* 51, 535-547 e539. 10.1016/j.immuni.2019.08.006.
- 2486 90. Jiang, Y., Ortega-Molina, A., Geng, H., Ying, H.Y., Hatzi, K., Parsa, S., McNally, D., Wang, L., Doane, A.S., Agirre, X., et al. (2017). CREBBP Inactivation Promotes the Development of HDAC3-Dependent Lymphomas. *Cancer Discov* 7, 38-53. 10.1158/2159-8290.CD-16-0975.
- 2487 91. Mondello, P., Tadros, S., Teater, M., Fontan, L., Chang, A.Y., Jain, N., Yang, H., Singh, S., Ying, H.Y., Chu, C.S., et al. (2020). Selective Inhibition of HDAC3 Targets Synthetic Vulnerabilities and Activates Immune Surveillance in Lymphoma. *Cancer Discov* 10, 440-459. 10.1158/2159-8290.CD-19-0116.
- 2488 92. Adelman, K., and Lis, J.T. (2012). Promoter-proximal pausing of RNA polymerase II: emerging roles in metazoans. *Nat Rev Genet* 13, 720-731. 10.1038/nrg3293.
- 2489 93. Core, L., and Adelman, K. (2019). Promoter-proximal pausing of RNA polymerase II: a nexus of gene regulation. *Genes Dev* 33, 960-982. 10.1101/gad.325142.119.
- 2490 94. Narita, T., Ito, S., Higashijima, Y., Chu, W.K., Neumann, K., Walter, J., Satpathy, S., Liebner, T., Hamilton, W.B., Maskey, E., et al. (2021). Enhancers are activated by p300/CBP activity-dependent PIC assembly, RNAPII recruitment, and pause release. *Mol Cell* 81, 2166-2182 e2166. 10.1016/j.molcel.2021.03.008.
- 2491 95. Barretina, J., Caponigro, G., Stransky, N., Venkatesan, K., Margolin, A.A., Kim, S., Wilson, C.J., Lehar, J., Kryukov, G.V., Sonkin, D., et al. (2012). The Cancer Cell Line Encyclopedia enables predictive modelling of anticancer drug sensitivity. *Nature* 483, 603-607. 10.1038/nature11003.
- 2492 96. Dempster, J.M., Boyle, I., Vazquez, F., Root, D.E., Boehm, J.S., Hahn, W.C., Tsherniak, A., and McFarland, J.M. (2021). Chronos: a cell population dynamics model of CRISPR experiments that improves inference of gene fitness effects. *Genome Biol* 22, 343. 10.1186/s13059-021-02540-7.
- 2493 97. Perez-Riverol, Y., Bandla, C., Kundu, D.J., Kamatchinathan, S., Bai, J., Hewapathirana, S., John, N.S., Prakash, A., Walzer, M., Wang, S., and Vizcaino, J.A. (2025). The PRIDE database at 20 years: 2025 update. *Nucleic Acids Res* 53, D543-D553. 10.1093/nar/gkae1011.
- 2494 98. Yu, C., Mannan, A.M., Yvone, G.M., Ross, K.N., Zhang, Y.-L., Marton, M.A., Taylor, B.R., Crenshaw, A., Gould, J.Z., Tamayo, P., et al. (2016). High-throughput identification of genotype-specific cancer vulnerabilities in mixtures of barcoded tumor cell lines. *Nature Biotechnology* 34, 419-423. 10.1038/nbt.3460.
- 2495 99. Stead, M.A., Rosbrook, G.O., Hadden, J.M., Trinh, C.H., Carr, S.B., and Wright, S.C. (2008). Structure of the wild-type human BCL6 POZ domain. *Acta Crystallographica Section F Structural Biology and Crystallization Communications* 64, 1101-1104. 10.1107/s1744309108036063.

- 2529 100. Evans, P. (2006). Scaling and assessment of data quality. *Acta Crystallogr D Biol*
2530 *Crystallogr* 62, 72-82. 10.1107/S0907444905036693.
- 2531 101. Evans, P.R., and Murshudov, G.N. (2013). How good are my data and what is the
2532 resolution? *Acta Crystallogr D Biol Crystallogr* 69, 1204-1214.
2533 10.1107/S0907444913000061.
- 2534 102. Agirre, J., Atanasova, M., Bagdonas, H., Ballard, C.B., Basle, A., Beilsten-
2535 Edmands, J., Borges, R.J., Brown, D.G., Burgos-Marmol, J.J., Berrisford, J.M., et
2536 al. (2023). The CCP4 suite: integrative software for macromolecular
2537 crystallography. *Acta Crystallogr D Struct Biol* 79, 449-461.
2538 10.1107/S2059798323003595.
- 2539 103. Cheng, H., Linhares, B.M., Yu, W., Cardenas, M.G., Ai, Y., Jiang, W., Winkler, A.,
2540 Cohen, S., Melnick, A., MacKerell, A., Jr., et al. (2018). Identification of Thiourea-
2541 Based Inhibitors of the B-Cell Lymphoma 6 BTB Domain via NMR-Based
2542 Fragment Screening and Computer-Aided Drug Design. *J Med Chem* 61, 7573-
2543 7588. 10.1021/acs.jmedchem.8b00040.
- 2544 104. Vagin, A.A., Steiner, R.A., Lebedev, A.A., Potterton, L., McNicholas, S., Long, F.,
2545 and Murshudov, G.N. (2004). REFMAC5 dictionary: organization of prior
2546 chemical knowledge and guidelines for its use. *Acta Crystallogr D Biol Crystallogr*
2547 60, 2184-2195. 10.1107/S0907444904023510.
- 2548 105. McCoy, A.J., Grosse-Kunstleve, R.W., Adams, P.D., Winn, M.D., Storoni, L.C.,
2549 and Read, R.J. (2007). Phaser crystallographic software. *J Appl Crystallogr* 40,
2550 658-674. 10.1107/S0021889807021206.
- 2551 106. Long, F., Nicholls, R.A., Emsley, P., Graaeulis, S., Merkys, A., Vaitkus, A., and
2552 Murshudov, G.N. (2017). AceDRG: a stereochemical description generator for
2553 ligands. *Acta Crystallogr D Struct Biol* 73, 112-122.
2554 10.1107/S2059798317000067.
- 2555 107. Casanal, A., Lohkamp, B., and Emsley, P. (2020). Current developments in Coot
2556 for macromolecular model building of Electron Cryo-microscopy and
2557 Crystallographic Data. *Protein Sci* 29, 1069-1078. 10.1002/pro.3791.
- 2558 108. Jenni, S., Goyal, Y., von Grotthuss, M., Shvartsman, S.Y., and Klein, D.E. (2015).
2559 Structural Basis of Neurohormone Perception by the Receptor Tyrosine Kinase
2560 Torso. *Mol Cell* 60, 941-952. 10.1016/j.molcel.2015.10.026.
- 2561 109. Demichev, V., Messner, C.B., Vernardis, S.I., Lilley, K.S., and Ralser, M. (2020).
2562 DIA-NN: neural networks and interference correction enable deep proteome
2563 coverage in high throughput. *Nat Methods* 17, 41-44. 10.1038/s41592-019-0638-
2564 x.
- 2565 110. Zhu, Y., Orre, L.M., Zhou Tran, Y., Mermelekas, G., Johansson, H.J., Malyutina,
2566 A., Anders, S., and Lehtio, J. (2020). DEqMS: A Method for Accurate Variance
2567 Estimation in Differential Protein Expression Analysis. *Mol Cell Proteomics* 19,
2568 1047-1057. 10.1074/mcp.TIR119.001646.
- 2569 111. Martin, M. (2011). Cutadapt removes adapter sequences from high-throughput
2570 sequencing reads. *EMBnet.journal* 17, 10. 10.14806/ej.17.1.200.
- 2571 112. Bray, N.L., Pimentel, H., Melsted, P., and Pachter, L. (2016). Near-optimal
2572 probabilistic RNA-seq quantification. *Nature Biotechnology* 34, 525-527.
2573 10.1038/nbt.3519.

- 2574 113. Love, M.I., Huber, W., and Anders, S. (2014). Moderated estimation of fold
2575 change and dispersion for RNA-seq data with DESeq2. *Genome Biol* 15, 550.
2576 10.1186/s13059-014-0550-8.
- 2577 114. Zhu, A., Ibrahim, J.G., and Love, M.I. (2019). Heavy-tailed prior distributions for
2578 sequence count data: removing the noise and preserving large differences.
2579 *Bioinformatics* 35, 2084-2092. 10.1093/bioinformatics/bty895.
- 2580 115. Chen, E.Y., Tan, C.M., Kou, Y., Duan, Q., Wang, Z., Meirelles, G.V., Clark, N.R.,
2581 and Ma'ayan, A. (2013). Enrichr: interactive and collaborative HTML5 gene list
2582 enrichment analysis tool. *BMC bioinformatics* 14, 128. 10.1186/1471-2105-14-
2583 128.
- 2584 116. Korotkevich, G.S., V.; Sergushichev, A. (2019). Fast gene set enrichment
2585 analysis. *bioRxiv*. 10.1101/060012.
- 2586 117. Kolde, R. (2018). pheatmap: Pretty Heatmaps.
- 2587 118. Meers, M.P., Bryson, T.D., Henikoff, J.G., and Henikoff, S. (2019). Improved
2588 CUT&RUN chromatin profiling tools. *eLife* 8. 10.7554/eLife.46314.
- 2589 119. Skene, P.J., Henikoff, J.G., and Henikoff, S. (2018). Targeted in situ genome-
2590 wide profiling with high efficiency for low cell numbers. *Nature protocols* 13,
2591 1006-1019. 10.1038/nprot.2018.015.
- 2592 120. Li, H., Handsaker, B., Wysoker, A., Fennell, T., Ruan, J., Homer, N., Marth, G.,
2593 Abecasis, G., Durbin, R., and Genome Project Data Processing, S. (2009). The
2594 Sequence Alignment/Map format and SAMtools. *Bioinformatics* 25, 2078-2079.
2595 10.1093/bioinformatics/btp352.
- 2596 121. Zhang, Y., Liu, T., Meyer, C.A., Eeckhoute, J., Johnson, D.S., Bernstein, B.E.,
2597 Nusbaum, C., Myers, R.M., Brown, M., Li, W., and Liu, X.S. (2008). Model-based
2598 Analysis of ChIP-Seq (MACS). *Genome Biology* 9, R137. 10.1186/gb-2008-9-9-
2599 r137.
- 2600 122. Quinlan, A.R., and Hall, I.M. (2010). BEDTools: a flexible suite of utilities for
2601 comparing genomic features. *Bioinformatics* 26, 841-842.
2602 10.1093/bioinformatics/btq033.
- 2603 123. Ramírez, F., Ryan, D.P., Grüning, B., Bhardwaj, V., Kilpert, F., Richter, A.S.,
2604 Heyne, S., Dündar, F., and Manke, T. (2016). deepTools2: a next generation web
2605 server for deep-sequencing data analysis. *Nucleic Acids Research* 44, W160-
2606 W165. 10.1093/nar/gkw257.
- 2607 124. Amemiya, H.M., Kundaje, A., and Boyle, A.P. (2019). The ENCODE Blacklist:
2608 Identification of Problematic Regions of the Genome. *Scientific Reports* 9.
2609 10.1038/s41598-019-45839-z.
- 2610 125. Perez, G., Barber, G.P., Benet-Pages, A., Casper, J., Clawson, H., Diekhans, M.,
2611 Fischer, C., Gonzalez, J.N., Hinrichs, A.S., Lee, C.M., et al. (2024). The UCSC
2612 Genome Browser database: 2025 update. *Nucleic Acids Res.*
2613 10.1093/nar/gkae974.
- 2614 126. Mayakonda, A., and Westermann, F. (2024). Trackplot: a fast and lightweight R
2615 script for epigenomic enrichment plots. *Bioinform Adv* 4, vbae031.
2616 10.1093/bioadv/vbae031.
- 2617 127. Riemondy, K.A., Sheridan, R.M., Gillen, A., Yu, Y., Bennett, C.G., and
2618 Hesselberth, J.R. (2017). valr: Reproducible genome interval analysis in R.
2619 *F1000Res* 6, 1025. 10.12688/f1000research.11997.1.